



**INSTITUTO POTOSINO DE INVESTIGACIÓN
CIENTÍFICA Y TECNOLÓGICA, A.C.**

POSGRADO EN GEOCIENCIAS APLICADAS

**Integrated methodology for the characterization of
active faulting and its link to the hydrogeological
system in the southern portion of the Villa de Reyes
Graben, S.L.P. and Guanajuato.**

Tesis que presenta

Fabián Esteban Monge Cerda

Para obtener el grado de

Doctor en Geociencias Aplicadas

Codirectores de la Tesis:

Dr. Omar Delgado Rodríguez

Dr. José Alfredo Ramos Leal

San Luis Potosí, S.L.P., Agosto de 2025



Constancia de aprobación de la tesis

La tesis “**Integrated methodology for the characterization of active faulting and its link to the hydrogeological system in the southern portion of the Villa de Reyes Graben, S.L.P. and Guanajuato.**” presentada para obtener el Grado de Doctor(a) en Geociencias Aplicadas fue elaborada por **Fabián Esteban Monge Cerda** y aprobada el **26 de agosto de 2025** por los suscritos, designados por el Colegio de Profesores de la División de Geociencias Aplicadas del Instituto Potosino de Investigación Científica y Tecnológica, A.C.

Dr. Omar Delgado Rodríguez
Codirector de la tesis

Dr. José Alfredo Ramos Leal
Codirector de la tesis

Dra. Mayla Alheli Ramos Vázquez
Miembro del Comité

Dr. José Ramón Torres Hernández
Miembro del Comité

Dr. Salvador Isidro Belmonte Jiménez
Miembro del Comité



Créditos Institucionales

Esta tesis fue elaborada en el Instituto Potosino de Investigación Científica y Tecnológica, A.C., bajo la codirección del Dr. Omar Delgado Rodríguez y José Alfredo Ramos Leal.

Durante la realización del trabajo el autor recibió una beca académica del Consejo Nacional de Ciencia y Tecnología (No. 869417) y del Instituto Potosino de Investigación Científica y Tecnológica, A. C.

Acta de examen

Dedications

To my parents, sister, wife and daughter.
This is because of and for you.

A mis padres, hermana, esposa, y a mi hija.
Esto es por y para ustedes.

Acknowledgements

To the Secretaría de Ciencia, Humanidades, Tecnología e Innovación (SECIHTI) for the assigned scholarship to complete my Doctorate in Applied Geosciences of the Instituto Potosino de Investigación de Científica y Tecnológica (IPICYT).

To the Instituto Potosino de Investigación de Científica y Tecnológica (IPICYT) and its Geophysics Laboratory technician David Torres Gaytan, for the support without which this work would not have been possible.

To my thesis advisors Dr. Omar Delgado-Rodríguez and Dr. José Alfredo Ramos Leal for the patience, kindness and understanding of difficult times I encountered throughout the completion of this work. Thank you, Dr. Omar, for all the geophysics knowledge you shared with me, your patience guiding me in the use of the different geophysics' software, and your willingness to always help me with the redaction and figure improving of this thesis. Thank you, Dr. Ramos, for sharing your vast geological knowledge, and for the countless hours we spent in your office improving this work's text and figures. I will always be in debt with both of you.

Thanks to my Doctoral committee members Dr. José Ramón Torres Hernández, Dr. Mayla Alheli Ramos Vázquez and Dr. Salvador Isidro Belmonte Jiménez, for your most valuable help in improving this document with their guidance and suggestions. Special thanks to Dr. José Ramón for all the help with the structural geology field work mentorship, and for sharing with me his non-ending knowledge about how faulting works, in ways that I could not have conceived before knowing him.

Special thanks to Dr. Lorena-Elisa Sánchez-Higuero for helping me with the redaction of the first paper derived from this work, and Dr. Oscar Guadalupe Almanza Tovar, for the field and software assistance of drone photographs.

To Juana-Edith Rodríguez-Delgadillo for all the administrative help and her kindness.

Thanks to my IPICYT friends Uli, Betty, Bere, Alexa, Daisy, Sebas, Patricia, Pavel, Roberto, Rubí, Karla, Erandi, Mayank, and my brother Mahendra, and my SLP friends, José Luis and his family, Ofe, Jorge, Dr. Memo and Irma, el Inge, Juan, Héctor, Vicky and Vicente, for all the good times.

Special thanks to all my Costa Rican friends Javier, Ari, Juan, Lorenzo, Berni and Karlita, for always keeping in touch. Special thanks to Dr. Alan López for being the one who encouraged me to pursue a graduate degree in México.

To Pechán and Ringo for being the most loyal and best friends I could ever ask for.

Finally, thank you to the Reynoso-Reynoso family, for all the support, hospitality, and for being there for me when my parents could not. Thanks dad, mom, my sister and her husband Frank for the never-ending love and support. Thanks to my wife Hali for being the pillar in which my life supports itself, without you all of this simply could not have been possible: your love, encouragement and inspiration have been my guiding light through the years. Thanks to my daughter Yami, you are new to this world, but the love I have for you is something I could not conceive of before, and I also want to thank you for bringing new inspiration to become a better person. This is for you.

Contents

| | |
|---|------|
| Constancia de aprobación de la tesis | ii |
| Créditos Institucionales | iii |
| Acta de examen | iv |
| Dedications | v |
| Acknowledgements | vi |
| Contents | viii |
| List of figures | x |
| Abstract | xi |
| Resumen | xiii |
| Chapter 1-. Generalities | 1 |
| 1.1 Introduction | 1 |
| 1.2 Previous studies | 5 |
| 1.2.1 Previous geological work in the study area | 5 |
| 1.2.2 Previous geophysical and hydrogeological work in the study area | 5 |
| 1.3 Study area | 6 |
| 1.4 Objectives | 8 |
| 1.4.1 General Objectives | 8 |
| 1.4.2 Particular objectives | 8 |
| 1.5 Justification | 8 |
| 1.6 Hypothesis | 9 |
| References | 9 |
| Chapter 2-. Geological and hydrogeological context | 16 |
| 2.1 Geological and tectonic setting | 16 |
| 2.1.1 General Geology | 16 |
| 2.1.2. Structural geology studies in the region | 24 |
| 2.2 General Hydrogeology | 29 |

| | |
|---|-----|
| 2.2.1 Hydrography | 29 |
| 2.2.2 Aquifer type | 29 |
| 2.2.3 Piezometric levels | 30 |
| References | 31 |
| Chapter 3-. Geoelectrical characterization of non-filled active faults in Jaral de Berrios, Guanajuato, México | 35 |
| Abstract | |
| 1. Introduction | 36 |
| 2. Geological and tectonic setting | 37 |
| 3. Methodology | 38 |
| 4. Results | 40 |
| 5. Discussion | 41 |
| 6. Conclusions | 42 |
| References | 43 |
| Chapter 4-. Geophysical, geological and tectonic study of active faulting inside the Villa de Reyes Graben, Central México | 45 |
| ABSTRACT | 46 |
| 1. INTRODUCTION | 47 |
| 2. GEOLOGICAL AND TECTONIC SETTING | 51 |
| 3. METHODS | 53 |
| 4. RESULTS | 60 |
| 5. DISCUSSION | 78 |
| 6. CONCLUSIONS | 84 |
| REFERENCES | 86 |
| Chapter 5-. Active faulting and its relationship with regional hydrogeological regimes: a case study in the Villa de Reyes Graben | 93 |
| Abstract | 94 |
| 1. Introduction | 95 |
| 2. Fault zone permeability | 99 |
| 3. Geological, hydrogeological and structural context of the Villa de Reyes Graben | 100 |
| 4. Methods and data processing | 105 |
| 5. Results | 109 |

| | |
|---|-----|
| 6. Discussion | 120 |
| 7. Conclusions and recommendations | 126 |
| References | 128 |
| Chapter 6-. Discussion | 134 |
| References | 137 |
| Chapter 7-. Conclusions and recommendations | 139 |
| 7.1 Conclusions | 139 |
| 7.2 Recommendations | 140 |

List of figures

Fig. 1. Study area located in central region of Mexico (Municipalities of Villa de Reyes in the State of San Luis Potosí and Jaral de Berrios in the State of Guanajuato, see cyan dot on inset map). Modified from Labarthe-Hernández et al. (1982), López-Loera & Tristán-González (2013) and Soto-García (2022), with redefinition of faulting limits Landsat 8 images, processed with ArcMap 10.8, version 10.0.0.10450, software (ESRI, 2019). 7

Fig. 2. Tectonic context of the study area: a Location of the study area. LS—Laguna de Santiaguillo; RCH-OG—Río Chico-Otinapa Graben; AG—Aguascalientes Graben; FVH—Fault Villa Hidalgo; FBV—Fault Buena Vista; FO—Fault El Obraje; FVA—Fault Villa de Arriaga; FLP—Fault Los Pájaros; CG—El Cuarenta Graben; FB—Fault El Bajío; GS—La Saucedá Graben; BG—Bledos Graben; VRG—Villa de Reyes Graben; VAG—Villa de Arista Graben; EG—Enramadas Graben; DQ—La Quemada Depression; SSM—Sierra de San Miguelito; SG—Sierra de Guanajuato; SC—Sierra de Catorce; SS—Sierra de Salinas; RC—Real de Catorce; G—Guanajuato; SLP—San Luis Potosí; SMR—Santa María del Río; SLDP—San Luis de La Paz; ND—Nombre de Dios; SMA—San Miguel de Allende; Q—Querétaro. ZG—Zacatecas Graben. Taken and modified after Nieto Samaniego *et al.* (2005). Epicenter data taken from SSN (2024). Topographic data after INEGI (2023); b Mesa Central Tectonic Province location in Central México. 28

Fig. 3. Geology and piezometric levels for the southern portion of the Villa de Reyes Graben. Geology and faults after López-Loera & Tristán-González (2013) and Soto-García (2022), with modifications and redefinition of faulting limits and geological contacts using Landsat 8 images, processed using ArcMap 10.8, version 10.0.0.10450 (ESRI,2019). Piezometric levels after (CEAG, 2021), processed using Surfer 16 (Golden Software, 2019). 31

Abstract

Integrated methodology for the characterization of active faulting and its link to the hydrogeological system in the southern portion of the Villa de Reyes Graben, S.L.P. and Guanajuato.

A geological, geophysical and structural study was performed in the southern sector of the Villa de Reyes Graben (VRG) in Central México, with the main objective of defining the structural style of the active faulting inside this graben. This was achieved through following a four-part methodology. The first and second steps of this methodology, geological survey and Electromagnetic Profiling (EMP) method, respectively, helped establish that most active faults outcrop as non-filled fractures generated by left-right lateral faulting, of NW-SE orientation in the southern study area and NE-SW in the northern part, which generate high-resistivity values in the EMP maps. The third part of this methodology allowed to characterize in depth these faults via the application of Electrical Resistivity Tomography (ERT) and Ground Penetrating Radar (GPR) methods. ERT sections show that sub-vertical fractures tend to join at depth, which is evidence of positive and negative flower structures, while GPR clearly show these structures with more detail. Moreover, ERT reveals the high-resistivity shallow faults become conductive at >20 m deep, probably relating to a local disturbance of the area's aquifer, while most fault traces are located below the water table, which reveal the purely geological origin of these faults. The fourth part of the methodology uses focal mechanism evidence to corroborate the main orientations and type of faulting, previously established with outcrop and geophysical evidence.

The previously mentioned methodology allowed to define the structural style of the VRG from a regional to an outcrop scale. To study the area on a basin scale, Aeromagnetic (AM) data was used to characterize the area with study depths of up to 2 km. This data helped confirm the previously mapped structures, and shows a pull-apart type structure, inside which there are alternate transtensive and transpressive stress fields, controls the structural style on the area. Hydrogeochemical (HGC) data reveal that the western sector of the VRG is more active than the eastern sector, since meteoric water influence is higher on the former than the latter. This also agrees with epicenter data from the seismic sequence of the September 5, 2021, San Felipe (Guanajuato) earthquake. Finally, the structural-geophysical model based on the integration of field, geoelectric, AM and major ion data reveals that the number and strike of faults remain constant for about 1000 m, while at 2000 m deep these shallower faults appear to join in a smaller number of traces, which reinforces the interpretation of positive-negative flower structures controlling the tectonics of the area. This means that these types of transpressive and transtensive structures are present at the outcrop, regional, and basin scales.

Keywords: No-filled fractures, Electrical Resistivity Tomography, Electromagnetic Profiling, Ground Penetrating Radar, Aeromagnetic data, Hydrogeochemical analysis, Positive and Negative flower structures, Active faulting, Villa de Reyes Graben.

Resumen

Integrated methodology for the characterization of active faulting and its link to the hydrogeological system in the southern portion of the Villa de Reyes Graben, S.L.P. and Guanajuato.

Se realizó un estudio geológico, geofísico y estructural en el sector sur del Graben de Villa de Reyes (VRG, por sus siglas en inglés) en el centro de México, con el objetivo principal de definir el estilo estructural del fallamiento activo en el interior de este graben. Esto se logró utilizando una metodología de cuatro pasos. El primer y segundo paso de esta metodología, geología de campo y Perfilaje Electromagnético (EMP, por sus siglas en inglés), respectivamente, ayudaron a establecer que la mayoría de las fallas activas afloran como fracturas no rellenas generadas por fallas laterales izquierda-derecha, con orientación NW-SE en el sector sur de la zona de estudio y NE-SW en la parte norte, lo que genera valores de resistividad alta en los mapas del EMP. La tercera parte de esta metodología permitió caracterizar en profundidad estas fallas mediante la aplicación de los métodos de Tomografía de Resistividad Eléctrica (ERT, por sus siglas en inglés) y Georadar (GPR, por sus siglas en inglés). Los perfiles ERT muestran que las fracturas subverticales tienden a unirse en profundidad, lo que es evidencia de estructuras de flor positivas y negativas, mientras que los perfiles de GPR muestra estas estructuras con mayor detalle. Además, las tomografías revelan que las fallas superficiales de resistividad alta se vuelven conductivas a más de 20 m de profundidad, provocado esto probablemente por una perturbación local del acuífero de la zona, mientras que la mayoría de las trazas de falla se ubican por debajo del nivel freático, lo que revela el origen puramente geológico de estas fallas. La cuarta parte de la metodología utiliza evidencia de mecanismos focal para corroborar las principales orientaciones y el tipo de fallamiento, previamente establecidos con evidencias de afloramiento y geofísica.

La metodología mencionada permitió definir el estilo estructural del VRG desde una escala regional hasta una de afloramiento. Para estudiar el área a escala de cuenca, se utilizaron datos aeromagnéticos (AM) para caracterizarla con profundidades de estudio de hasta 2 km. Estos datos confirmaron las estructuras previamente mapeadas y muestran una estructura de tipo pull-apart, dentro de la cual existen esfuerzos transtensivos y transpresivos alternados, controla el estilo estructural del área. Los datos hidrogeoquímicos revelan que el sector occidental del VRG es más activo que el oriental, ya que la influencia del agua meteórica es mayor en el primero que en el segundo. Esto también concuerda con los datos de epicentros de la secuencia sísmica del sismo del 5 de septiembre de 2021, de San Felipe (Guanajuato). Finalmente, el modelo estructural-geofísico, basado en la integración de datos de campo, geoelectrónicos, AM y de iones, revela que el número y rumbo de las fallas se mantienen constantes por aproximadamente 1000 m, mientras que, a 2000 m de profundidad, estas fallas menos profundas parecen unirse en un número menor de trazas, lo que refuerza la interpretación de estructuras de flor positiva-

negativa que controlan la tectónica del área. Esto significa que estos tipos de estructuras transpresivas y transtensivas están presentes a escala de afloramiento, regional y de cuenca.

Palabras clave: Fracturas vacías, Tomografía de Resistividad Eléctrica, Perfilaje Electromagnético, Georradar, Datos Aeromagnéticos, Análisis Hidrogeoquímico, Estructuras de flor positiva-negativa, Fallamiento activo, Graben de Villa de Reyes.

Chapter 1-. Generalities

1.1 Introduction

The Villa de Reyes Graben (VRG) is an approximately 100 km long valley filled with alluvial sediments, pyroclastic flows, and lacustrine deposits, which ranges in thickness from 50 to about 250 m, with a northward dip (Tristán-González, 1986; Fig. 1), and which is also located in the central portion of the tectonic province known as the Mesa Central. Until now, structural studies have focused on the Oligocene age normal faults that originated the VRG (Labarthe-Hernández *et al.*, 1982; Tristán-González, 1986; Henry & Aranda-Gómez, 1992; Stewart, 1998; López-Loera & Tristán-González, 2013; Del Pilar-Martínez *et al.*, 2020; Cauch-Kau *et al.*, 2021), but little to no attention has been given to the active faulting inside the VRG that is producing (or contributing to) land subsidence, cracks on the ground, and seismic activity. Since the causes of this phenomena are not well studied, this represents a challenge in the urban and economic development of the region.

Geophysical methods have a wide range of applications among which, location of oil reserves, groundwater modeling, engineering applications, are some of the most important ones (Martos, 2012). The application of geoelectrical methods in the study of active faults have been successfully applied to these types of studies for several decades, while Aeromagnetic (AM) methods have also been successfully applied to these kinds of studies, but they normally work better on a regional scale (Kuria *et al.*, 2010; Suski *et al.*, 2010; Monahan, 2013; Cinti *et al.*, 2015; Boubaya, 2017; Wang *et al.*, 2017; Bran *et al.*, 2018; Ahmad *et al.*, 2020; Gunda *et al.*, 2020; Nabi *et al.*, 2020; Aray-Castellano *et al.*, 2021; Hasan *et al.*, 2021; Meneisy & Al-Deep, 2021; Porras *et al.*, 2022; Bustamante-Orozco *et al.*, 2023; Galone *et al.*, 2024).

For instance, Nabi *et al.* (2020) applied Electric Resistivity Tomography (ERT) across active and concealed faults in Karachi Arc, in southern Kirthar Fold Belt

(Pakistan), studying three main faults: the Sona, Kirthar, and Khud faults. The results of the geophysical analysis, aided by fault trenching, revealed that the Sona fault has not experienced recent movement, with the most recent faulting activity predating the Quaternary cover deposition. The Kirthar fault does not extend as much as previously thought, and that most of the displacement is accommodated by folding. Finally, the Khud Fault in the north is active, as indicated by lithological differences revealed in the ERT section. Gunda *et al.* (2020) performed a comprehensive Ground Penetrating Radar (GPR) complemented with total station surveys along active faults in the South Andaman Island to characterize its sub-surface geometry and structural style. The GPR imaging illustrated the sub-surface expression of a fault scarp being generated by a thrust fault strand with very low angle, which very clearly cuts the basement rock. The high-resolution GPR has also revealed the presence of two antithetic fault strands cutting the basement and reaching the surface in the form of a piggyback basin and pop-up scarps. Kuang *et al.* (2022) mapped the distribution of basement faults in the Tarim Basin in mainland China, based on newly acquired aeromagnetic (AM) and seismic data. The authors used four main filters: the horizontal gradient derivative, the first vertical derivative, the tilt derivative, and the upward continuation method. Based on the strikes, amplitudes, and textures of the AM maps and models, the authors were able to define: five crystalline basement domains; the origin of the Tarim Central Highly Anomaly as caused by the Archean crystalline basement; a Neoproterozoic rifting that modified the Archean crystalline basement; and the weakly magnetic Southeastern Domain that was sutured to the highly magnetic Central Tadong Domain along the Tadong South Fault during the Paleoproterozoic.

Hydrogeological methods have been extensively used to study the link between faulting and groundwater for several decades, especially to study fault zone permeability for aquifer potential and contaminant pathway assessment (Caine *et al.*, 1996; Bense and Pearson, 2006; Bense *et al.*, 2013; Cilona *et al.*, 2015; Bauer *et al.*, 2016; Fronzi *et al.*, 2021; Piña-González *et al.*, 2021; Sproule *et al.*, 2021).

For example, Bauer *et al.* (2016) presented a comparative, field-based hydrogeological assessment of non-active geological faults in low-porosity Triassic dolostones and limestones of the Hochschwab massif (Austria), by the integration of field-based structural analysis, fault-rock classification, and fracture-network assessments, complemented with thin-section analysis, electron microscopy, and porosity/permeability laboratory measurements. The authors' main conclusions are that in massive, low porosity carbonates that lack features such as bedding, faults form the most important pathways for potential fluid infiltration, migration and karstification. Faults zones also were found to be accompanied by significant fault-parallel volumes of fractured host-rock, with fracture densities varying by a factor of up to 10. Finally, Monte Carlo simulations of a conceptual fault network support the interpretation that most of the storage capacity in limestones reside within the pore volume of the fault network. Sproule *et al.* (2021) studied the effect of fault zone cementation on the permeability of fault zones, conducting a series of aquifer pumping tests in wells installed within tens of meters of the variably cemented Loma Blanca Fault, located in the Río Grande Rift (New Mexico). The authors conclude that the fault zone cementation can act as a barrier to groundwater flow at the field scale, finding that the cementation reduces the fault zone hydraulic conductivity by at least 6-22 times relative to the host sediment. This is important because for the Loma Blanca Fault that has not clay in its core, and unlithified silty sand on both sides, most conceptual models for the hydrogeology of faults would predict that it would not be a barrier to groundwater flow, so this study highlights the importance of having a network of observation wells for identifying hydrogeologic boundaries.

As can be gathered from the above-mentioned studies, the different types of methodologies used are usually not integrated, which could leave out interpretations that reduce the degree of uncertainty inherent to each one of them. Moreover, most of those studies deal with non-active faulting. This is why in this work an integrated methodology is proposed in which geological and geophysical analysis was used to **define** the type of active-structural style present in the southern sector of the VRG (see Fig. 1). Geoelectric methods: Electromagnetic Profiling (EMP), Electrical

Resistivity Tomography (ERT), Ground Penetrating Radar (GPR), and existing AM data were performed and analyzed to further **identify** the type of geological structures, and hydrogeological methods to **know** the trajectory of the material derived from the faulting and, finally, **analyze** the possible impact in the composition of groundwater.

The thesis work is structured as follows: **Chapter 1** deals with the generalities of the study zone, the main objectives and justification of this work, and with the previous studies similar in nature to this present work, both internationally as well as nationally. **Chapter 2** describes in detail the geological, structural and hydrogeological context of the Villa de Reyes Graben.

The results achieved in the present work are shown in the format of papers in **Chapters 3, 4 and 5**: the first one, presented in **Chapter 3**, is an paper published in the *Journal of Applied Geophysics*, in which geoelectrical methods were applied in the “Banco de Material” site to map non-filled active faults, to observe the response and types of models that can be achieved in these types of fractures, and to determine their suitability to these kinds of structural studies. The second and third (**Chapters 4 and 5**) as manuscripts under review in journals registered in the Journal Citation Reports. **Chapter 4**, based on a paper accepted for publication by **Near Surface Geophysics**, in which a geological and geophysical methodology for the study of active faults was established and applied to map active faults in four sites inside the VRG and understand the structural style inside this basin. **Chapter 5** shows the results of the third article, sent to the JCR publication **Pure and Applied Geophysics** where AM and hydrogeochemical data was used with the main objective of establishing the extent to which active faults can be pathways for contaminants and also one to assess if the geological structures mapped in this work’s second article play a role in the hydrogeological regime of the studied area. **Chapter 6** discusses the main points made in this work, and finally in **Chapter 7** the concluding remarks of this work are presented.

1.2 Previous studies

1.2.1 Previous geological work in the study area

Geological work in the Villa de Reyes Graben (GVR) has mostly focused on normal faulting affecting the study area and the detailed description of its lithology. Amongst many of those studies are of special interest: Labarthe-Hernández *et al.* (1982); Tristán-González (1986); Henry & Aranda-Gómez (1992); Stewart (1998); Nieto Samaniego *et al.* (2007); Tristán-González *et al.* (2009); López-Loera & Tristán-González (2013); Botero-Santa *et al.* (2020); Del Pilar-Martínez *et al.* (2020); Cauch-Kau *et al.* (2021) and Soto-García (2022).

A detailed description of the structural geology and lithology of the study area will be given in Chapter 2.

1.2.2 Previous geophysical and hydrogeological work in the study area

There have been several studies which applied different types of geophysical and hydrogeological methods, mainly for structural and hydrogeological purposes (Ramos-Leal *et al.*, 2007; López-Loera & Tristán-González, 2013; Pérez-Martínez *et al.*, 2021; Hernández-Bocanegra, 2023; Sánchez-Barrientos, 2023). Among those studies, the following are of special interest for this work:

López-Loera & Tristán-González (2013) studied the subsurface geology and tectonics of the VRG by means of aeromagnetic data processing. Through the filtering of these data, the authors were able to generate the following maps: Residual Magnetic Field, Reduced to Pole, Upward Continuation (1,2,3,5, 7.5 and 10 km), First and Second Derivates, and Analytical Signals. The interpretation of these maps shows the underlying geology of the area as being made up of mostly volcanic rocks covered by plio-quadernary deposits. Faults zones and water recharge areas were correlated to magnetic lows. Finally, the authors were able to designate intertwined fault zones associated with aeromagnetic lineaments as the most promising zones for the location of new sources of water supply, mainly located in the SW portion of the VRG.

Hernández-Bocanegra (2023) integrated geophysical methods: Electrical Resistivity Tomography (ERT), and Aeromagnetic (AM) data, with Radon measurements, and hydrogeochemical and isotopic analysis to characterize faulting and its relationship to the local hydrogeology in three sites of VRG. The author interpreted that most lineaments follow a NE-SW trend which agrees with the faulting direction of the VRG's normal faults, but there are also active faults with NW-SE trends. Hydrogeological results show that the VRG groundwater is predominantly of a regional-intermediate flow. Finally, the geological and hydrogeological integrated results make clear that active faulting in these three sites are of tectonic origin, since most faults are found more than 100 m deep on the ground (below the local water table).

1.3 Study area

The study area is located in the states of San Luis Potosí and Guanajuato, inside the Villa de Reyes Graben (VRG). Most of the VRG borders are very steep, since they are mostly controlled by normal faulting (Fig. 1), which is the most common type of faulting that exists in the region and originated the VRG (Tristán-González, 1986). Four sites were visited inside the southern sector of this Graben. Each of the sites was named after local characteristics and/or previous use given to them: "Banco de material" (an old quarry), "Presa El Hundido" (a colonial period dam), "Jaral" (a town in Guanajuato) and "Río Jaral" (an unnamed river).

These sites were chosen since they were the ones where surface evidence of faults was most evident, and because of being in the vicinity of the most important towns in the area.

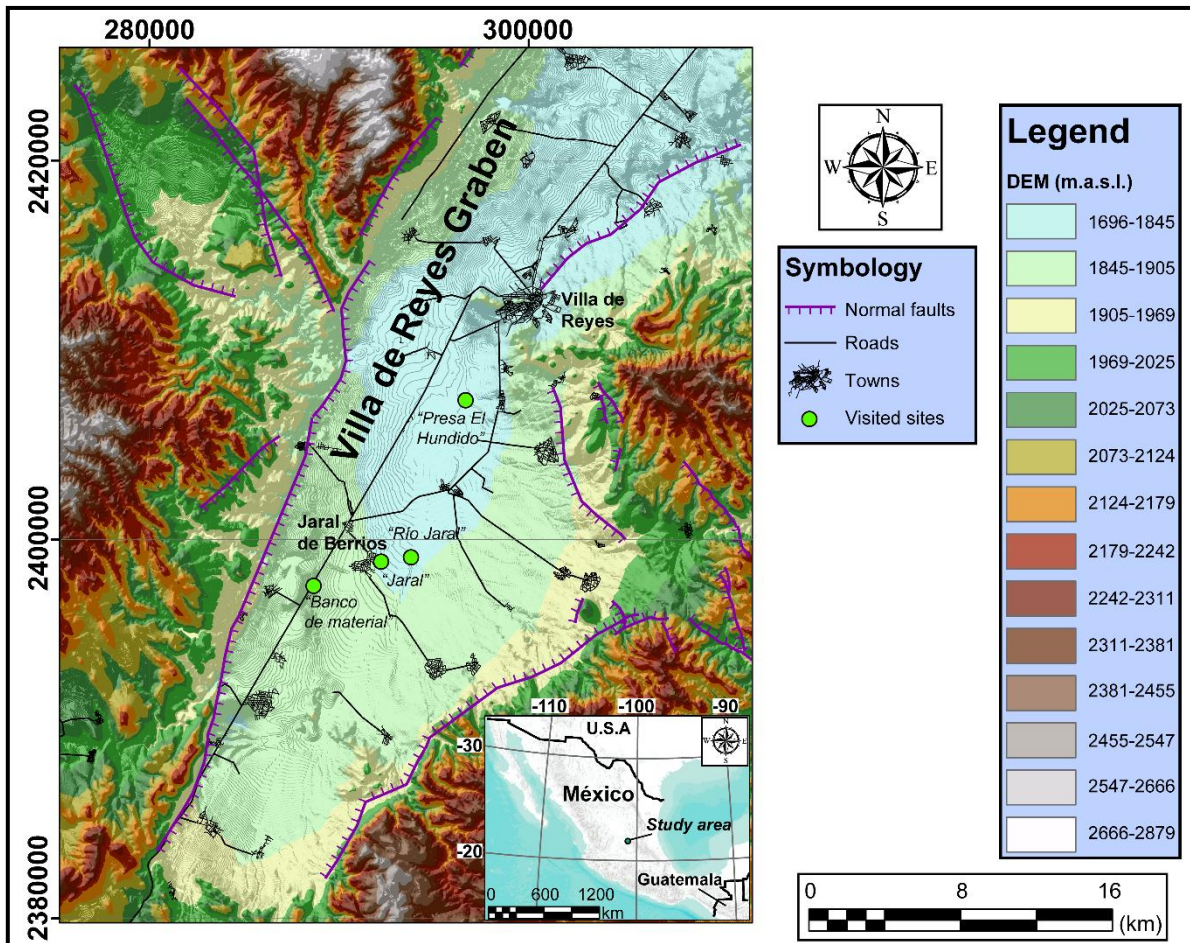


Fig. 1. Study area located in central region of Mexico (Municipalities of Villa de Reyes in the State of San Luis Potosí and Jaral de Berrios in the State of Guanajuato). Modified from Labarthe-Hernández *et al.* (1982), López-Loera & Tristán-González (2013) and Soto-García (2022), with redefinition of faulting limits Landsat 8 images, processed with ArcMap 10.8, version 10.0.0.10450, software (ESRI, 2019).

1.4 Objectives

1.4.1 General Objectives

Define, identify, and analyze the conditions in the southern sector of the Villa de Reyes Graben, which are causing fracturing and land subsidence and related phenomena, through the integration of geological methods, fault analysis, geophysics and hydrogeology.

1.4.2 Particular objectives

- Map and define the characteristics of the faults and fractures in the area.
- Locate surficial faults and further characterize them in depth using geoelectric methods.
- Establish the origin (geological, anthropogenic, or mixed) and type of faulting, integrating direct measurements with indirect ones (geophysical methods).
- Confirm the presence of transtensive and transpressive structures in the study area.
- Define the possible modification of the hydrogeological regime of the area due to faulting.
- Analyze the possible effects that the material derived from the faulting and other contaminants exert on the aquifer.

1.5 Justification

The importance of this study lies in the fact that in Mexico, where arid areas abound, faulting and/or overexploitation of aquifers produces or exacerbates fracturing and land subsidence. Thus, by establishing an integrated methodology, based on geological, geophysical, and hydrogeological data, it would help to characterize aquifers prone to these phenomena, and to know their exact causes, whether they are geological, anthropogenic, or mixed.

The results of this work will also contribute to the decision making of local farmers and landowners when choosing the best places for their activities, since the dimensions of faulted areas will be established.

1.6 Hypothesis

There are fractures in the Villa de Reyes Graben of tectonic, anthropogenic origin, or a combination of both, whose activity can modify the hydrogeological regime of the area. There are also strike-slip faults that produce geomorphological features such as positive and negative type flower structures, which also contribute to land fracturing and subsidence. Faults can be detected on the surface with geological methods and characterized in depth with geophysical methods given by the contrasts in the electrical and magnetic properties they generate.

References

- Ahmad, N., Xiaodong, L., Zhijun, G., & Abbas, A., (2020) Electrical resistivity imaging of active faults in palaeoseismology: case studies from Karachi Arc, southern Kirthar Fold Belt, Pakistan. *NRIAG Journal of Astronomy and Geophysics* 9(1), 116-128. <https://doi.org/10.1080/20909977.2020.1722524>
- Aray-Castellano, J.C., Lacan, P., Garduño-Monroy, V.H., Ávila-García, J., Gómez-Cortés, J., Audmard-M, F.A., Lázaro-Mancilla, O., & Bandy, W., (2021) Geophysical characterization of a potentially active fault in the Agua Fría micrograben, Los Azufres, México. *Boletín de la Sociedad Geológica Mexicana* 73(2), A040121. <https://doi.org/10.18268/BSGM2021v73n2a040121>
- Bauer, H., Schröckenfuchs, T. C., & Decker, K., (2016) Hydrogeological properties of fault zones in a karstified carbonate aquifer (Northern Calcareous Alps, Austria). *Hydrogeology Journal* 24(5), 1147. <https://doi.org/10.1007/s10040-016-1388-9>

- Bense, V. F., & Person, M. A., (2006) Faults as conduit-barrier systems to fluid flow in siliciclastic sedimentary aquifers. *Water Resources Research* 42(5). <https://doi.org/10.1029/2005WR004480>
- Bense, V. F., Gleeson, T., Loveless, S. E., Bour, O., & Scibek, J., (2013) Fault zone hydrogeology. *Earth-Science Reviews* 127, 171-192. <http://dx.doi.org/10.1016/j.earscirev.2013.09.008>
- Botero-Santa, P.A., Xu, S., Nieto-Samaniego, Á.F., & Alaniz-Álvarez, S.A., (2020) Efecto de las fracturas de enfriamiento en la formación de fallas normales: El ejemplo de Santa María del Río, San Luis Potosí, México. [Influence of cooling fractures on the formation of normal faults: a case study in Santa María del Río, San Luis Potosí, México]. *Boletín de la Sociedad Geológica Mexicana* 72(1). <https://doi.org/10.18268/bsgm2020v72n1a011019>
- Boubaya, D. (2017) Combining resistivity and aeromagnetic geophysical surveys for groundwater exploration in the Maghnia plain of Algeria. *Journal of Geological Research* 2017(1), 1309053. <https://doi.org/10.1155/2017/1309053>
- Bran, D.M., Tassone, A., Menichetti, M., Cerredo, M.E., Lozano, J.G., Lodolo, E., & Vilas, J.F., (2018) Shallow architecture of Fuegian Andes lineaments based on Electrical Resistivity Tomography (ERT). Evidences of transverse extensional faulting in the central Beagle Channel area. *Andean Geology* 45(1), 1-34. <http://dx.doi.org/10.5027/andgeov45n1-3002>
- Bustamante-Orozco, M. R., Medrano-Pérez, O. R., Neri-Flores, I., & Ángeles-Cordero, E. (2023) Interpretación de datos aeromagnéticos y gravimétricos satelitales para la identificación de zonas con potencial acuífero en la porción oeste de la cuenca Grijalva, México. [Interpretation of aeromagnetic and satellite gravimetric data for the identification of zones with aquifer potential on the western Grijalva basin, México]. *Boletín de la Sociedad Geológica Mexicana*, 75(1).
- Caine, J. S., Evans, J. P., & Forster, C. B., (1996) Fault zone architecture and permeability structure. *Geology* 24(11), 1025-1028. [https://doi.org/10.1130/0091-7613\(1996\)024<1025:FZAAPS>2.3.CO;2](https://doi.org/10.1130/0091-7613(1996)024<1025:FZAAPS>2.3.CO;2)

- Cauich-Kau, D.D.A., Cardona-Benavides, A., Castro-Larragoitia, G.J. & Rde, T.R., (2021) Understanding Arsenic and Uranium Sources and Mobility in Groundwater Flow Systems from Two Areas in San Luis Potosi, Mexico: Cerritos and Villa de Reyes Basins. *Lehr-und Forschungsgebiet Hydrogeologie* No. RWTH-2021-09796. <https://doi.org/10.18154/RWTH-2021-09796>.
- Cilona, A., Aydin, A., & Johnson, N. M., (2015) Permeability of a fault zone crosscutting a sequence of sandstones and shales and its influence on hydraulic head distribution in the Chatsworth Formation, California, USA. *Hydrogeology Journal* 23(2), 405. <https://doi.org/10.1007/s10040-014-1206-1>
- Cinti, F.R., Pauselli, C., Livio, F., Ercoli, M., Brunori, C.A., Ferrario, M.F., Volpe, R., Civico, R., Pantosti, D., Pinzi, S., De Martini, P.M., Ventura, G., Alfonsi, L., Gambillara, R., & Michetti, A.M., (2015) Integrating multidisciplinary, multiscale geological and geophysical data to image the Castrovillari fault (Northern Calabria, Italy). *Geophysical Journal International* 203(3), 1847–1863. <https://doi.org/10.1093/gji/ggv404>
- Del Pilar-Martnez, A., Nieto-Samaniego, A.F., Alaniz-lvarez, S.A., & ngeles-Moreno, E., (2020) Geology of the southern Mesa Central of Mexico: recording the beginning of a polymodal fault system. *Journal of Maps* 16(2), 199-211. <https://doi.org/10.1080/17445647.2020.1719911>
- ESRI, (2019) ArcMap 10.8 (Version 10.0.0.10450) [Software]
- Fronzi, D., Mirabella, F., Cardellini, C., Caliro, S., Palpacelli, S., Cambi, C., ... & Tazioli, A., (2021) The role of faults in groundwater circulation before and after seismic events: Insights from tracers, water isotopes and geochemistry. *Water* 13(11), 1499. <https://doi.org/10.3390/w13111499>
- Galone, L., Villani, F., Colica, E., Pistillo, D., Baccheschi, P., Panzera, F., Galindo-Zaldvar, J., & D'Amico, S., (2024) Integrating near-surface geophysical methods and remote sensing techniques for reconstructing fault-bounded valleys (Mellieha valley, Malta). *Tectonophysics* 875, 230263. <https://doi.org/10.1016/j.tecto.2024.230263>

- Gunda, G.K.T., Balaji, S., Champati-Ray, P.K., Bhat, G.R., Balakrishna, & Kannaujiya, S., (2020) Geophysical Characterization of the Active Fault Geometry and Trends in Tectonic Deformation in the Shallow Stratigraphy along Active Faults, South Andaman, India. *Journal of the Geological Society India* 95, 286–292. <https://doi.org/10.1007/s12594-020-1427-y>
- Hasan, M., Shang, Y., Meng, H., Shao, P., & Yi, X., (2021) Application of electrical resistivity tomography (ERT) for rock mass quality evaluation. *Scientific Reports* 11(1), 23683. <https://doi.org/10.1038/s41598-021-03217-8>
- Henry, C.D., & Aranda-Gómez, J.J., (1992) The real southern Basin and Range: Mid to late Cenozoic extension in Mexico. *Geology* 20, 701-704. [https://doi.org/10.1130/0091-7613\(1992\)020<0701:TRSBAR>2.3.CO;2](https://doi.org/10.1130/0091-7613(1992)020<0701:TRSBAR>2.3.CO;2)
- Hernández-Bocanegra, P.I., (2023) Exploración geofísica e hidrogeoquímica en el graben de Villa de Reyes, para estudiar el origen de las fallas activas y sus implicaciones en el acuífero. [Geophysical and hydrogeochemical exploration inside the Villa de Reyes Graben, to study the area's active faulting and its effects on the aquifer] [Master Dissertation] Instituto Potosino de Investigación Científica y Tecnológica (IPICYT).
- Kuang, X., Zhu, X., Ning, F., Li, W., Zheng, Q., Li, B., & Zhou, D., (2022) Aeromagnetic-imaged basement fault structure of the Eastern Tarim Basin and its tectonic implication. *Frontiers in Earth Science* 9, 825498. <https://doi.org/10.3389/feart.2021.825498>
- Kuria, Z.N., Woldai, T., Van Der Meer, F.D., & Barongo, J.O., (2010) Active fault segments as potential earthquake sources: Inferences from integrated geophysical mapping of the Magadi fault system, southern Kenya Rift. *Journal of African Earth Sciences* 57, 345-359. <https://doi.org/10.1016/j.jafrearsci.2009.11.004>
- Labarthe-Hernández, G., Tristán-González, M., & Aranda-Gómez, J.J., (1982) Revisión estratigráfica del Cenozoico de la parte central del Estado de San Luis Potosí. [Stratigraphic revision of the Cenozoic of central part of the State of San Luis Potosí]. Universidad Autónoma de San Luis Potosí, San Luis Potosí.

- López-Loera, H., & Tristán-González, M., (2013) Geología y magnetometría aérea del Graben de Villa de Reyes, San Luis Potosí, Mesa Central de México: Implicaciones tectónicas y geohidrológicas. [Geological and aeromagnetic mapping of the Villa de Reyes Graben, San Luis Potosí, Mesa Central of México: Hydrogeological and tectonic implications]. *Boletín de la Sociedad Geológica Mexicana* 65(1), 137-156. <https://doi.org/10.18268/BSGM2013v65n1a11>
- Martos, J.R., (2012) Fault Mapping with the Refraction Microtremor and seismic refraction methods along the Los Osos Fault Zone [Master Dissertation]. California Polytechnic State University.
- Meneisy, A. M., & Al Deep, M. (2021) Investigation of groundwater potential using magnetic and satellite image data at Wadi El Amal, Aswan, Egypt. *The Egyptian Journal of Remote Sensing and Space Science* 24(2), 293-309. <https://doi.org/10.1016/j.ejrs.2020.06.006>
- Monahan, S.M., (2013) Investigating Fault Structure Using Electrical Resistivity Tomography. [Bachelor of Science dissertation]. California Polytechnic State University, San Luis Obispo.
- Nabi, A., Liu, X., Gong, Z., & Ali, A., (2020) Electrical resistivity imaging of active faults in palaeoseismology: case studies from Karachi Arc, southern Kirthar Fold Belt, Pakistan. *NRIAG Journal of Astronomy and Geophysics* 9(1), 116-128. <https://doi.org/10.1080/20909977.2020.1722524>
- Nieto-Samaniego, A.F., Alaniz-Alvarez, S.A., & Camprubí, A., (2005) La Mesa Central de México: estratigrafía, estructura y evolución tectónica cenozoica. [Mesa Central of México: Stratigraphy, structure, and Cenozoic tectonic evolution]. *Boletín Sociedad Geológica Mexicana* 57(3), 285-318. <https://doi.org/10.18268/bsgm2005v57n3a3>
- Pérez-Martínez, I., Ramos-Leal, J.A., Cardona-Benavides, A., & Morán-Ramírez, J. (2021) Hydrogeochemical characterization for the identification and quantification of the flows that give rise to groundwater in a tectonic valley. *Environmental Earth Sciences* 80, 772. <https://doi.org/10.1007/s12665-021-10057-2>

- Piña-González, V., Miranda-Avilés, R., Hernández-Anguiano, J. H., Knappett, P. S., Morales-Martinez, J. L., Puy-Alquiza, M. D. J., Naves, A., Bian, J., Liu, J., Ramírez-González, L.M., Navarro-Céspedes, J.M., & Li, Y. (2022) Influence of geological faults on dissolved arsenic concentrations in an overexploited aquifer with shallow geothermal heat. *Applied Geochemistry* 144, 105395. <https://doi.org/10.1016/j.apgeochem.2022.105395>
- Porras, D., Carrasco, J., Carrasco, P., & González, P.J., (2022) Imaging extensional fault systems using deep electrical resistivity tomography: A case study of the Baza fault, Betic Cordillera, Spain. *Journal of Applied Geophysics* 202, 104673. <https://doi.org/10.1016/j.jappgeo.2022.104673>
- Ramos-Leal, J. A., López-Loera, H., Martínez Ruiz, V. J., & Aranda-Gómez, J. J. (2007) Sucesión de eventos y geometría de la parte central del acuífero del graben de Villa de Reyes (San Luis Potosí, México) inferida a partir de datos geoelectrónicos. [Event succession and geometry of the central part of the Villa de Reyes Graben aquifer]. *Revista Mexicana de Ciencias Geológicas* 24(1), 31-46.
- Sánchez-Barrientos, A.S., (2023) Aplicación de métodos geofísicos para la prospección de agua subterránea: caso Graben de Villa de Reyes, San Luis Potosí. [Application of geophysical methods for the prospection of ground water: the Villa de Reyes Graben case] [Master Dissertation] Instituto Potosino de Investigación Científica y Tecnológica (IPICYT).
- Soto-García, A.G., (2022) Análisis estructural del Graben de Santa Rosa, San Luis Potosí y Guanajuato. [Structural Analysis of the Santa Rosa Graben, San Luis Potosí and Guanajuato] [Master Dissertation] Universidad Autónoma de San Luis Potosí (UASLP).
- Sproule, T. G., Spinelli, G. A., Wilson, J. L., Fort, M. D., Mozley, P. S., & Ciarico, J., (2021) The effects of fault-zone cementation on groundwater flow at the field scale. *Groundwater* 59(3), 396-409. <https://doi.org/10.1111/gwat.13062>
- Stewart, J.H., (1998) Regional characteristics, tilt domains, and extensional history of the late Cenozoic Basin and Range province, western North America.

- Special Paper of the Geological Society of America* 47-74.
<https://doi.org/10.1130/0-8137-2323-X.47>
- Suski, B., Brocard, G., Authemayou, C., & Consenza, B., (2010) Localization and characterization of an active fault in an urbanized area in central Guatemala by means of geoelectrical imaging. *Tectonophysics* 480, 88-698.
<https://doi.org/10.1016/j.tecto.2009.09.028>
- Tristán-González, M., (1986) Estratigrafía y tectónica del graben de Villa de Reyes, en los estados de San Luis Potosí y Guanajuato, México, Folleto Técnico 107. [Stratigraphy and tectonics of the Villa de Reyes Graben, in the states of San Luis Potosí and Guanajuato, México, Technical Report number 107]. Universidad Autónoma de San Luis Potosí (UASLP), San Luis Potosí.
- Tristán-González, M., Aguillón-Robles, A., Barboza-Gudiño, J.R., Torres-Hernández, J.R., Herve, B., López-Doncel, R., Rodríguez-Ríos, R., & Labarthe-Hernández, G., (2009) Geocronología y distribución espacial del vulcanismo en el Campo Volcánico de San Luis Potosí. [Geochronology and spatial distribution of de vulcanism inside de Volcanic Field of San Luis Potosí]. *Boletín de la Sociedad Geológica Mexicana* 61 (3), 287-303.
- Wang, Z., Cai, X., Yan, J., Wang, J., Liu, Y., & Zhang, L., (2017) Using the integrated geophysical methods detecting active faults: A case study in Beijing, China. *Journal of Applied Geophysics* 156, 82-91.
<https://doi.org/10.1016/j.jappgeo.2017.01.030>

Chapter 2-. Geological and hydrogeological context

2.1 Geological and tectonic setting

The Villa de Reyes Graben (VRG) is a tectonic basin located inside a bigger tectonic province known as the Mesa Central (Fig. 2); which is an elevated plateau mostly covered by Cenozoic volcanic rocks, encompassing portions of the states of Aguascalientes, Durango, Guanajuato, Jalisco, San Luis Potosí, and Zacatecas (Nieto Samaniego *et al.*, 2005; Botero-Santa *et al.*, 2020; Cauich-Kau *et al.*, 2021). In the following section, a review of the main structural geology of our study area is presented to have a better understanding of the VRG faulting dynamics.

2.1.1 General Geology

In this section, the main geological formations of our study area will be briefly described (Fig. 3).

2.1.1.1. Cretaceous

Cretaceous marine sediments

This unit, locally named Caracol Formation, is found outcropping on in a small outcrop W of Villa de Reyes. The rocks of this unit are of marine flysch type facies, with dominant lithology of layers of ocher green sandstone with medium to coarse grains of feldspar and quartz in a calcareous matrix, some muscovite and calcite veinlets. Its thickness varies from laminations to meter long strata (Tristán-González, 1986; López-Loera & Tristán-González, 2013).

Its lower contact with the Indidura formation is concordant and transitional. It underlies the Tertiary continental clastic sediments of the Cenicera formation, Portezuelo Latite, Lower and Upper Panalillo Rhyolite, and is intruded by the Nuevo Valle Intrusive. A Coniacian to Maastrichtian age is assigned to this unit (Tristán-González, 1986).

2.1.1.2. Paleogene

Santa María Ignimbrite

The outcrops in the Villa de Reyes Graben (VRG) area are of a sporadic nature, located on the SW flank of the Sierra de San Pedro (5 km SW of Villa de Reyes), at the intersection of the VRG with that of Santa Rosa, and SE of San Bartolo de Berrios (Tristán-González, 1986).

This formation is a well-welded ash flow, pinkish gray to reddish in color, with a porphyritic and eutaxitic texture, with phenocrysts of quartz and sanidine, with abundant magnetite altered to hematite, in a partially devitrified matrix, with elongated fragments of collapsed pumice. Its thickness varies between 60-100 m (Tristán-González, 1986; López-Loera & Tristán-González, 2013).

This formation unconformably overlies the Caracol formation. It also unconformably underlies the Portezuelo Latite, Ojo Caliente Trachyte, San Miguelito Rhyolite, and the Cantera Ignimbrite. This rock package forms the basis of the volcanic sequence of the Oligocene volcanic field of San Luis Potosí (Tristán-González, 1986; Tristán-González *et al.*, 2009).

Trachyte Ojo Caliente

Its main outcrops are located on the outer edge of the graben SW of Villa de Reyes. It is a lava spill, light gray to reddish brown in color, with a holocrystalline texture, with sanidine crystals, a devitrified matrix, plagioclase and clinopyroxenes crystals altered to serpentine, iron oxides and some isolated quartz crystals. The strong jointing and flow structures cause this rock to disintegrate in the form of chips (Tristán-González, 1986).

This unit unconformably overlies the Santa María Ignimbrite, and outside the study area the Del Carmen Rhyodacite. It underlies the Portezuelo Latite and in some places the Panalillo Rhyolite, in both cases, unconformably. Emplacement took

place through large exogenous domes. Its assigned age is 31.8 ± 0.7 Ma (Tristán-González *et al.*, 2009).

Portezuelo Latite

The distribution of this rock, both inside and outside the graben, is very wide, although it is not continuous since its placement was in the form of domes. This rock is a lava spill in domes of the exogenous type and of grayish brown color, holocrystalline, porphyritic texture, aphanitic matrix with phenocrysts of sanidine, quartz, and the matrix consists of plagioclase microliths, with accessory minerals such as magnetite, zircon, and apatite (Tristán-González, 1986).

This formation unconformably overlies several Mesozoic marine formations, the Santa María Ignimbrite, and the Ojo Caliente Trachyte. It underlies the San Miguelito Rhyolite, Cantera Ignimbrite, and sporadically the two members of the Panalillo Rhyolite and the Cabras Basalt. In addition, it is intruded by the Nuevo Valle Intrusive (Tristán-González, 1986). On the other hand, according to Del Pilar-Martínez *et al.* (2020) its lower contact is not exposed. A thickness range of this unit of 208-530 m has been reported in the VRG (Soto-García, 2022).

Its age was determined with the K/Ar method, being 30.6 ± 1.5 Ma, which places it in the Early Oligocene (Labarthe-Hernández *et al.*, 1982). Del Pilar-Martínez *et al.* (2020) dates this unit with an age of 30.53 ± 0.24 Ma.

San Miguelito Rhyolite

This unit is of great extension in the study area, emplaced in the form of at least four large domes across the margins of the graben, but predominating in the NW, with NW-SE preferential orientation. Within the graben, there is only one outcrop in the vicinity of San Felipe and another where the graben is truncated by the Sierra de Guanajuato. In the wells drilled in the Valley of Villa de Reyes and San Luis Potosí, this unit has not been reported (Tristán-González, 1986; López-Loera & Tristán-González, 2013).

The rocks of this unit are made up of two generations of rhyolitic domes, separated by an ash flow, with the following three members being best appreciated in the State of Guanajuato (Tristán-González, 1986):

-Lower Member: This is the predominant one in the Sierra de San Miguelito, and has large areas of breccia, vitrophid, glass and deposits of chalcedony and opal in its central parts, its margins being a light gray lava flow with a holo to microcrystalline texture, porphyritic, with an aphanitic matrix, with disseminated sanidine, quartz, and magnetite crystals, where the matrix is devitrified with great development of flow folds. The maximum thickness observed is 30 m.

-Middle Member: It is composed of layers, variable between outcrops, of grayish porphyritic rocks and/or rocks from the previous member, glass layers, ash flows with different degrees of welding, tuffs, and at the top rocks with fluid structures (sometimes of the third member of this unit). Its thickness is very variable.

-Upper Member: This member outcrops in greater detail in the portion corresponding to the State of Guanajuato and is characterized by being topaciferous rhyolitic domes. It is a pinkish brown rock, with a holocrystalline, porphyritic texture, with phenocrysts of sanidine, quartz, and a devitrified matrix.

The San Miguelito Rhyolite overlies the Santa María Ignimbrite, Portezuelo Latite and underlies the Cantera Ignimbrite, the two members of the Panalillo Rhyolite, and the Cabras Basalt. Its age determined with the K/Ar method is 30.0 ± 1.5 Ma, places it in the Late Oligocene (Tristán-González, 1986).

Cantera Ignimbrite

Its most important outcrops are found in the Sierra de San Miguelito and Sierra Las Mesas, generally being closely associated with the domes of the San Miguelito Rhyolite. This unit is made up of a package of four pyroclastic spills that vary from well-welded to unwelded, generally separated by vitrophids and air-deposited tuffs (Tristán-González, 1986; López-Loera & Tristán-González, 2013).

The characteristics of the welded zones are commonly a pinkish gray to grayish brown rock, with phenocrysts of quartz, sanidine, and some biotite. The matrix is microcrystalline, completely to partially vitrified. Towards its base, lithics and well-collapsed pumice preferably abound, which tends to align parallel and form a eutaxitic texture. Unwelded to partially welded ash flow zones are characterized by the abundance of lithics and un-collapsed pumice into centimeter fragments. Its thickness is variable but can reach up to about 300 m (Tristán-González, 1986; López-Loera & Tristán-González, 2013).

This unit overlies the Portezuelo Latite and San Miguelito Rhyolite, all of which in a discordant fashion. It underlies the two members of the Panalillo Rhyolite. Its age is 29.0 ± 1.5 Ma, which places it in the Late Oligocene (Tristán-González, 1986; Tristán-González *et al.*, 2009; López-Loera and Tristán-González, 2013). Del Pilar-Martínez *et al.* (2020) dated two samples of this unit, obtaining ages of 30.62 ± 0.23 Ma and 30.14 ± 0.16 Ma.

Panalillo Rhyolite

This unit is found along almost the entire length of the sunken part of the VRG, and transverse grabens, and in the outer parts, sporadic outcrops of the Upper Member of this rhyolite predominate, which forms extensive plateaus in the upper parts of the hills. The Panalillo Rhyolite has been divided into two members (Labarthe-Hernández *et al.*, 1982; Tristán-González, 1986; Torres-Hernández *et al.*, 2006; Alva-Valdivia *et al.*, 2012):

-Lower Member: It is a poorly welded pyroclastic flow, cream to slightly reddish in color, well stratified, graded, in layers that vary between 5 and 50 cm from very fine to sandy grain, to conglomeratic, with an abundance of lithics, with phenocrysts of sanidine, quartz and plagioclase, with abundant pumice without collapsing. Its thickness is very variable, ranging from 40 to 150 m in wells inside the VRG (Torres-Hernández *et al.*, 2006; Alva-Valdivia *et al.*, 2012; López-Loera & Tristán-Martínez, 2013).

-Upper Member: This member consists in some places of two well-welded ash flows; The lower one is a reddish to light brown ignimbrite, with phenocrysts of quartz and sanidine, in a partially devitrified matrix, with well-collapsed pumice and isolated lithic stones. The upper flow is a pinkish-gray to reddish ignimbrite, with phenocrysts of quartz and sanidine, and some plagioclase in an almost completely devitrified matrix. Inside the VRG, this unit is buried by clastic and lacustrine deposits, and its thickness ranges from 20 to 50 m in most wells, while near the margins of the graben it does not surpass 20 m (López-Loera & Tristán-Martínez, 2013).

The volcanic event that gave rise to these rocks is bimodal, so basalts and andesites occur, where basalts are reported at the intersections of the Santa Rosa and Villa De Reyes Grabens faults. Most of the rocks of this unit are buried by great thicknesses of alluvial sediments of the order of 250 m and on lacustrine and alluvial deposits from the Cenozoic, especially in the valleys of Villa de Reyes and San Luis Potosí, while in the valleys of San Felipe and Nuevo Valle are covered only by thin layers of conglomerates (Tristán-González, 1986; Tristán-González *et al.*, 2009).

The Panalillo Rhyolite unconformably overlies the Caracol formation. It underlies the Cabras basalt and Quaternary sediments. For the Upper member, an age of 28.9 Ma has been reported (Tristán-González *et al.*, 2009).

Placa Basalt

It is a dark gray rock with phenocrysts of plagioclase and altered olivine. It is found interbedded with the Panalillo Rhyolite and has an age of 28.0 ± 0.6 to 26.9 ± 0.4 Ma. (Tristán-González *et al.*, 2009).

Santa Rosa Basalt

Named and described by Soto-García (2022), it had originally been described as “basalt” in the San Francisco geological map mentioning an intercalation between the two members of the Panalillo Rhyolite.

It consists of a dark gray to black rock with a melanocratic composition and aphanitic texture, holocrystalline and sometimes vesicular, it can present phenocrysts of up to 3 mm, sometimes they occur as subhedral plagioclase and olivine microcrystals that can be altered within a matrix devitrified in a very massive way, it may also present ferromagnesian minerals in the interstices, according to its mineralogical composition, it is interpreted as a rock with an andesitic composition. In specific areas it is found towards the base as a vitrofid with oxide alteration.

In the study area it crops out in the northern part of the Santa Rosa Graben, unconformably underlying the graben in the remnants of the upper Panalillo Rhyolite where it is delimited by the northern fault of the study area. It also overlies an isolated remnant of the lower Panalillo Rhyolite (see Fig. 3).

Cabras Basalt

Formally proposed by Labarthe *et al.* (1982), taking the name of the type locality of the community of Cabras in Villa de Reyes, S.L.P. This unit crops out in small remnants inside and outside the graben, and it is very common to find it on the marginal faults of the graben. It is a basaltic, aphanitic rock, dark brown to black in color. It presents phenocrysts of olivine, plagioclase and hypersthene (Tristán-González, 1986).

Its thickness is variable, not exceeding 150 m in the Sierra de Guanajuato where it is thickest. The Cabras Basalt unconformably overlies the Panalillo Rhyolite and conglomeratic alluvial deposits. Its age is 21.5 ± 0.5 Ma (Tristán-González, 1986; Torres-Hernández *et al.*, 2006; Tristán-González *et al.*, 2009).

Los Castillos Andesite

To the SE of the Villa de Arriaga valley, there are outcrops of a brown to dark gray rock, with a porphyritic texture with plagioclase phenocrysts in a matrix of plagioclase microliths with abundant oxidized magnetite. This rock is classified as trachyte, and

its thickness does not exceed 50 m. Its age is 20.9 to 20.3 Ma (Torres-Hernández *et al.*, 2006; Tristán-González *et al.*, 2009; López-Loera & Tristán González, 2013).

El Carmen Rhyodacite

It is a reddish brown or yellowish rock, with porphyritic texture with 15% of phenocryst up to 6 cm of plagioclase, sanidine, quartz, and iron oxides with devitrified matrix. In some sites, it is very altered, with iron oxide nodules. Its thickness in the town of El Carmen is about 550 m. It outcrops as windows in the SE shoulder of VRG (Labarthe-Hernández *et al.* 1982; Cauch-Kau *et al.*, 2021).

El Quiote Tuff

In the south-eastern portion of the VRG, SE of Villa de Reyes there are windows of a pyroclastic flow, unwelded at its base and welded at its top. The rock is white to pink in color, with 15% phenocrysts of quartz and sanidine, with abundant pumice and lithics. Its thickness at Cerro del Quiote is about 50 m (Labarthe-Hernández *et al.*, 1982).

2.1.1.3. Quaternary

Conglomerate

At different locations of our study area there are sedimentary deposits, corresponding to oligomictic and polymictic conglomerates with fragments of the rocks that outcrop in the area, with clasts and blocks > 10 cm of subrounded to angular shapes, with a structure of supported clasts and sometimes embedded in an ash matrix, derived from materials remobilized from the Santa María Ignimbrite. These deposits are found filling depressions throughout the area. In specific places, it appears as polymictic relicts overlying very fine materials that were remobilized from the same unit (Soto-García, 2022).

Quaternary Sediments

The Plio-Quaternary package in the Valleys of Villa de Reyes and San Luis Potosí, accumulated within the graben, reaches thicknesses of 400 m, and consists of gravel, sand, and silt. Lacustrine deposits are also found in the southern part of the study area. (Tristán-González, 1986; Torres-Hernández, 2009; Cauch-Kau *et al.*, 2021).

2.1.2. Structural geology studies in the region

Tristán-González (1986) described the following structural events:

1. During crustal breaking processes, normal faults originated because of the warping effects of the upper mantle. These faults are mainly located in marine sediments and have generated many intermontane valleys with a preferential N and NW orientation, which are mainly preserved northward and northeastward, with little to no associated vulcanism. These faults in the Graben area are buried by a thick volcanic cover and, around 32 Ma, were the main conduits through which the first magmas ascended.
2. With the spill of the Latita Portezuelo lavas, the beginning of the collapse of the graben started and, concurrently with the subsidence of the valley, the exit of the different volcanic formations of the area, culminating with the Cantera Ignimbrite. This process took place between 39 and 32 Ma. A system of parallel marginal faults of the graben underwent a change in direction, from N-NW to NE, which suggests a control of the VRG due to the proximity of the interdigitation of the Mesozoic Basin of Central Mexico with the Valles-San Luis Potosí Platform. These faults are mainly high angles (60° to 75°), which are more clearly seen where volcanic units outcrop, given rise to large fault scarps.

The other fault system of importance has an almost perpendicular behavior (NW) to the graben fault system (NE), giving rise to a series of grabens and horsts limited by high angle faults (60° - 70°), and represents the graben extension system.

3. After the development of the previously described structures, the eruption of the Panalillo Rhyolite took place, with more violence towards the south, filling a large part of the graben and transverse valleys near the area. This marks the end of faulting within the grabens. Net block displacement is hard to measure with precision since most of the graben is filled with alluvial and volcanoclastic deposits. Nonetheless, based on three 600 m deep exploration wells in the VRG, Tristán-González (1986) was able to calculate between 450-500 m in our study area.

Henry and Aranda-Gómez (1992) established the beginning of east-northeast extension as early as 30 Ma, in areas north of the Trans-Mexican volcanic belt. The best-known episodes of extension in México, which begun between 23 and 12 Ma, seem to be part of regionally extensive episodes in the central Basin and Range province (whose Mexican part constitutes about half the area of said province). In the Guanajuato-San Luis Potosí area (Fig. 2) grabens strike NW and NE, with K-Ar ages of host rocks and vein adularia indicate that faulting began between 32 and 28 Ma. Intraplate alkali basalts, which erupted between 11-14 Ma and in the Quaternary, near San Luis Potosí suggest episodes of extension at these times. A graben with NE strike terminates against de Bajío fault north of Guanajuato, suggests that NW extension is younger than NE extension. Conversely, several small NW striking grabens terminate against NE oriented faults south of San Luis Potosí. All of this suggests that the VRG main extension phase is contemporaneous with the southern extension of the Basin and Range province (Henry and Aranda-Gómez, 1992; Stewart, 1998).

Nieto-Samaniego *et al.* (2005) defined the Mesa Central (Fig. 2) as an elevated plateau located in the central part of México, with more than half of its total area found above 2000 m.a.s.l., with topographic highs within are less than 600 m. The Mesa Central plateau is bounded to the N and E by the Sierra Madre Oriental, W by the Sierra Madre Occidental, and to the S by the El Bajío Basin. The study area is located south of a major fault system called the San Luis-Tepehuanes Fault System (Fig. 2), a NW-SE striking lineament, which roughly separates the northern and

southern regions of the Mesa Central. The northern sector is in a more advanced state of erosion (with topographic heights of less than 2000 m.a.s.l.) and shows almost no evidence of Neogene tectonics, while the southern sector is where major extensional tectonics events took place during the Oligocene, with minor events in the Miocene to Quaternary as well. In the southern region of Mesa Central, detailed studies have revealed that there was also Oligocene volcanism coeval with extensional crustal deformation, with principal extensions of around 20% in the E-W direction and 10% in the N-S direction. As can be seen on Fig. 2, this southern section of the Mesa Central is where most seismic recent seismic activity has concentrated, which is especially true for the western part the study area (Fig. 2). This recent seismic activity (from 1993 to 2024, SSN (2024)) makes it evident that extensional tectonics and active faulting are still taking place to this day inside the VRG.

Del Pilar-Martínez *et al.* (2020) detailed the stratigraphy, complementing with thirteen new U-Pb ages (which before this study were lacking in previous works) of the southern Mesa Central, to establish when the deformation of the Cenozoic volcanic rocks began. They were able to establish four lithostratigraphic groups affected by major fault activity:

- 1) Early Rupelian volcanic rocks (34.4 to 30.4 Ma), are mostly felsic in composition, and subordinate andesitic-dacitic lavas, associated with NW trending domino style normal faults.
- 2) Middle Rupelian volcanic rocks (30 Ma), dominated by effusive volcanism of felsic composition, predate the beginning of the polymodal normal fault system.
- 3) Late Rupelian rocks (28 Ma) of a thick succession of rhyolitic ignimbrites, that correspond to the zenith of the polymodal faulting, when all the fault systems were still active.
- 4) Chattian rocks (23 Ma), which are separated from the Rupelian rocks by a hiatus of about 4.2 million years. This episode was associated with a minor

faulting phase. The last faulting phase occurred in the Miocene, and it was coeval with reactivation of the VRG and the El Bajío Fault.

These authors also date the main phase of activity of the VRG, coevally with the volcanism between 28 and 27 Ma, and show that the extensional system of the VRG formed on top of a previous domino-like fault domain boundaries of the early Rupelian systems.

To date, studies focusing on the active tectonics inside the VRG have not been made, with only anecdotal evidence of transtensional and transpressional stresses, generated by left lateral faults and right lateral faults, with associated positive and negative flower structures. The active faulting inside the southern portion of the VRG will be the focus of this work.

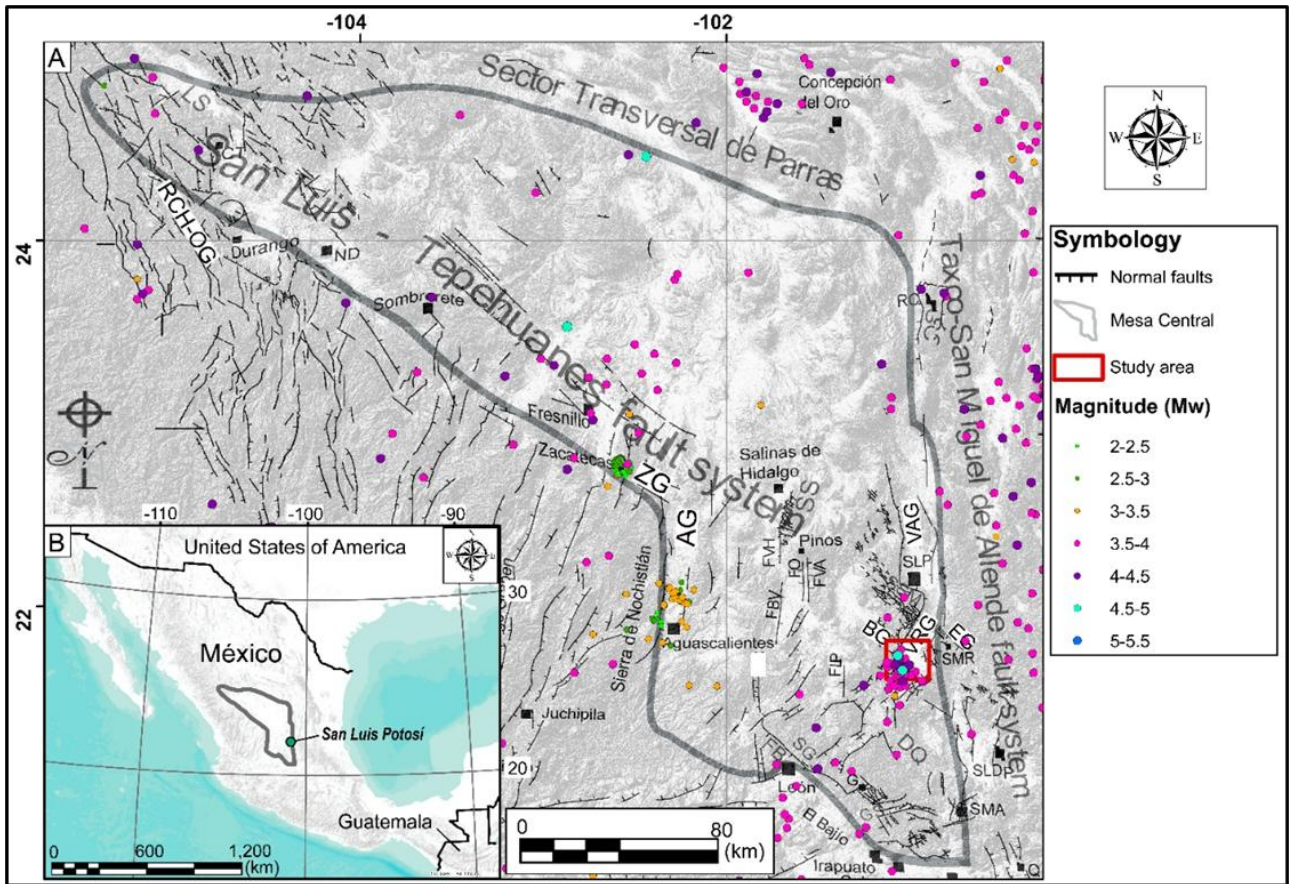


Fig. 2. Tectonic context of the study area: (a) Location of the study area. LS—Laguna de Santiaguillo; RCH-OG—Río Chico-Otinapa Graben; AG—Aguascalientes Graben; FVH—Fault Villa Hidalgo; FBV—Fault Buena Vista; FO—Fault El Obraje; FVA—Fault Villa de Arriaga; FLP—Fault Los Pájaros; CG—El Cuarenta Graben; FB—Fault El Bajío; GS—La Saucedá Graben; BG—Bledos Graben; VRG—Villa de Reyes Graben; VAG—Villa de Arista Graben; EG—Enramadas Graben; DQ—La Quemada Depression; SSM—Sierra de San Miguelito; SG—Sierra de Guanajuato; SC—Sierra de Catorce; SS—Sierra de Salinas; RC—Real de Catorce; G—Guanajuato; SLP—San Luis Potosí; SMR—Santa María del Río; SLDP—San Luis de La Paz; ND—Nombre de Dios; SMA—San Miguel de Allende; Q—Querétaro. ZG—Zacatecas Graben. Taken and modified after Nieto Samaniego *et al.* (2005). Epicenter data taken from SSN (2024). Topographic data after INEGI (2023); (b) Mesa Central Tectonic Province location in Central México.

2.2 General Hydrogeology

The main aquifer that encompasses the study area is defined as the Jaral de Berrios-Villa de Reyes aquifer, labeled by Comisión Nacional del Agua, CONAGUA (National Water Commission) with the code 2412. This aquifer is located in central Mexico, covering northern Guanajuato, corresponding to the Jaral de Berrios Valley, and southeast San Luis Potosí, corresponding to the Villa de Reyes Graben (VRG), with a total area of 2370 km² (CONAGUA, 2023).

2.2.1 Hydrography

The study area is located within Hydrological Region 26 (Pánuco) and in the southwestern portion of the Tamún river basin. The main streams which drain the area are the San Bartolo River (Guanajuato area) and the Altamira River, later named the Santa María River (San Luis Potosí area), both with an intermittent regimen. In the Guanajuato portion, the main hydrographic axis is formed by the San Bartolo River, while in the San Luis Potosí portion the Altamira River represents the main hydrographic system. The Santa Ana dam represents the main source of water in this area for the population (CONAGUA, 2023).

2.2.2 Aquifer type

Based on the petrophysical properties of the rocks that are part of the stratigraphy of the study area, CONAGUA (2023) differentiates two lithological sequences according to their porosity: primary (intergranular) or secondary (by fracturing). Hence, for most of the volcanic sequence, water movement takes place through fractures, except for sandy tuffs who present both types of porosity. On the other hand, sedimentary materials of fluvial facies present textural properties that allow to assume that water circulation is manifested through a porous media.

According to the aquifer constitution, it can be described vertically in two parts: the upper part located in the left bank of the Altamira River is a hanging aquifer,

unconfined and embedded in in the alluvial fill of the graben, with a saturated thickness between 5 to 25 m. Since the static level is found to be between 0.5 and 6 m deep, water extraction is done with dug wells and by manual traction for domestic uses and, to a lesser extent, mechanically for irrigation of small plots for self-consumption. The lower part of the aquifer is constituted by alluvial, lacustrine, pyroclastic deposits as well as fractured volcanic rocks withing the graben. Thickness varies between 200 and 450 m, and piezometric levels are found between 40 to 120 m (Cauich-Kau *et al.*, 2021; CONAGUA, 2023).

2.2.3 Piezometric levels

According to Carillo-Rivera *et al.* (1992), the water table levels for shallow groundwaters in Villa de Reyes valley closely follow local topography, which indicates a general flow pattern towards the axis of the valley and north-eastward along the direction of surface drainage. On the other hand, for deep groundwaters, the piezometric surface has been substantially modified by water extraction over the past decades. Nevertheless, a similar flow direction which is influenced by topography is apparent.

Similarly, according to Cauich-Kau *et al.* (2021), groundwater flow presents a direction from the recharge areas (mountain ranges) towards the central part of the valley, however to the northeast of Villa de Reyes groundwater flow takes a northeast direction, probably related to zones with high exploitation. We report similar results to the latter author, using piezometric data from the Comisión Estatal de Agua de Guanajuato (Guanajuato State Water Commission) CEAG (2021), with the difference that in this study piezometric level map (Fig. 3) water depletion zones are more evident near the most populated communities (Jaral de Berrios and Villa de Reyes), which is to be expected. In this work, a connection between groundwater and fault zones is established, as will be discussed in Chapter 5.

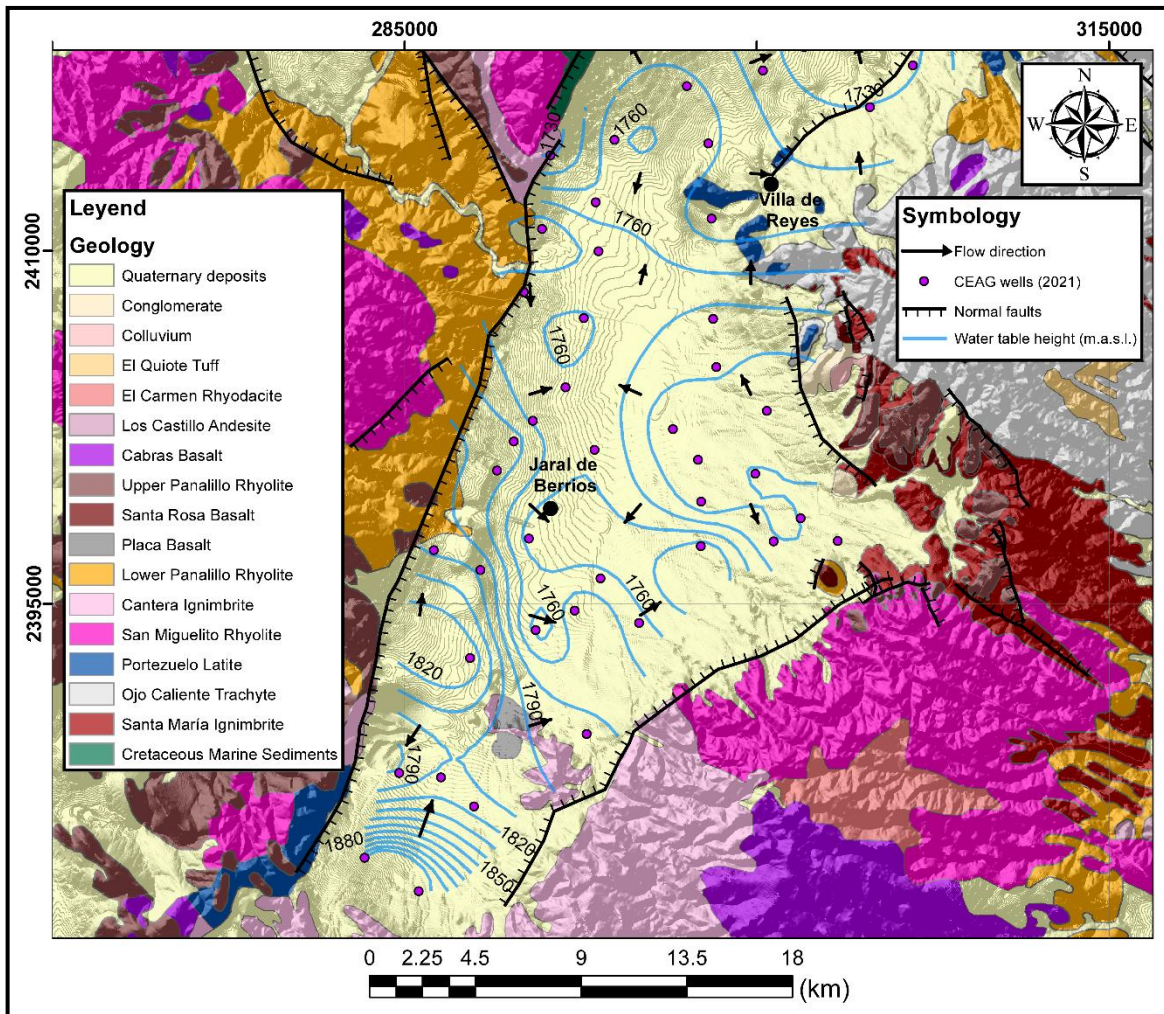


Fig. 3. Geology and piezometric levels for the southern portion of the Villa de Reyes Graben. Geology and faults after López-Loera & Tristán-González (2013) and Soto-García (2022), with modifications and redefinition of faulting limits and geological contacts using Landsat 8 images, processed using ArcMap 10.8, version 10.0.0.10450 (ESRI,2019). Piezometric levels after (CEAG, 2021), processed using Surfer 16 (Golden Software, 2019).

References

- Alva-Valdivia, L.M., Torres-Hernández, J.R., González-Rangel, J.A., Caballero-Miranda, C.I., Rosas-Elguera, J.G., & Villalobos-Romero, N., (2012) Paleomagnetismo en la determinación de la temperatura de emplazamiento

- de la ignimbrita Panalillo, Juachín, San Luis Potosí, México [Paleomagnetism in determining emplacement temperature of the Panalillo Ignimbrite, Juachín, San Luis Potosí, México]. *Revista Mexicana de las Ciencias Geológicas* 29(3),619-638.
- Botero-Santa, P.A., Xu, S., Nieto-Samaniego, Á.F., & Alaniz-Álvarez, S.A., (2020) Efecto de las fracturas de enfriamiento en la formación de fallas normales: El ejemplo de Santa María del Río, San Luis Potosí, México. [Influence of cooling fractures on the formation of normal faults: a case study in Santa María del Río, San Luis Potosí, México]. *Boletín de la Sociedad Geológica Mexicana* 72(1). <https://doi.org/10.18268/bsgm2020v72n1a011019>
- Carrillo-Rivera, J.J., Clark, I.D., & Fritz, P., (1992) Investigating Recharge Of Shallow And Paleo-Groundwaters In The Villa De Reyes Basin, SLP, Mexico, With Environmental Isotopes. *Applied Hydrogeology* 1(4), 35–48.
- Cauich-Kau, D.D.A., Cardona-Benavides, A., Castro-Larragoitia, G.J. & Rúde, T.R., (2021) Understanding Arsenic and Uranium Sources and Mobility in Groundwater Flow Systems from Two Areas in San Luis Potosi, Mexico: Cerritos and Villa de Reyes Basins. *Lehr-und Forschungsgebiet Hydrogeologie* No. RWTH-2021-09796. <https://doi.org/10.18154/RWTH-2021-09796>.
- Comisión Estatal de Agua de Guanajuato (CEAG) (2021). Historia de Piezometría 2015-2021, acuífero Jaral de Berrios-Villa de Reyes (Piezometric levels history 2015-2021, Jaral de Berrios-Villa de Reyes aquifer) [Data set].
- Comisión Nacional del Agua (CONAGUA) (2023) Actualización de la disponibilidad media anual de agua en el acuífero Jaral de Berrios-Villa de Reyes (2412), Estado de San Luis Potosí. Ciudad de México. (Update of the average annual water availability in the Jaral de Berrios-Villa de Reyes aquifer (2412), State of San Luis Potosi. Mexico City).
- Del Pilar-Martínez, A., Nieto-Samaniego, A.F., Alaniz-Álvarez, S.A., & Ángeles-Moreno, E., (2020) Geology of the southern Mesa Central of Mexico:

- recording the beginning of a polymodal fault system. *Journal of Maps* 16(2), 199-211. <https://doi.org/10.1080/17445647.2020.1719911>
- ESRI, (2019) ArcMap 10.8 (Version 10.0.0.10450) [Software]
- Golden Software, (2019) Surfer 16 (Version 16.3.408) [Software]
- Hasan, M., Shang, Y., Meng, H., Shao, P., & Yi, X., (2021) Application of electrical resistivity tomography (ERT) for rock mass quality evaluation. *Scientific Reports* 11(1), 23683. <https://doi.org/10.1038/s41598-021-03217-8>
- Henry, C.D., & Aranda-Gómez, J.J., (1992) The real southern Basin and Range: Mid to late Cenozoic extension in Mexico. *Geology* 20, 701-704. [https://doi.org/10.1130/0091-7613\(1992\)020<0701:TRSBAR>2.3.CO;2](https://doi.org/10.1130/0091-7613(1992)020<0701:TRSBAR>2.3.CO;2)
- Instituto Nacional de Estadística y Geografía (INEGI), (2023) Continuo de Elevaciones Mexicano. <https://www.inegi.org.mx/app/geo2/elevacionesmex/> (accessed 10 April 2023).
- Labarthe-Hernández, G., Tristán-González, M., & Aranda-Gómez, J.J., (1982) Revisión estratigráfica del Cenozoico de la parte central del Estado de San Luis Potosí. [Stratigraphic revision of the Cenozoic of central part of the State of San Luis Potosí]. Universidad Autónoma de San Luis Potosí, San Luis Potosí.
- López-Loera, H., & Tristán-González, M., (2013) Geología y magnetometría aérea del Graben de Villa de Reyes, San Luis Potosí, Mesa Central de México: Implicaciones tectónicas y geohidrológicas. [Geological and aeromagnetic mapping of the Villa de Reyes Graben, San Luis Potosí, Mesa Central of México: Hydrogeological and tectonic implications]. *Boletín de la Sociedad Geológica Mexicana* 65(1), 137-156. <https://doi.org/10.18268/BSGM2013v65n1a11>
- Nieto-Samaniego, A.F., Alaniz-Alvarez, S.A., & Camprubí, A., (2005) La Mesa Central de México: estratigrafía, estructura y evolución tectónica cenozoica. [Mesa Central of México: Stratigraphy, structure, and Cenozoic tectonic evolution]. *Boletín Sociedad Geológica Mexicana* 57(3), 285-318. <https://doi.org/10.18268/bsgm2005v57n3a3>

- Servicio Sismológico Nacional (SSN), (2024) Earthquake Catalog. National Seismological Survey website. <http://www2.ssn.unam.mx:8080/catalogo/> (accessed 22 March 2024).
- Soto-García, A.G., (2022) Análisis estructural del Graben de Santa Rosa, San Luis Potosí y Guanajuato. [Structural Analysis of the Santa Rosa Graben, San Luis Potosí and Guanajuato] [Master Dissertation] Universidad Autónoma de San Luis Potosí (UASLP).
- Stewart, J.H., (1998) Regional characteristics, tilt domains, and extensional history of the late Cenozoic Basin and Range province, western North America. *Special Paper of the Geological Society of America* 47-74. <https://doi.org/10.1130/0-8137-2323-X.47>
- Torres-Hernández, J.R., Labarthe-Hernández, G., Aguillón-Robles, A., Gómez-Anguiano, M., & Mata-Segura, J.L., (2006) The pyroclastic dikes of the Tertiary San Luis Potosí volcanic field: Implications on the emplacement of Panalillo ignimbrite. *Geofísica Internacional* 45(4), 243-253.
- Torres-Hernández, J.R., (2009) Origen y emplazamiento de las ignimbritas Cantera y Panalillo del campo volcánico de San Luis Potosí. [Emplacement and origin of the Cantera and Panalillo ignimbrites in the Volcanic Field of San Luis Potosí] [Doctoral Dissertation] Universidad Nacional Autónoma de México (UNAM).
- Tristán-González, M., (1986) Estratigrafía y tectónica del graben de Villa de Reyes, en los estados de San Luis Potosí y Guanajuato, México, Folleto Técnico 107. [Stratigraphy and tectonics of the Villa de Reyes Graben, in the states of San Luis Potosí and Guanajuato, México, Technical Report number 107]. Universidad Autónoma de San Luis Potosí (UASLP), San Luis Potosí.
- Tristán-González, M., Aguillón-Robles, A., Barboza-Gudiño, J.R., Torres-Hernández, J.R., Herve, B., López-Doncel, R., Rodríguez-Ríos, R., & Labarthe-Hernández, G., (2009) Geocronología y distribución espacial del vulcanismo en el Campo Volcánico de San Luis Potosí. [Geochronology and spatial distribution of de vulcanism inside de Volcanic Field of San Luis Potosí]. *Boletín de la Sociedad Geológica Mexicana* 61 (3), 287-303.

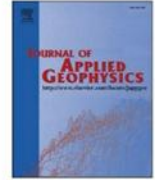
Chapter 3-. Geoelectrical characterization of non-filled active faults in Jaral de Berrios, Guanajuato, México

This chapter is based on an article where geoelectrical methods were tested to observe their response on non-filled active faults and fractures, by authors: M.Sc. Fabián Esteban Monge-Cerda, Dr. Omar Delgado-Rodríguez, Dr. José Alfredo Ramos-Leal and Dr. Lorena Elisa Sánchez-Higueredo. It was published by the **Journal of Applied Geophysics** in 2024.



Contents lists available at ScienceDirect

Journal of Applied Geophysics

journal homepage: www.elsevier.com/locate/jappgeo

Geoelectrical characterization of non-filled active faults in Jaral de Berrios, Guanajuato, México

Fabián Esteban Monge-Cerda, Omar Delgado-Rodríguez*, José Alfredo Ramos-Leal, Lorena Elisa Sánchez-Higueredo

División de Geociencias Aplicadas, Instituto Potosino de Investigación Científica y Tecnológica A.C. (IPICYT), San Luis Potosí 78216, Mexico

ARTICLE INFO

Keywords:

Non-filled fractures
Electrical resistivity tomography
Electromagnetic profiling
Resistive lineament
Active fault

ABSTRACT

Electromagnetic and electrical methods have a great number of applications and have become a commonly used tool for the study of active geological faults, where they are usually detected as low resistivity anomalies. However, this is not always the case. We used both Electromagnetic Profiling (EMP) and Electrical Resistivity Tomography (ERT) methods with the aim of mapping active geological faults which affect agricultural plots and a former quarry near the town of Jaral de Berrios, State of Guanajuato. The apparent resistivity map derived from EMP survey shows how NW-SE on site measured faults (which reach at least 400 m in length and 0.4 m in width) match with high apparent resistivity anomalies. Two ERT profiles reveal the subsurface continuity of the main fault zones, as well as the main high apparent resistivity lineaments, for at least 40 m below the surface. The resistive lineaments in the apparent resistivity map showed a coincidence with the faults modeled in the geoelectric section of the ERT1 profile; this result gives reliability to the methodology used in the study site. All of this means that faulting presently evident on the surface continues at depth and has a wider extension than previously thought, and that since the fractures are non-filled with minerals and/or moisture the preponderance of high resistivity anomalies make sense. The results of this work provide the basis for future studies that help in determining the type of faulting affecting our study area, so long term urban planning and development in the area may be possible.

1. Introduction

Three important geophysical applications in the study of active faults include: 1) Areas where erosion or anthropogenic activity had effectively erased surface expression of active faults; 2) faulting is covered by a thick cover of Quaternary deposits; or 3) where there is no budget available for more expensive survey techniques that make confirmation of a fault zone possible (e.g., fault trench studies or radiometric dating).

Geoelectric methods are increasingly used in near surface geophysics such as mining (Mendoza et al., 2021; Mustafa et al., 2023), hydrogeological exploration (Rolia and Sutjiningsih, 2018; Mollehuar-Canales et al., 2020; Alzahrani et al., 2022), agricultural studies (Doser et al., 2019; Cordero-Vázquez et al., 2021, 2023), environmental studies (Delgado-Rodríguez, 2017; Gómez-Hernández et al., 2020), and geotechnical studies (Aizebeokhai and Oyeyemi, 2015; Martínez et al., 2021).

Surface geophysical methods in the study of geological faults have been used successfully for several decades (Cinti et al., 2015; Wang et al., 2018; Gunda et al., 2020; Aray-Castellano et al., 2021). Specifically, geoelectrical methods usually detect highly fractured and weathered fault zones as low resistivity anomalies, in contrast to unaltered fault wall rocks (Monahan, 2013; Bran et al., 2018; Ahmad et al., 2020; Meng et al., 2020; Hasan et al., 2021; Sana et al., 2021; Porras et al., 2022). For example, the Electromagnetic Profiling (EMP) method was applied on the active Conclud fault in the Iberian Cordillera (NE Spain), where it showed the advantages of this fast-forward method for mapping fault planes. A conductive anomaly with a contrast of >25 mS/m marked the fault plane zone up to 20–25 m deep (Pueyo-Anchuela et al., 2016). Drahor and Berge (2017) used electric and electromagnetic methods in conjunction with seismic and magnetometric techniques, in a fault zone located in the southwestern part of the city of İzmir, Western Anatolia, Turkey. After the integrated interpretations of the geophysical surveys, it was possible to locate the fault core and some evidence of

* Corresponding author.

E-mail address: omar.delgado@ipicyt.edu.mx (O. Delgado-Rodríguez).

<https://doi.org/10.1016/j.jappgeo.2024.105431>

Received 26 July 2023; Received in revised form 5 June 2024; Accepted 14 June 2024

Available online 15 June 2024

0926-9851/© 2024 Published by Elsevier B.V.

active faulting in the investigated area. Bran et al. (2018) carried out a geoelectric study to investigate the shallow architecture of the Beagle Channel, located in the foothills of the Fuegian Andes, in the Chile-Argentina border. Resistivity patterns were established that allowed inferring an extensional control over the oblique depressions due to postglacial deformations along the area. Khalili and Mirzakerdeh (2019) used microtremor and geoelectrical methods to detect subsurface geological structures (hidden faults) in a suburb of Shiraz, Iran. The authors modeled the fault zone as a transition zone from high to low resistivity values. The VES method with Schlumberger configuration was used by Winarto et al. (2019) to identify the geologic subsurface and active fault zone in an area of the Garut regency, southern West Java, where they collected geoelectric data from seven profile lines. In general, two resistive strata were found (resistivity >50 Ohm.m), which are separated by a conductive layer (resistivity < 15 Ohm.m), interpreted as a fault. Arjwech et al. (2020) used 2D and 3D Electrical Resistivity Tomography (ERT) to study an active fault in Thailand. Their geoelectrical models showed a resistive sandstone unit and a conductive sandy-clay sediment unit. The two units are separated by a transition zone of approximately 12 m wide, being defined as the fault core.

The studies mentioned above have in common that faults were observed to be conductors or a transition zone between high and low resistivity. However, Nobes and Hornblow (2021) clarify that the electrical properties near the surface of faults can change depending on the nature of the materials that fill the faults and the type of climate. A prolonged period of dry weather can dry out (i.e. leave fractures "empty") the near-surface sections of faults, thereby increasing the electrical resistivity. Conversely, a prolonged period of rain increases the moisture content of the porous material filling the faults, thus decreasing the resistivity. In the case of unfilled faults, a resistive response would be expected, however, there is a lack of geoelectrical studies demonstrating their effectiveness in detecting and characterizing active unfilled faults. Since these types of faults are (at least in similar studies like the mentioned above) uncommon, we considered an important experiment

applying conventional geophysical methods in unfilled active faults to observe their response and the types of models that can be achieved.

In this study, EMP and ERT methods were used primarily to map the active non-filled fault planes which affect plots in the municipality of Jaral de Berrios, State of Guanajuato.

1.1. Study area

The study site is in the State of Guanajuato inside the bigger tectonic setting of the Villa de Reyes Graben (VRG), an approximately 100 km long valley filled with alluvial sediments, pyroclastic flows, and lacustrine deposits, which ranges in thickness from 50 to about 250 m, with a northward dip. The type of climate of the region is semiarid and it is located inside the physiographic province known as the Mesa Central (Diario Oficial de la Federación (DOF), 2015), which the latter will be further discussed in Section 2. Most of the VRG borders are very steep, since they are controlled by normal faulting (Fig. 1), which is the most common type of faulting that exists in the region (Tristán-González, 1986). The study area comprises approximately 25 ha of agricultural plots, including a former quarry. The site is located next to Federal Highway 37 and approximately 2.5 km from the town of Jaral de Berrios (Fig. 2).

The economy is based on primary activities (rainfed agriculture), with beans and corn as seasonal crops (Diario Oficial de la Federación (DOF), 2015). This semiarid region is limiting water not only to climate conditions but also due to the increase in the number and length of fractures on the soil surface. These fractures facilitate the fast infiltration of irrigation water and the loss of agricultural soil, thus reducing arable areas.

2. Geological and tectonic setting

The VRG is located inside a bigger tectonic province known as the Mesa Central, which is an elevated plateau mostly covered by Cenozoic

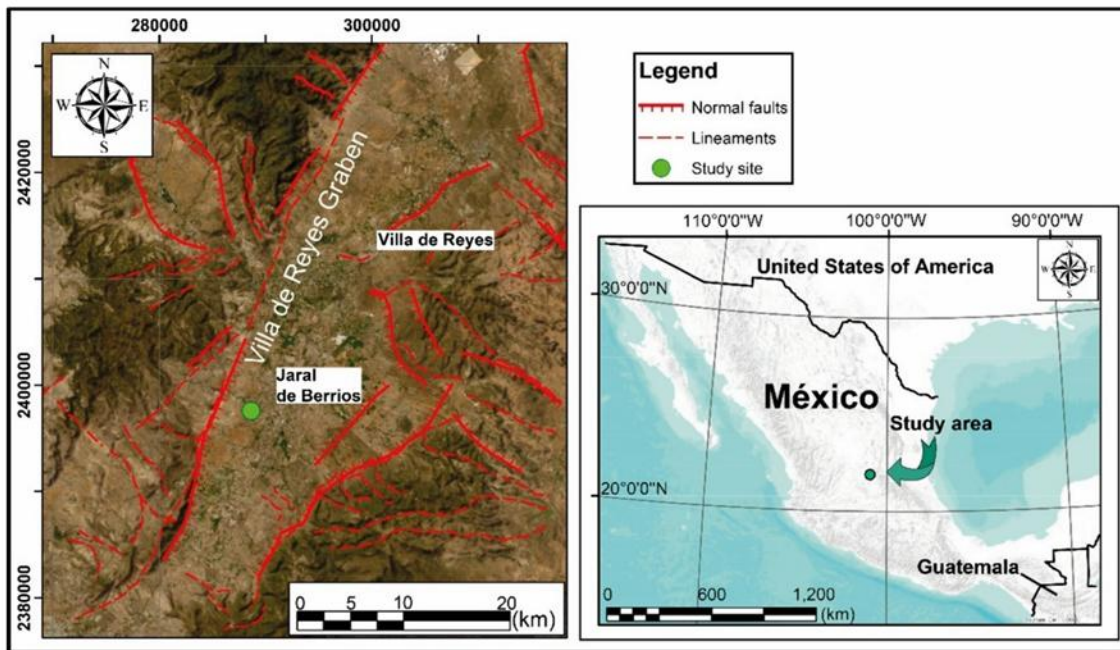


Fig. 1. Study area located in central region of Mexico (Municipalities of Villa de Reyes in the State of San Luis Potosí and Jaral de Berrios in the State of Guanajuato). Modified from López-Loera and Tristán-González (2013) and redefinition of faulting limits and lineaments using Landsat 8 images, processed with ArcMap 10.8, version 10.0.0.10450, software (ESRI, 2019).

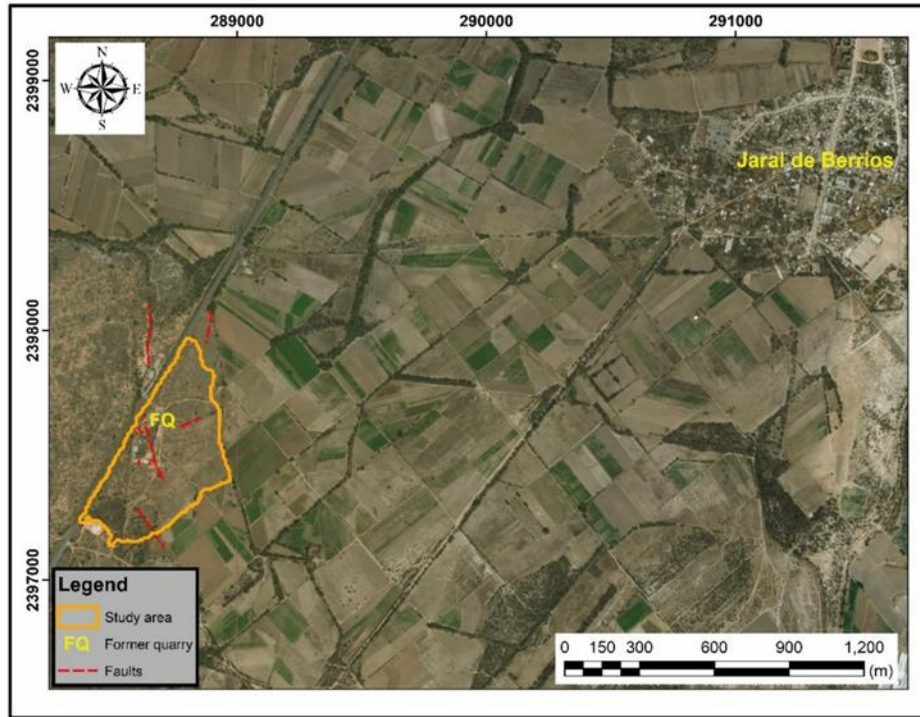


Fig. 2. Study site location. Red discontinuous lines represent the faults mapped in this work. (For interpretation of the references to colour in this figure legend, the reader is referred to the web version of this article.)

volcanic rocks and bordered by the Sierra Madre Oriental at the north and east, the Sierra Madre Occidental at the west, and in the south by the Trans Mexican Volcanic Belt, encompassing portions of the states of Aguascalientes, Durango, Guanajuato, Jalisco, San Luis Potosí, and Zacatecas (Nieto-Samaniego et al., 2007; Botero-Santa et al., 2020; Cauich-Kau et al., 2021).

The VRG formation started in the main extension phase of the Mesa Central (26–28 Ma, mostly Chattian in age), which is also part of the Cuencas y Sierras Province of the Mexican Republic, i.e., the southern extension of the Basin and Range Province (Labarthe-Hernández et al., 1982; Tristán-González, 1986; Henry and Aranda-Gómez, 1992; Stewart, 1998; López-Loera and Tristán-González, 2013; Del Pilar-Martínez et al., 2020). Faulting in this area was polymodal, a fault system compound of three or more fault sets forming and slipping simultaneously, normally under triaxial deformation fields. The extensional system of the VRG formed on top of a previous domino-like fault domain boundaries, which were formed in the Rupelian under a biaxial stress field (Del Pilar-Martínez et al., 2020).

The study area mostly includes rocks corresponding to the Volcanic Field of San Luis Potosí (VFSLP) and the Volcanic Field of Santa María del Río (VFMR), whose composition varies from dacites to rhyolites, and mostly of effusive origin. The main geological formations (Fig. 3) are: San Miguelito Rhyolite (late Oligocene); Cantera Ignimbrite (late Oligocene); Lower and Upper Panalillo Rhyolites (both from late Oligocene); Placa Basalt (late Oligocene), and finally the entire volcanic sequence is topped by up to 400 m of Quaternary deposits, mainly composed of alluvial and lacustrine deposits (Tristán-González, 1986; Tristán-González et al., 2009; López-Loera and Tristán-González, 2013; Cauich-Kau et al., 2021).

3. Methodology

3.1. Geoelectrical methods

To analyze the subsurface continuity of faults and fractures, we used the Electromagnetic Profiling (EMP) method to quickly and accurately define resistivity lineaments associated with the subsurface location of faults. The Electrical Resistivity Tomography (ERT) method was used to characterize the faults. Its basic operating principles are briefly described below.

3.1.1. EMP survey

To perform the EMP survey, we used the CMD MiniExplorer 6 L conductivity meter, in which both the transmitter (Tx) and receiver (Rx) coils are inside a cylindrical device, which is hand-carried along the profile (see Fig. 4). Data acquisition and georeferencing can be programmed automatically, which makes the EMP survey faster and easier. Considering walking at an average speed of 4 km/h, an acquisition of conductivity measurement every 2 s was programmed, thus an apparent electrical conductivity value was recorded approximately every 1 m along each path. For the CMD MiniExplorer 6 L, maximum survey depths of 0.3, 0.5, 0.8, 1.1, 1.6, and 2.3 m are reached. However, in this study, only the 2.3 m depth map will be shown since it shows less affectation by anthropic sources (e.g., agricultural tillage) and whose depth is of interest to the objectives of this work.

Since data acquisition is automatic, we were able to survey our study area in many parallel grid lines in a relatively short amount of time, which were subsequently interpolated to create the apparent resistivity map shown in Fig. 6 and discussed in Section 4.

3.1.2. ERT survey

For our measurements, we used the SuperSting R8 multielectrode resistivity meter (Fig. 5). In this methodology, multichannel cables that

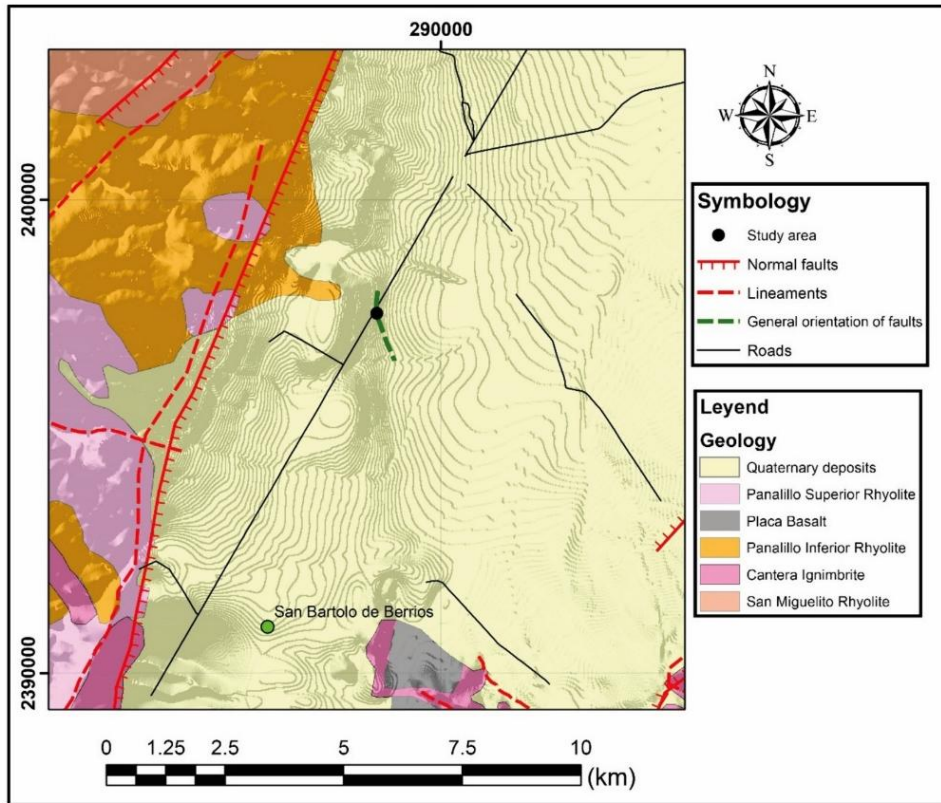


Fig. 3. Local geology of the study area. Geology and faults after López-Loera and Tristán-González (2013), with modifications and redefinition of faulting limits, lineaments, and geological contacts using Landsat 8 images, processed using ArcMap 10.8, version 10.0.0.10450 (ESRI, 2019). The green discontinuous line represents the general orientation of faults mapped in this work. (For interpretation of the references to colour in this figure legend, the reader is referred to the web version of this article.)



Fig. 4. CMD-MiniExplorer 6 I EM conductivity meter.



Fig. 5. SuperSting R8 multi-electrode resistivity meter.

include 56 electrodes are used to both inject electricity into the soil and to measure electrical potential, resulting in obtaining apparent resistivity values. Data is obtained automatically, which makes the survey faster when compared with manual ERT measurements. We used the

Dipole-Dipole array since it facilitates simultaneous data acquisition through different channels depending on the characteristics of the resistivity meter; for each current injection, eight apparent resistivity values are determined, saving time in the field. Thabit and Al-Zubedi (2015), demonstrated that this array is the best choice when

horizontal resolution is paramount (vertical bodies, such as faults and dykes are best modeled), which makes it most suitable for our objectives.

3.2. Data acquisition and processing

3.2.1. Previous measuring

We measured fault and fracture planes directly at outcrops. Around fifty measurement points were taken, both directly at rock outcrops and ground subsidence spots, using a Brunton type compass. Individual ground subsidence spots were joined to delineate fracture lengths. Sense of movement criteria on fault planes (which tends to be scarce on the study area), was interpreted after Petit (1987).

3.2.2. Electromagnetic mapping

After fault planes and fracturing boundaries were established, we covered around 25 ha of the study area using the CMD MiniExplorer 6 L conductivity meter, for 2.3 m depth mapping, to see how well the directly measured faults match with the geophysical anomalies. At least 35 parallel grid lines were necessary to cover the entire study area. From the field survey, around 13,000 apparent conductivity values were processed using Surfer 16.3.408 (Golden Software, 2019) for both converting the apparent conductivity data (in $mS.m^{-1}$) to apparent resistivity (Ohm.m), and for contour map creation. Field survey was also greatly facilitated, as the topography of most of the study area is flat, except in the quarry portion. In this case, great care was taken to obtain the automatic data at a steady pace as far as possible so as not to affect its acquisition.

3.2.3. Electrical resistivity tomography

For any surface geophysical method, vertical resolution decreases with increasing study depth. For ERT, the spatial resolution depends on the electrode spacing. The smaller the electrode spacing, the higher the resolution. On the other hand, the study depth depends on the total distance covered by the electrode array.

Considering the above, two ERT profiles using Dipole-Dipole array

were designed (see ERT lines A-B and C-D in Fig. 6) to obtain and compare data at different resolutions. In the first one (ERT1), an electrode spacing of 5 m resulted in a 56-electrode array length of 275 m, guaranteeing a maximum study depth of 55 m. Subsequently, six 68.75 m roll along were added giving an ERT1 length of 687.5 m. After processing the ERT1 data, a second ERT2 profile with an electrode spacing of 3 m and a 56-electrode array length of 165 m, provided higher resolution and a shallower study depth (33 m). Four 41.25 m roll along were added for a total length of 330 m. ERT profiles were performed exclusively on flat topography, so field work was also greatly expedited. This also means that raw data did not need topographic corrections.

From the ERT survey, an apparent electrical resistivity section is obtained, which is then tomographically inverted into a recovered electrical resistivity section using Res2DInv, version 3.4, software (Geotomo Software, 2002). The Res2DInv software uses an inversion routine based on Gauss-Newton least squares methods with smoothness and finite element constraints (Sasaki, 1992; Loke and Barker, 1996; Suski et al., 2010). In cases where the subsurface consists of homogeneous bodies creating sharp resistivity contrasts with each other (e.g., igneous dykes or faults), the robust inversion method produces better results (Loke, 2021). To measure the difference between the calculated and measured apparent resistivity, the root-mean-square (RMS) error was used, with convergence achieved after a maximum of five iterations, and RMS errors of <5%. After inversion, the data was plotted in Surfer 16.3.408 (Golden Software, 2019) to improve the quality image of both ERT profiles.

4. Results

4.1. Fault plane measurements

Most faults, fractures, and ground subsidence spots have a roughly NW-SE orientation, with fractures up to 240 m long and at least 0.4 m wide (F5 fault in Fig. 6). As we mentioned before, the sense of movement is hard to interpret at fault planes due to extensive weathering. Nevertheless, we were able to interpret a right-lateral sense of movement.

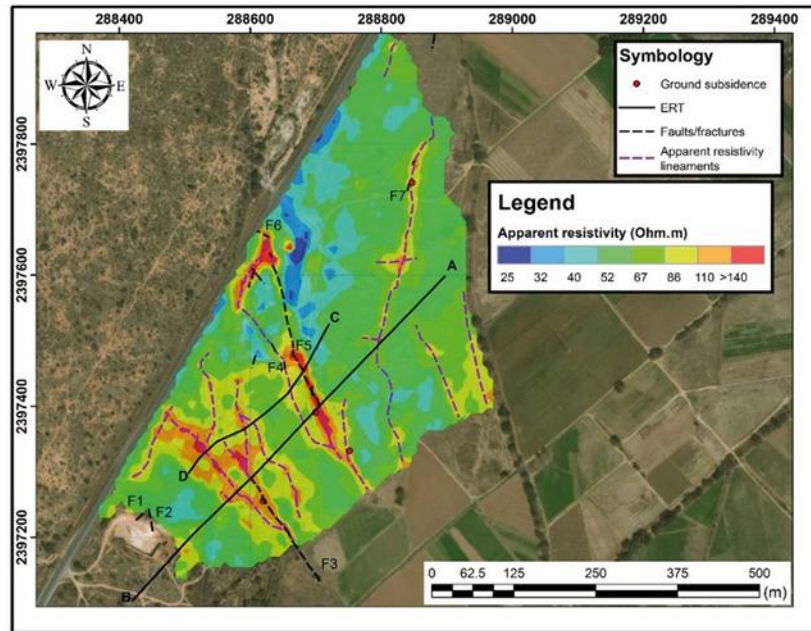


Fig. 6. Apparent resistivity mapping results and location of the two ERTs of this study. Notice how well the measured fractures (discontinuous black lines) agree with the high apparent resistivity anomalies (orange polygons and purple discontinuous lines). The figure also shows the location of the two ERT profiles (A-B and C-D) performed in our study area. (For interpretation of the references to colour in this figure legend, the reader is referred to the web version of this article.)

4.2. Apparent resistivity mapping and ERT sections

Fig. 6 shows the results obtained with the MiniExplorer 6 L equipment, for an exploration depth of 2.3 m, covering 25 ha of land. Note how the NW-SE trend continues to be the predominant one, with the orientation of the fractures measured in the field matching with that of the geophysical anomalies. As can be seen in Fig. 6, the presence of mainly high apparent resistivity lineaments is revealed in orange colour. Also, possible traces of secondary faults can be identified which intertwine with the main ones. Fig. 6 also shows the location of the two ERT profiles.

Although in less detail, the ERT1 section (Fig. 7A) shows the resistivity contrasts caused by the unfilled fractures. ERT2 section (Fig. 7B), with higher resolution than ERT1, shows details of the fractures in the uppermost subsurface such as their dip-angle.

Fig. 7A shows the ERT1 section, which reveals the subsurface continuity of F3 and F5 faults, as well as two of the longest high apparent resistivity lineaments shown in Fig. 6. Fig. 7B shows the results of the second ERT carried out in the study area. This section also reveals the subsurface continuity of F5 fault, as well as several high apparent resistivity lineaments with the same NW-SE trend observed for that fault. Fig. 7A and B also show the possible width of the main fault zone (50 m on ERT1 and 55 m for ERT2, respectively).

5. Discussion

Both geological and geophysical studies confirm the subsurface continuity of the structures seen on the surface. Most fractures measured on site are not filled with minerals and/or moisture, which is atypical for active fault sites (e.g., Kuria et al., 2010; Suski et al., 2010, among others), so this explains why most geophysical anomalies in our study

area associated with faulting are of high resistivity values (see Figs. 6, 7 and 8). The main structure in our study area is an F5 fault (Fig. 6), with at least 400 m in length and 0.4 m in width and NW-SE orientation, for which there is both field evidence, such as measurable fractures and ground subsidence spots, as well as geophysical evidence in the form of high apparent resistivity lineaments, (see Figs. 6 and 7). This map also makes it clear that the faulting that is currently evident on the surface continues at depth and has a wider extension than what can be currently seen in the field.

The ERT1 section (Fig. 7A) also shows that the F5 fault is the main structure in the area, with its fault zone being almost vertical for the first 30 m. This supports our previous interpretation of a lateral fault since no clear dip-slip component can be interpreted. At depths >30 m, this fault zone seems to become less vertical. The explanation for this might be that the local water table is being disturbed by this fault, but more studies are needed to ascertain this. Similarly, the ERT2 section (Fig. 7B) reveals that the F5 fault is the main fracture zone, with the same dip angle change shown in the ERT 1 section. Also, since ERT2 has a higher resolution than ERT1, the former image has more faults than the latter.

Finally, Fig. 9 shows a comparison of the results of the apparent resistivity mapping and ERT1 section. The locations of F3 and F5 faults on the apparent resistivity map (the longest ones in our study area) agree very well with the subsurface interpretation of these faults on the ERT section. Fig. 9 also shows how both F3 and F5 faults affect at least 40 m of our study area's subsurface.

In this work, as with most geophysical work, several sources of ambiguities can arise:

- Fault geometry and electrode placement ambiguities were dealt placing electrodes and survey lines as perpendicular to the field expression of faults as possible, to achieve accuracy in fault plane dip

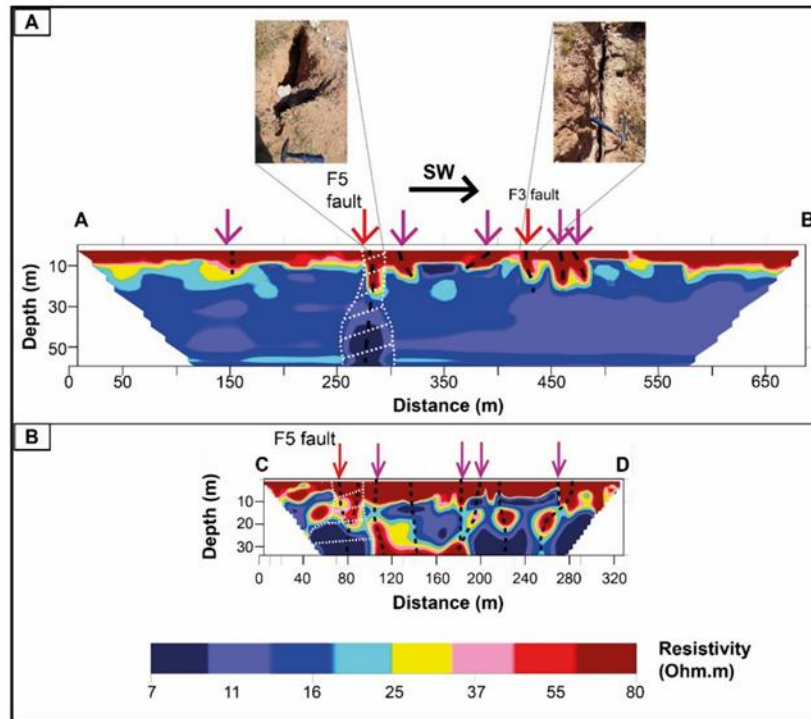


Fig. 7. A) ERT1 section obtained in the study area (A-B in Fig. 6). B) ERT2 section obtained in the study area (C-D in Fig. 6). Discontinuous lines represent possible fault planes, red arrows represent the location of directly measured faults and fractures, and purple arrows represent the location of high apparent resistivity anomalies. The white dashed polygon represents the possible width of the fault zone. The figure also shows why non-filled fractures (field photographs) produce high resistivity anomalies. (For interpretation of the references to colour in this figure legend, the reader is referred to the web version of this article.)

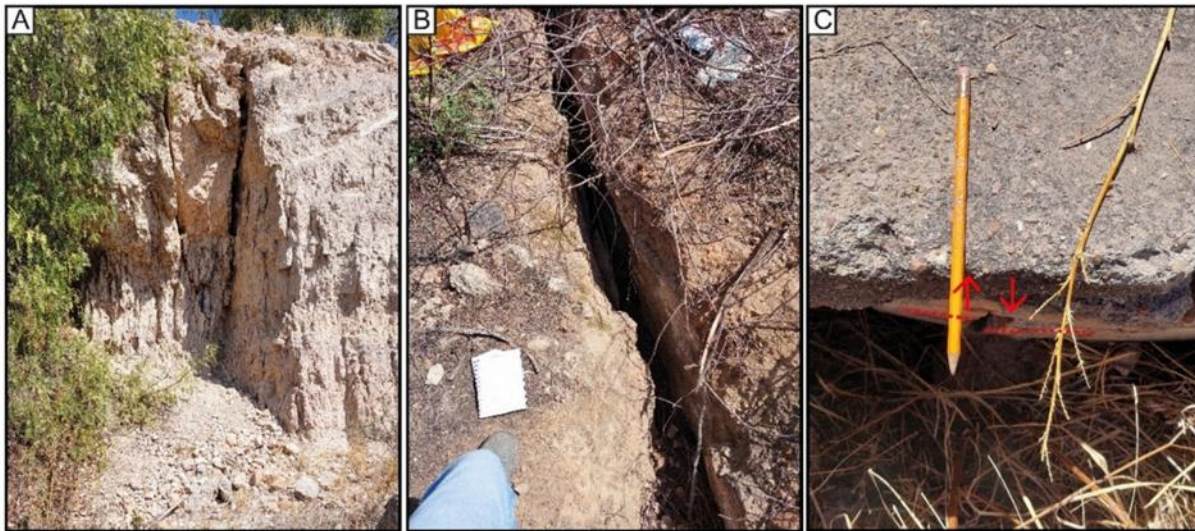


Fig. 8. a) Vertical fracture (F5 fault in Fig. 6). b) Fracture without mineral filling. Both pictures show non-filled fractures, which explains why their anomaly response is of high resistivity values. c) Man-made structure being affected by right-lateral type faulting.

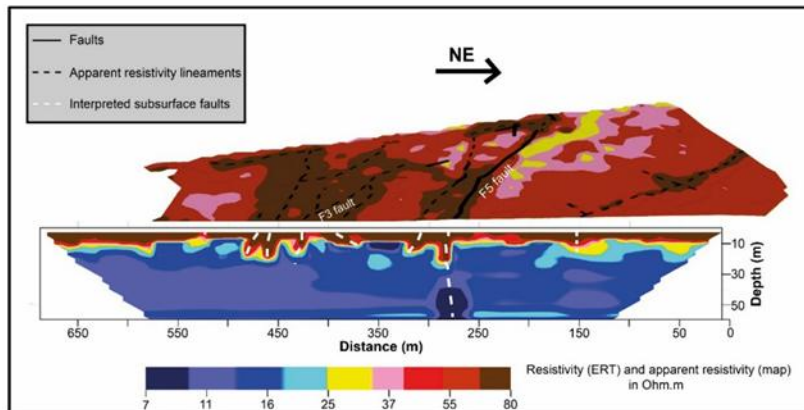


Fig. 9. 3D comparison of the resistivity map shown on Fig. 6 and ERT1 shown on Fig. 7A. Notice how well the apparent resistivity lineaments interpreted on the apparent resistivity map agree with the subsurface interpretation of the ERT. Differences between the map's and ERT's colors are due to the former showing apparent resistivity values while the latter shows true resistivity (after inversion).

angle imaging, and avoid violating the 2D assumption of the inversion software.

- Even though we were not able to obtain other sources of information to compare our data (e.g., seismic and drilling data), we are confident in our interpretations since faulting evidence in the study area is pretty evident in the exposed faulted rocks at the old quarry site (see Fig. 8 for some examples).
- Despite that resistivity anomalies do not always indicate the presence of active faults, our study site presented active faulting evidence such as: new fractures and ground subsidence spots appearing in practically each visit to the study site, fractures affecting agricultural plots, and displaced man-made structures (Fig. 8c), among others.

6. Conclusions

A geoelectric study was performed in the southern portion of the Villa de Reyes Graben (VRG) at a landfill site near the city of Jaral de Berrios, Guanajuato. One apparent resistivity anomaly map and two ERT

profiles were performed with the main objective of characterizing at depth several non-filled faults and fractures that outcrop in the field.

The apparent resistivity map shows mainly high apparent resistivity signatures, which match very well with on-site measured fractures, both with a mainly NW-SE orientation and reaching at least 400 m in length and 0.4 m in width. Since the fractures are non-filled with minerals and or water, the preponderance of high apparent resistivity anomalies makes sense. The ERT survey reveals the subsurface continuity of the faults and fractures, which are almost vertical in the first few meters of the profile and change to a lower dip angle at depth. The vertical plane of the shallowest portion of the fractures is probably due to them being right lateral faults, which agrees with our field geological structure interpretation. The dip angle change at deeper levels could possibly be related to the local disturbance of the water table, but this has not been possible to confirm yet. When comparing the results of the apparent resistivity map and ERT1 section, they tend to agree very well with each other, especially on the locations of the main faults in our study site: faults F3 and F5. This gives confidence to our geological and geophysical

interpretation and in our choice of the methodology used in this study.

All of this indicates that the faulting that is currently evident on the surface not only continues at depth but also has a wider extension than what is seen on site, so the risk of the expansion of this faulting is very high. We regard our study as a first step in characterizing and mapping several active faults and contributing to the decision making of local farmers and landowners when choosing the best places for their activities.

Thus, we expect this study to be followed up by more detailed investigations (like drilling and direct rock sampling at high-resistivity anomalies sites) that help define the type of faulting affecting our study area and its relationship with the tectonics of the VRG so both short- and long-term urban planning and local development may be possible. We also hope that this work may be of use for other studies in similar geological environments.

CRedit authorship contribution statement

Fabián Esteban Monge-Cerda: Writing – review & editing, Writing – original draft, Visualization, Methodology, Investigation, Conceptualization. **Omar Delgado-Rodríguez:** Writing – review & editing, Supervision, Methodology, Conceptualization. **José Alfredo Ramos-Leal:** Writing – review & editing, Supervision, Methodology, Conceptualization. **Lorena Elisa Sánchez-Higuero:** Writing – review & editing.

Declaration of competing interest

The authors declare that they have no known competing financial interests or personal relationships that could have appeared to influence the work reported in this paper.

Data availability

Data will be made available on request.

Acknowledgments

This work was supported by grants from the Instituto Potosino de Investigación Científica y Tecnológica A.C. (IPICYT) and by the Consejo Nacional de Humanidades, Ciencias y Tecnologías (CONAHCYT). Special thanks to David Ernesto Torres Gaytán, Ana Beatriz Rubio Arellano, Alexa Sofía Sánchez Barrientos, Karen Hernández Reyes, Montserrat Lemus Rueda, Saira Diego Olmedo, and Ulises Gerón Flores for their field work assistance, without which this work would not have been possible.

References

Almad, N., Xiaodong, L., Zhijun, G., Abbas, A., 2020. Electrical resistivity imaging of active faults in paleoseismology: case studies from Karachi Arc, southern Kirthar Fold Belt, Pakistan. *NRIAG J. Astronom. Geophys.* 9 (1), 116–128. <https://doi.org/10.1080/20909977.2020.1722524>.

Aizebeokhai, A.P., Oyeyemi, K.D., 2015. Application of geoelectrical resistivity imaging and VLF-EM for subsurface characterization in a sedimentary terrain, Southwestern Nigeria. *Arab. J. Geosci.* 8, 4083–4099. <https://doi.org/10.1007/s12517-014-1482-z>.

Alzahrani, H., Abdelrahman, K., Hazaea, S.A., 2022. Use of geoelectrical resistivity method for detecting near surface groundwater potential zones at Riyadh city, Saudi Arabia. *J. King Saud Univ. –Sci.* 34 (7), 102253 <https://doi.org/10.1016/j.jksus.2022.102253>.

Aray-Castellano, J.C., Lacan, P., Garduño-Monroy, V.H., Ávila García, J., Gómez-Cortés, J., Audmard M, F.A., Lázaro Mancilla, O., Bandy, W., 2021. Geophysical characterization of a potentially active fault in the Agua Fria micrograben, Los Azufres, México. *Bolet. de la Soc. Mexicana* 73 (2), A040121. <https://doi.org/10.18268/BSGM2021v73n2a040121>.

Arjwech, R., Boonsungnem, W., Sriwongpon, P., Somchat, K., Pondthai, P., 2020. Using integrated geophysics data set to delineate Phetchabun active fault in Thailand. *Data Brief* 30, 105608. <https://doi.org/10.1016/j.dib.2020.105608>.

Botero-Santa, P.A., Xu, S., Nieto-Samaniego, Á.F., Alaniz-Álvarez, S.A., 2020. Efecto de las fracturas de enfriamiento en la formación de fallas normales: El ejemplo de Santa María del Río, San Luis Potosí, México [Influence of cooling fractures on the

formation of normal faults: a case study in Santa María del Río, San Luis Potosí, México]. *Bol. Soc. Geol. Mex.* 72 (1) <https://doi.org/10.18268/bsgm2020v72n1a011019>.

- Bran, D.M., Tassone, A., Menichetti, M., Cerredo, M.E., Lozano, J.G., Lodolo, E., Vilas, J. F., 2018. Shallow architecture of Fuegian Andes lineaments based on Electrical Resistivity Tomography (ERT). Evidences of transverse extensional faulting in the Central Beagle Channel area. *Andean Geol.* 45 (1), 1–34. <https://doi.org/10.5027/andgeov45n1-3002>.
- Cauich-Kau, D.D.A., Cardona-Benavides, A., Castro-Larragoitia, G.J., Rüde, T.R., 2021. Understanding Arsenic and Uranium Sources and Mobility in Groundwater Flow Systems from Two Areas in San Luis Potosí, Mexico: Cerritos and Villa de Reyes Basins. *Lehr- und Forschungsgebiet Hydrogeologie, No. RWTH-2021-09796*. <https://doi.org/10.18154/RWTH-2021-09796>.
- Cinti, F.R., Pauselli, C., Livio, F., Ercoli, M., Brunori, C.A., Ferrario, M.F., Volpe, R., Civico, R., Pantosti, D., Pinzi, S., De Martini, P.M., Ventura, G., Alfonsi, L., Gambillara, R., Michetti, A.M., 2015. Integrating multidisciplinary, multiscale geological and geophysical data to image the Castrovallari fault (Northern Calabria, Italy). *Geophys. J. Int.* 203 (3), 1847–1863. <https://doi.org/10.1093/gji/ggv404>.
- Cordero Vázquez, C.Y., Delgado Rodríguez, O., Peinado Guevara, H.J., Ladrón de Guevara-Torres, M.A., Hernández-Ramos, J.O., Peinado-Guevara, V.M., 2021. Determination of Soil Properties from Electrical Measurements in Agricultural Plots, Villa de Arriaga, San Luis Potosí, Mexico. *Geofis. Int.* 60 (1), 76–100. <https://doi.org/10.22201/igeof.00167169p.2021.60.1.2037>.
- Cordero Vázquez, C.Y., Delgado Rodríguez, O., Cisneros Almazán, R., Peinado Guevara, H.J., 2023. Determination of Soil Physical Properties and Pre-Sowing Irrigation Depth from Electrical Resistivity, Moisture, and Salinity Measurements. *Land* 12, 877. <https://doi.org/10.3390/land12040877>.
- Del Pilar Martínez, A., Nieto Samaniego, A.F., Alaniz Álvarez, S.A., Ángeles Moreno, E., 2020. Geology of the southern Mesa Central of Mexico: recording the beginning of a polymodal fault system. *J. Maps* 16 (2), 199–211. <https://doi.org/10.1080/17445647.2020.1719911>.
- Delgado-Rodríguez, O., 2017. Mapping of hydrocarbon and scrap metal contaminated soil using volatile organic compounds and electromagnetic profiling methods. *Near Surf. Geophys.* 15, 312–332. <https://doi.org/10.3997/1873-0604.2017008>.
- Diario Oficial de la Federación (DOF), 2015. Resultado de los Estudios Técnicos de aguas Nacionales Subterráneas del Acuífero Jaral de Berrios Villa de Reyes (2412). [Results of technical studies of national ground waters of the Jaral de Berrios-Villa de Reyes acuífer (2412)]. https://www.dof.gob.mx/nota_detalle.php?codigo=5413967&fecha=3/11/2015.
- Doser, D.L., Ornelas, M.A., Martínez, I., Jin, L., Ortiz, A., Kaip, G.M., 2019. Using Geophysics to Investigate Texture and Salinity of Agricultural Soils and their Impact on Crop Growth in El Paso County, Texas. *J. Environ. Eng. Geophys.* 24 (3), 465–477. <https://doi.org/10.2113/JEEG24.3.465>.
- Drahor, M.G., Berge, M.A., 2017. Integrated geophysical investigations in a fault zone located on southwestern part of İzmir city, Western Anatolia, Turkey. *J. Appl. Geophys.* 136, 114–133. <https://doi.org/10.1016/j.jappge.2016.10.021>.
- ESRI, 2019. ArcMap 10.8 Software (Version 10.0.0.10450) [Computer software].
- Geotomo Software, 2002. Red2DInv Software (Version 3.4) [Computer software].
- Golden Software, 2019. Surfer 16 Software (Version 16.3.408) [Computer software].
- Gómez Hernández, A., Rodríguez, R., Lara del Río, A., Ruiz Huerta, E.A., Armienta, M.A., Dávila Harris, P., Sen Gupta, B., Delgado Rodríguez, O., Del Angel Rios, A., Martínez-Villegas, N., 2020. Alluvial and gypsum karst geological transition favors spreading arsenic contamination in Matchuala, Mexico. *Sci. Total Environ.* 707, 135340 <https://doi.org/10.1016/j.scitotenv.2019.135340>.
- Gunda, G.K.T., Balaji, S., Champati Ray, P.K., Bhat, G.R., Balakrishna Kannaujya, S., 2020. Geophysical Characterisation of the active Fault Geometry and Trends in Tectonic Deformation in the Shallow Stratigraphy along active Faults, South Andaman, India. *J. Geol. Soc. India* 95, 286–292. <https://doi.org/10.1007/s12594-020-1427-y>.
- Hasan, M., Shang, Y., Meng, H., Shao, P., Yi, X., 2021. Application of electrical resistivity tomography (ERT) for rock mass quality evaluation. *Sci. Rep.* 11, 23683. <https://doi.org/10.1038/s41598-021-03217-8>.
- Henry, C.D., Aranda-Gómez, J.J., 1992. The real southern Basin and Range: Mid to late Cenozoic extension in Mexico. *Geology* 20, 701–704. [https://doi.org/10.1130/0091-7613\(1992\)020<0701:TRSBR>2.3.CO;2](https://doi.org/10.1130/0091-7613(1992)020<0701:TRSBR>2.3.CO;2).
- Khalili, M., Mirzakerdeh, A.V., 2019. Fault detection using microtremor data (HVSR-based approach) and electrical resistivity survey. *J. Rock Mech. Geotech. Eng.* 11 (2), 400–408. <https://doi.org/10.1016/j.jrmge.2018.12.003>.
- Kuria, Z.N., Woldai, T., Van Der Meer, F.D., Barongo, J.O., 2010. Active fault segments as potential earthquake sources: Inferences from integrated geophysical mapping of the Magadi fault system, southern Kenya Rift. *J. Afr. Earth Sci.* 57, 345–359. <https://doi.org/10.1016/j.jafrearsci.2009.11.004>.
- Labarthe-Hernández, G., Tristán-González, M., Aranda-Gómez, J.J., 1982. Revisión estratigráfica del Cenozoico de la Parte Central del Estado de San Luis Potosí. [Stratigraphic Revision of the Cenozoic of Central Part of the State of San Luis Potosí]. Technical Report number 85. Universidad Autónoma de San Luis Potosí, Instituto de Geología y Metalurgia.
- Loke, M.H., 2021. Tutorial: 2-D and 3D Electrical Imaging Surveys, 216 pp. 18. Geotomo Software, RES2DINV ver. 3.59. 2D Resistivity and IP Inversion Program.
- Loke, M.H., Barker, R.D., 1996. Rapid least-squares inversion of apparent resistivity pseudosections using a quasi Newton method. *Geophys. Prospect.* 44, 131–152. <https://doi.org/10.1111/j.1365-2478.1996.tb00142.x>.
- López-Loera, H., Tristán-González, M., 2013. Geología y magnetometría aérea del Graben de Villa de Reyes, San Luis Potosí, Mesa Central de México: implicaciones tectónicas y geohidrológicas. [Geological and magnetic mapping of the Villa de Reyes Graben, San Luis Potosí, Mesa Central of México: hydrogeological and tectonic

- implications]. *Bol. Soc. Geol. Mex.* 65 (1), 137–156. <https://doi.org/10.18268/BSGM2013v65n1a11>.
- Martínez, J., Mendoza, R., Rey, J., Sandoval, S., Hidalgo, M.C., 2021. Characterization of Tailings Dams by Electrical Geophysical Methods (ERT, IP): Federico Mine (La Carolina, Southeastern Spain). *Minerals* 11, 145. <https://doi.org/10.3390/min11020145>.
- Mendoza, R., Rey, J., Martínez, J., Hidalgo, M.C., Sandoval, S., 2021. Geophysical characterisation of geologic features with mining implications from ERT, TDEM and seismic reflection (Mining District of Linares-La Carolina, Spain). *Ore Geol. Rev.* 139, Part B, 104581 <https://doi.org/10.1016/j.oregeorev.2021.104581>.
- Meng, F., Zhang, G., Qi, Y., Zhou, Y., Zhao, X., Ge, K., 2020. Application of combined electrical resistivity tomography and seismic reflection method to explore hidden active faults in Pingwu, Sichuan, China. *Open Geosci.* 12 (1), 174–189. <https://doi.org/10.1515/geo-2020-0040>.
- Mollehuara-Canales, R., Kozlovskaya, E., Lunkka, J.P., Guan, H., Banks, E., Moiso, K., 2020. Geoelectric interpretation of petrophysical and hydrogeological parameters in reclaimed mine tailings areas. *J. Appl. Geophys.* 181, 104139 <https://doi.org/10.1016/j.jappgeo.2020.104139>.
- Monahan, S.M., 2013. Investigating Fault Structure using Electrical Resistivity Tomography. [Bachelor of Science dissertation, California Polytechnic State University]. California Polytechnic State University, San Luis Obispo.
- Mustafa, H., Maulana, A., Irfan, U.R., Tonggihroh, A., 2023. *IOP Conf. Ser.: Earth Environ. Sci.* 1134, 012035. <https://doi.org/10.1088/1755-1315/1134/1/012035>.
- Nieto Samaniego, A.F., Alaniz Alvarez, S.A., Camprubí, A., 2007. Mesa Central of México: Stratigraphy, structure, and Cenozoic tectonic evolution. In: Alaniz Alvarez, S.A., Nieto-Samaniego, A.F. (Eds.), *Geology of México: Celebrating the centenary of the Geological Society of México*, 422. Geological Society of America Special Papers, pp. 41–70. <https://doi.org/10.18268/bsgm2005v57n3a3>.
- Nobes, D.C., Hornblow, S.M., 2021. Not all faults are conductive: the effects of seasonal weather changes on the near-surface expression of faults. *Geophys. Prospect.* 69 (7), 1503–1514. <https://doi.org/10.1111/1365-2478.13126>.
- Petit, J.P., 1987. Criteria for the sense of movement on fault surfaces in brittle rocks. *J. Struct. Geol.* 9 (5–6), 597–608. [https://doi.org/10.1016/0191-8141\(87\)90145-3](https://doi.org/10.1016/0191-8141(87)90145-3).
- Porras, D., Carrasco, J., Carrasco, P., González, P.J., 2022. Imaging extensional fault systems using deep electrical resistivity tomography: a case study of the Baza fault, Betic Cordillera, Spain. *J. Appl. Geophys.* 202, 104673 <https://doi.org/10.1016/j.jappgeo.2022.104673>.
- Pueyo-Anchuela, Ó., Lafuente, P., Arlegui, L., Liesa, C.L., Simón, J.L., 2016. Geophysical characterization of buried active faults: the Concul Fault (Iberian Chain, NE Spain). *Int. J. Earth Sci. (Geol. Rundsch.)* 105, 2221–2239. <https://doi.org/10.1007/s00531-015-1283-y>.
- Rolia, E., Sutjningsih, D., 2018. Application of geoelectric method for groundwater exploration from surface (a literature study). *AIP Conf. Proc.* 1977, 020018–1–020018–9. <https://doi.org/10.1063/1.5042874>.
- Sana, I.I., Taborik, P., Valenta, J., Bhat, F.A., Flašar, J., Štěpančíková, P., Khwaja, N.A., 2021. Detecting active faults in intramountain basins using electrical resistivity tomography: a focus on Kashmir Basin, NW Himalaya. *J. Appl. Geophys.* 192, 104395 <https://doi.org/10.1016/j.jappgeo.2021.104395>.
- Sasaki, Y., 1992. Resolution of resistivity tomography inferred from numerical SIMULATION1. *Geophys. Prospect.* 40 (4), 453–463.
- Stewart, J.H., 1998. Regional characteristics, tilt domains, and extensional history of the later Cenozoic Basin and Range Province, western North America. Book Chapter, USGS Publications Warehouse, 10.1130/0-8137-2323-X.47.
- Suski, B., Brocard, G., Authemayou, C., Consenza, B., 2010. Localization and characterization of an active fault in an urbanized area in Central Guatemala by means of geoelectrical imaging. *Tectonophysics* 480, 88–698. <https://doi.org/10.1016/j.tecto.2009.09.028>.
- Thabit, J.M., Al Zubeidi, A.S., 2015. Evaluation of three important electrode arrays in defining the vertical and horizontal structures in 2D imaging surveys. *Iraqi J. Sci.* 56 (2B), 1465–1470.
- Tristán-González, M., 1986. Estratigrafía y tectónica del graben de Villa de Reyes, en los estados de San Luis Potosí y Guanajuato, México. In: [Stratigraphy and Tectonics of the Villa de Reyes Graben, in the States of San Luis Potosí and Guanajuato, México]. Folleto Técnico 107. Instituto de Geología Y Metalurgia. Universidad Autónoma de San Luis Potosí.
- Tristán-González, M., Aguillón-Robles, A., Barboza-Gudiño, J.R., Torres-Hernández, J.R., Herve, B., López Doncel, R., Rodríguez Ríos, R., Labarthe Hernández, G., 2009. Geocronología y distribución espacial del vulcanismo en el Campo Volcánico de San Luis Potosí. [Geochronology and spatial distribution of de vulcanism inside de Vocanic Field of San Luis Potosí]. *Bol. Soc. Geol. Mex.* 61 (3), 287–303.
- Wang, Z., Cai, X., Yan, J., Wang, J., Liu, Y., Zhang, L., 2018. Using the integrated geophysical methods detecting active faults: a case study in Beijing, China. *J. Appl. Geophys.* 156, 82–91. <https://doi.org/10.1016/j.jappgeo.2017.01.030>.
- Winarto, J.B., Sukiyah, E., Haryanto, A.D., Haryanto, I., 2019. Sub Surface active Fault Identification on Quaternary and Tertiary Rocks using Geoelectric Method in Cilaki Drainage Basin, Southern part of West Java, Indonesia. *Int. J. Adv. Sci. Eng. Informat. Technol.* 9 (5) <https://doi.org/10.18517/ijaseit.9.5.8111>.

Chapter 4-. Geophysical, geological and tectonic study of active faulting inside the Villa de Reyes Graben, Central México

This chapter is based on an article where a four-part methodology was developed, mainly using geoelectrical methods on four sites in the southern portion of the Villa de Reyes Graben, to establish the structural style inside this graben, by authors: M.Sc. Fabián Esteban Monge-Cerda, Dr. José Alfredo Ramos-Leal, Dr. Omar Delgado-Rodríguez, Dr. José Ramón Torres-Hernández, Dr. Salvador Isidro Belmonte-Jimenez and M. Sc. David Ernesto Torres-Gaytan. It has been accepted for publication by **Near Surface Geophysics**, and it is currently under production.

Geophysical, geological and tectonic study of active faulting inside the Villa de Reyes Graben, Central México.

Fabián Esteban Monge-Cerda¹ • José Alfredo Ramos-Leal^{1*}(0000-0003-4715-7411) • Omar Delgado-Rodríguez¹(0000-0001-7027-2560) • José Ramón Torres-Hernández²(0000-0002-0624-0780) • Salvador Isidro Belmonte-Jiménez³(0000-0001-7205-417X), • David Ernesto Torres-Gaytán¹

¹División de Geociencias Aplicadas, Instituto Potosino de Investigación Científica y Tecnológica A.C. (IPICYT), San Luis Potosí, 78216, México

² Facultad de Ingeniería, Universidad Autónoma de San Luis Potosí, San Luis Potosí, 78290, México

³ Instituto Politécnico Nacional, CIIDIR-Oaxaca, Oaxaca, 71230, México

*Corresponding autor: jalfredo@ipicyt.edu.mx

ABSTRACT

The Villa de Reyes Graben is a 100 km long valley in which most studies have mainly focused on the Oligocene normal faults that originated it. This study integrates geological, geophysical (Electromagnetic Profiling, Electrical Resistivity Tomography, Ground Penetrating Radar), photogrammetric, and focal mechanism solution data on four sites inside the southern portion of the Villa de Reyes Graben to study the faulting inside this graben that is currently producing land subsidence, cracks on the ground and seismic activity. It was also possible to apply a methodology which uses the above-mentioned methods for the study of faulting inside of active tectonic basins. The northern portion of the study area is mainly impacted by NE-SW left-lateral faults, while the southern portion is dominated by NW-SE right-lateral faults. Field evidence also agrees with earthquake focal mechanism solutions evidence. It was possible to report for the first time evidence of positive and negative flower structures inside the graben, related to transpressional and transtensional deformation. Finally, the methodology for studying active faulting inside a tectonic basin can be summed up as follows: 1) Surveying the study area for evidence of faulting; 2) Using Electromagnetic Profiling for fast and accurate mapping of the study site faulting distribution; 3) further characterize the previously defined fault zones using more detailed methods such

as Electrical Resistivity Tomography or Ground Penetrating Radar; 4) Use other type of evidence, such as earthquake focal mechanism solutions, to help confirming the fault kinematics affecting the studied area.

Keywords: Acquisition, Electromagnetics, Imaging, Interpretation, Resistivity, Seismics, Tomography.

1. INTRODUCTION

Geophysical methods have a wide range of applications among which, location of oil reserves, groundwater modeling, engineering applications, are some of the most important ones (Martos 2012). The application of geoelectrical methods in the study of active faults have been successfully applied to these types of studies for several decades (Kuria *et al.* 2010; Suski *et al.* 2010; Carpentier *et al.* 2012; Monahan 2013; Cinti *et al.* 2015; Konon *et al.* 2016; Drahor & Berge 2017; Wang *et al.* 2017 Bran *et al.* 2018; Ahmad *et al.* 2020; Gunda *et al.* 2020; Aray-Castellano *et al.* 2021; Hasan *et al.* 2021; Porras *et al.* 2022; Galone *et al.* 2024; Monge-Cerda *et al.* 2024).

For example, Cinti *et al.* (2015) studied the Castrovillari fault (in Calabria, Italy), which outcrops as three scarps, to characterize the geometry at the surface and at depth, and to obtain constraints on the fault slip history. The study combined data from quantitative geomorphological analyses, electrical resistivity tomography (ERT) and ground penetrating radar (GPR) surveys, and paleoseismological trenching along a 40 m high scarp. Despite the varying resolutions of each method, each one suggests the presence of sub-parallel fault planes below the scarps at approximately the same location. Wang *et al.* (2017) studied active geological faults crossing the Beijing plain (North China), by means of the integration of gravity methods, Controlled Source Audio-Frequency Magnetotellurics (CSAMT), seismic reflection, Direct Current (DC) resistivity and paleomagnetism to locate faults and characterize their activity. These methods were useful for imaging buried fault at shallower and to analyze the fault slip rate. Array-Castellano *et al.* (2021) used magnetic, Ground Penetrating Radar (GPR) and seismic refraction data to identify, localize, and characterize a partly blind fault in the Llano Grande basin within the Agua Fría Graben (Los Azufres Volcanic Complex, central México). The authors were able to

identify anomalies and lineaments of different orientations, structurally characterize the main magnetic lineament identified in the basin and to interpret it as a high angle north-dipping fault. Galone *et al.* (2024) employed different near-surface geophysical techniques (Electrical Resistivity Tomography (ERT), active and passive seismic methods, GPR) as well as remote sensing techniques, to investigate the structural configuration of the southern sector of the Mellieha valley (Island of Malta). The result enabled the authors to identify the structural settings of the valley, including the presence of a previously unmapped fault, and characterize an asymmetric graben.

The above-mentioned studies have in common that, while several geophysical methods are used, a common and clear methodology to study active faults is not established, which is one of the goals of the present study. Additionally, the presence of positive and negative type flower structures, which until now have been only anecdotally reported, have yet to be properly established in the study area, and although studies like Carpentier *et al.* (2012) have used GPR to characterize these structures, there is lack of studies in which there is a differentiation between positive and negative types.

Specifically, in northern-central México (where the study area is located), active geological faults and associated structures are partially responsible for triggering Structurally Controlled Differential Subsidence which creates hazards such as cracking and collapsing of civil structures (Figuroa-Miranda *et al.* 2018). The importance of the present study lies in the fact that delineating these fault traces can be crucial in the decision making of local farmers and landowners when choosing the best places for their activities.

A geological and geophysical study was conducted at four sites located in the southern portion of the Villa de Reyes Graben, located in central México (GVR, Figures 1 and 2). Each of the sites was named after local characteristics and/or previous use given to them: "Banco de material" (an old quarry), "Presa El Hundido" (a colonial period dam), "Jaral " (a town in Guanajuato) and "Río Jaral" (an unnamed

river), and even though each site is very different from a structural geology standpoint, a common methodology for the study of active faults was able to be used.

Electromagnetic Profiling (EMP), Electrical Resistivity Tomography (ERT) and Ground Penetrating Radar (GPR) methods were applied mainly to confirm the subsurface presence and continuity of faulting that can be seen directly on the field using standard geological and photogrammetric techniques. It is the goal of this study to integrate geological, geophysical, photogrammetric, and earthquake focal mechanism solutions evidence for the study of faulting inside an active tectonic basin. Additionally, it is also one of the main goals of this work to map faults inside the VRG and understand its relationship with the Mesa Central active tectonics.

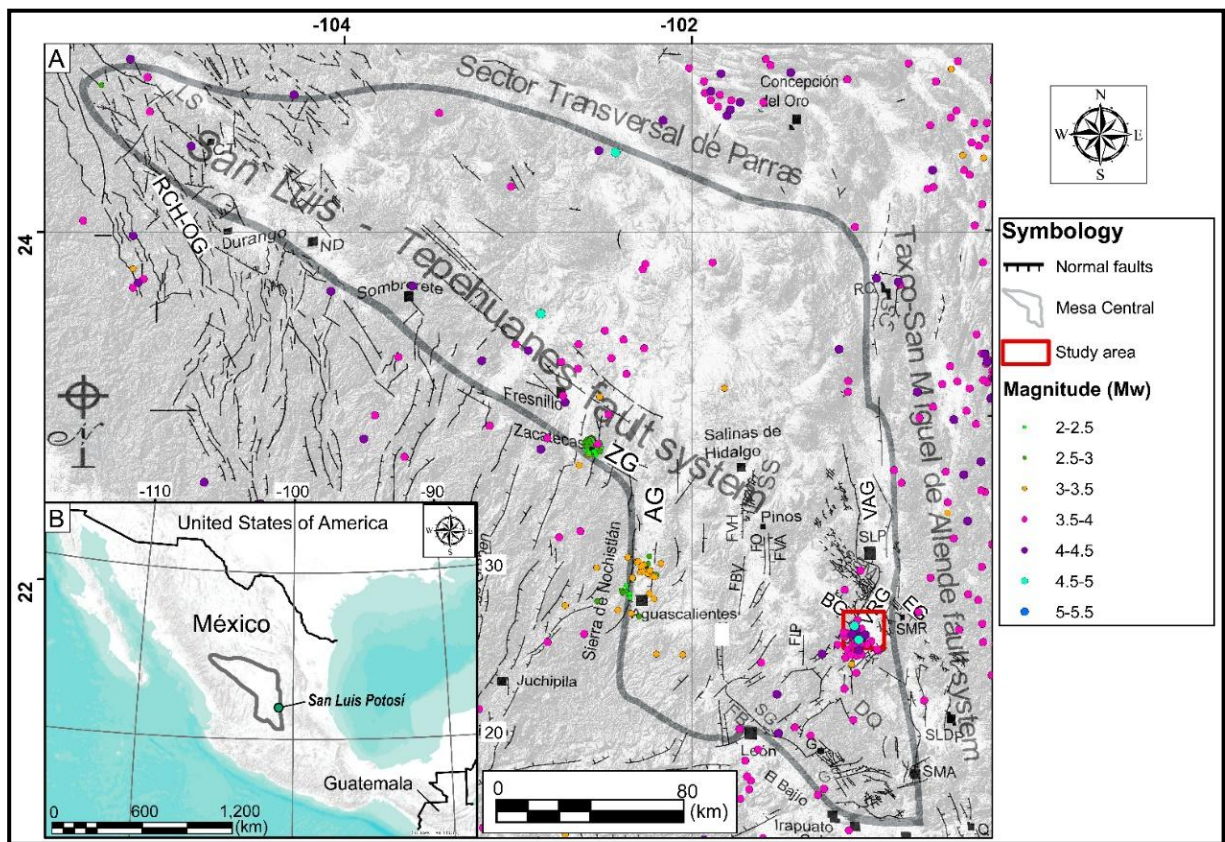


Figure 1 Tectonic context of the study area: (a) Location of the study area. LS—Laguna de Santiaguillo; RCH-OG—Río Chico-Otinapa Graben; AG—Aguascalientes Graben; FVH—Fault Villa Hidalgo; FBV—Fault Buena Vista; FO—Fault El Obraje; FVA—Fault Villa de Arriaga; FLP—Fault Los Pájaros; CG—El Cuarenta Graben; FB—Fault El Bajío; GS—La Sauceda Graben; BG—Bledos Graben; VRG—Villa de Reyes Graben; VAG—Villa de

Arista Graben; EG—Enramadas Graben; DQ—La Quemada Depression; SSM—Sierra de San Miguelito; SG—Sierra de Guanajuato; SC—Sierra de Catorce; SS—Sierra de Salinas; RC—Real de Catorce; G—Guanajuato; SLP—San Luis Potosí; SMR—Santa María del Río; SLDP—San Luis de La Paz; ND—Nombre de Dios; SMA—San Miguel de Allende; Q—Querétaro. ZG—Zacatecas Graben. Taken and modified after Nieto Samaniego et al. (2005). Epicenter data taken from SSN (2024). Topographic data after INEGI (2023); (b) Mesa Central Tectonic Province location in Central México.

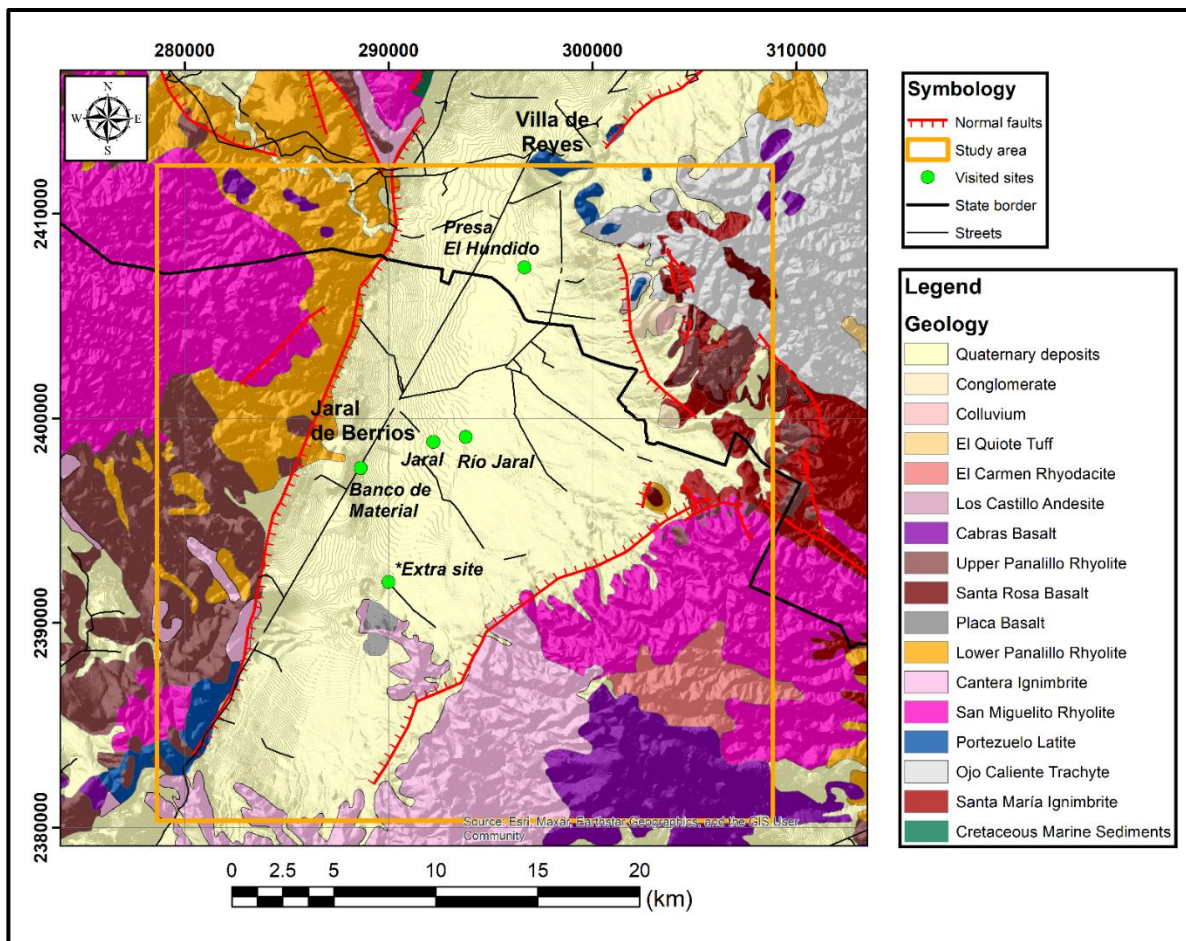


Figure 2 Study area located in central region of Mexico (Municipalities of Villa de Reyes in the State of San Luis Potosí (north) and Jaral de Berrios in the State of Guanajuato (south)). Geology and faults after Labarthe-Hernández *et al.* (1982), López-Loera & Tristán-González (2013) and Soto-García (2022), with redefinition of faulting limits and geological contacts using Landsat 8 images, processed with ArcMap 10.8, version 10.0.0.10450, software (ESRI 2019). An additional site labeled “extra site” was used to establish the continuity of faulting trends present in the “Banco de material” site.

2. GEOLOGICAL AND TECTONIC SETTING

The study area is located in the States of San Luis Potosí and Guanajuato inside the bigger tectonic structure of the Villa de Reyes Graben (VRG). The VRG is a ~ 100 km long valley filled with alluvial sediments, pyroclastic flows, and lacustrine deposits, which ranges in thickness from 50 to about 250 m (Tristán-González 1986). Until now, structural studies have focused on the Oligocene age normal faults that originated the VRG (Labarthe-Hernández *et al.* 1982; Tristán-González 1986; Henry and Aranda-Gómez 1992; Stewart 1998; López-Loera & Tristán-González 2013; Del Pilar-Martínez *et al.* 2020; Cauich-Kau *et al.* 2021) but little to no attention has been given to the active faulting inside the graben's Quaternary deposits that is producing land subsidence, cracks on the ground, and seismic activity. Since the causes of this phenomena are not well studied, this represents a challenge in the urban and economic development of the region. This was one of the main motivators for starting this study.

The study area consists of four sites inside this Graben, which from south to north are named: “Banco de material”, “Jaral”, “Río Jaral”, and “Presa El Hundido”. These four sites were chosen since they were the ones where surface evidence of faulting was most evident, and because of being in the vicinity of the most important towns in the area. Additionally, a fifth site located 5 km to the SE of the “Banco de material” site was visited, where only 160 m long NW-SE trending fracture was measured (Figure 2).

The VRG is located inside the bigger tectonic structure of the physiographic province known as the Mesa Central (Figure 1); an elevated plateau mostly covered by Cenozoic volcanic rocks, and bordered by the Sierra Madre Oriental at the north and east, the Sierra Madre Occidental at the west, and in the south by the Trans Mexican Volcanic Belt, encompassing portions of the states of Aguascalientes, Durango, Guanajuato, Jalisco, San Luis Potosí, and Zacatecas (Nieto Samaniego *et al.* 2005; Botero-Santa *et al.* 2020; Cauich-Kau *et al.* 2021). In the following section, a brief review of the tectonics of the VRG is presented, so the reader has a better understanding of its faulting dynamics.

2.1. Structural geology studies in the region

The VRG was mainly formed during crustal normal faulting, from which predominantly rhyolitic magma ascended 32 Ma. The beginning of the collapse of the graben started with the spill of the Latita Portezuelo lavas and, simultaneously with the subsiding block, the different volcanic units of the area were formed, and culminated with the formation of the Cantera Ignimbrite (32 to 27 Ma, Tristán-González (1986)). Since the main extension phase of the VRG is contemporaneous with the southern extension of the Basin and Range province of California, Arizona, New Mexico, and Texas, several authors have considered both extensional regions continuous (Henry & Aranda-Gómez 1992; Stewart 1998; López-Loera & Tristán-González 2013).

Nieto-Samaniego *et al.* (2005) defined the Mesa Central (Figure 1) as an elevated plateau located in the central part of México, with most of its total area found above 2000 m.a.s.l. The VRG is located south of a major fault system called the San Luis-Tepehuanes Fault System (Figure 1), a NW-SE fault lineament, which approximately separates the northern and southern regions of Mesa Central. The northern sector is in a more advanced state of erosion and shows almost no evidence of Neogene tectonics, while the southern sector (where our study area is located, Figure 1) is where major extensional tectonics events took place during the Oligocene, with minor events in the Miocene to Quaternary as well. This is especially true for the southern sector of the VRG, where low intensity seismic activity dominates. This recent seismic activity (from 1993 to 2024, SSN (2024)) makes it clear that active tectonics are still taking place to this day.

To date, studies focusing on the active tectonics inside the VRG Quaternary filling have not been made, with only anecdotal evidence of transtensional and transpressional stresses, generated by left lateral faults and right lateral faults, which seem to be generating small-scale (meter long) positive and negative flower structures.

2.2 Main geological formations

The study area mostly includes rocks corresponding to the Volcanic Field of San Luis Potosí (VFSLP), Volcanic Field of Santa María del Río (VFSMR) (Labarthe-Hernández et al. 1982), later called Volcanic Complex Sierra de San Miguelito (VCSSM), and Volcanic Complex of Santa María del Río (VCSMR). These fields consist of a package of volcanic rocks that vary from dacites to high silica rhyolites (formed between 32 and 29 Ma), with 80% of these rocks having an effusive origin, while the rest are pyroclastic products associated with the opening of ducts through which the magmas came out (Labarthe-Hernández et al. 1982; Tristán-González 1986; Tristán-González et al. 2009).

The main geological formations (Figure 2) are: Santa María Ignimbrite (early Oligocene), Ojo Caliente Trachyte (early Oligocene); Portezuelo Latite (early Oligocene); San Miguelito Rhyolite (mid-late Oligocene); Cantera Ignimbrite (mid-late Oligocene); El Zapote Rhyolite (mid-late Oligocene); Lower Panalillo Rhyolite (late Oligocene); Placa Basalt (late Oligocene); Santa Rosa Basalt (late Oligocene); Upper Panalillo Rhyolite (late Oligocene); Los Castillo Andesite (late Oligocene); El Carmen Rhyodacite (late Oligocene); Cabras Basalt (late Oligocene); and finally the entire volcanic sequence is topped by up to 400 m of Quaternary deposits, mainly composed of polymictic, alluvial, colluvial and lacustrine deposits (Tristán-González 1986; Tristán-González *et al.* 2009; López-Loera & Tristán González 2013; Cauch-Kau *et al.*, 2021; Soto-García 2022).

3. METHODS

To study the active faults, after directly measuring fault planes at outcrops, the following geoelectrical methods were applied: Electromagnetic Profiling (EMP), as a fast forward method for the surface location of fractures in the subsurface; Electrical Resistivity Tomography (ERT) to characterize in depth the fractures located using

EMP method. Finally, once the main fault zones are established, the Ground Penetrating Method (GPR) method was applied to study in detail the fault structure.

3.1. Methodology for the study of active faults

By means of the integration of the above-mentioned methods, and the use of additional non-geological information such as earthquake focal mechanism solutions, a methodology for the study of active faults was used (Figure 3), which could be potentially applied to similar geological environments if its limitations are considered.

3.2. Geological and photogrammetric data

Fault planes and ground subsidence spots (which are considered nascent faults in this study) were measured directly at outcrops. Sense of movement criteria on fault planes was interpreted after Petit (1987). Since most fault planes tended to be very weathered or non-existent (when measurements took place in unconsolidated sediments), Petit (1987) criteria were not always readily applicable. In those cases, in-situ measurements of fractures length, high resolution drone photos and alternative sense of movement criteria such as faulted man-made structures, were helpful to better map and understand fault kinematics. Drone photos were taken using the Mavic 2 Pro equipment.

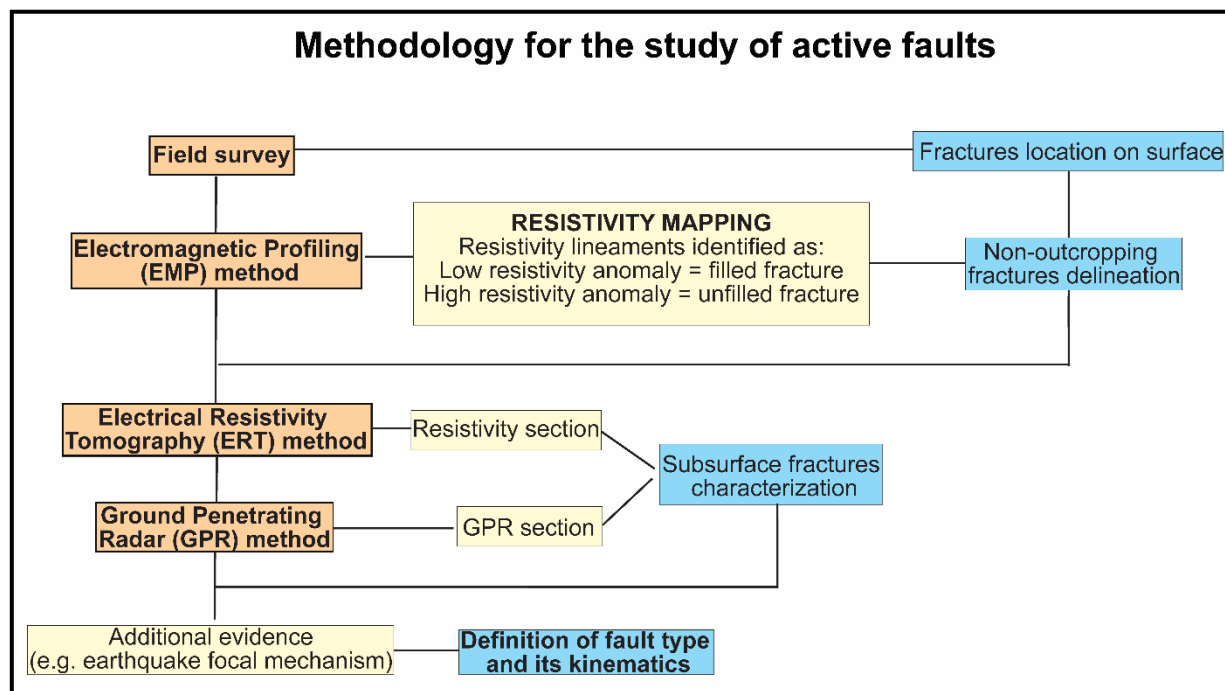


Figure 3 Flow diagram describing the methodology for the study of active faults derived from this work.

3.3. Geophysical methods

3.3.1. Electromagnetic Profiling method

The Electromagnetic Profiling (EMP) method consists in passing an alternating current of frequency f through a transmitter coil (Tx), generating a primary magnetic field of frequency f . The primary magnetic field induces a secondary magnetic field of the same frequency f in the subsurface. Both primary and secondary magnetic fields are recorded in a receiver coil (Rx) separated at a distance S from the coil Tx (Figure 4a). From the ratio between the primary and secondary magnetic fields, a conductivity (or its inverse, resistivity) value is calculated for the entire geologic sequence from the surface to a maximum depth of study that depends on S , f , and the electrical properties of subsurface (McNeill 1980; Figure 4a).

The Czech-made CMD MiniExplorer 6L CMD was used to carry out the EMP survey. It consists of a sensor tube containing one Tx coil and six Rx coils separated at

different S values, which allows the calculation of six apparent resistivity values for six study depths (0.3, 0.5, 0.8, 1.1, 1.6 and 2.3 m). For the purposes of this study, only the apparent resistivity map for the 2.3 m survey depth will be shown.

This method was applied in two of our four study sites with the following survey area dimensions (all measurements in hectares (ha)):

- Presa El Hundido: 95 ha.
- Banco de material: 8 ha.

After fault planes and fracturing boundaries were established, each of the study sites were surveyed using the CMD MiniExplorer 6L conductivity meter, for 2.3 m depth mapping, to establish how well the directly measured faults match with the geophysical anomalies. Data was processed using Surfer 16, version 16.3.408 (Golden Software 2019) for both converting the apparent conductivity data (in $\text{mS}\cdot\text{m}^{-1}$) to apparent resistivity ($\text{Ohm}\cdot\text{m}$), and for contour map creation.

It is worth mentioning that these EM data were not inverted, since the main objective in using this rapid acquisition method was to obtain a qualitative first set of data to be used to apply more detailed methods such as ERT. From the EMP results, the lateral variations of ground conductivity were obtained, which allowed locating the fault planes not visible on the ground surface. ERT profiles were planned perpendicular to the fractures planes to characterize the faults at depth.

3.3.2. Electric Resistivity Tomography method

As a result of the application of the Electrical Resistivity Test (ERT) method, a geoelectric image of the subsurface is obtained by means of electrical measurements made on the surface along a profile. In the field, a multicore cable is used, to which several steel electrodes are inserted into the ground at a fixed distance according to the type of electrode array selected. The electrodes are used both for the injection of electrical current into the subsurface and for voltage measurements, and to determine the apparent resistivity values at depth along the profile (Loke 2021).

In this study, the Dipole-Dipole array, which offers high horizontal resolution (Thabit & Al-Zubedi 2015), makes simultaneous data acquisition easier through different channels. This array performs its measurements using a current dipole (C) and a potential dipole (P), both of length "a". The distance between the two dipole centers is an integer multiple of "a", i.e. "na", where $n = 1, 2, 3, \text{etc.}$, increasing the distance between the dipoles increases the study depth (Figure 4b, Adepelumi *et al.* 2006; Loke 2021).

At two of the four sites visited in our study, an Electrical Resistivity Tomography (ERT) profile was performed using the SuperSting R8 multi-electrode resistivity meter. The specifications of each profile are as follows:

- Presa El Hundido: 1100 m long, with electrode spacing of 10 m.
- Jaral: 540 m long, with electrode spacing of 10 m.

An apparent electrical resistivity section is obtained as the result of the ERT survey, which is then inverted into a "true" electrical resistivity section using the Res2DInv, version 3.4, software (Geotomo Software 2002). This software uses an inversion routine based on Gauss-Newton least squares methods with smoothness and finite element constraints (Sasaki 1992; Loke & Barker 1996; Suski *et al.* 2010). The robust inversion method produces better results where there exist homogeneous bodies creating sharp resistivity contrasts with each other (e.g., faults) (Loke 2021). As a measure of the difference between the calculated and measured apparent, the root-mean-square (RMS) error was used, with convergence achieved (when possible) after a maximum of five iterations, and RMS errors of (ideally) less than 5 %.

Using an electrode spacing of 10 m, a maximum exploration depth of up to 110 m was achieved. The main drawback of such a depth of survey is that it considerably decreases the resolution of the geoelectric model, especially in the first 20 m depth. The use of the ground penetrating radar technique is an attempt to recover some of that lost resolution in the shallower part of the geological section.

3.3.3. Ground Penetrating Radar method

The Ground Penetrating Radar (GPR) is an electromagnetic pulse reflection method based on physical principles analogous to those of seismic reflection surveys. This method uses reflections of short pulses of electromagnetic (EM) energy spanning a wide range of frequencies. Reflections and refractions of electromagnetic waves occur at the boundaries between rock strata and objects with different electrical properties. (Milsom 2003; Blindow 2009).

A GPR system usually consists of a control unit (CRU) connected to receiver and transmitter units, each of which is in turn connected to an antenna of a given frequency, which sends an EM pulse from the surface penetrating into the ground, and a boundary layer is reflected when this pulse passes through two objects with different physical values (Figure 4c). Subsequently, the reflected wave returns to the ground surface and is intercepted by the receiving antenna that measures the reflected signal as a function of time (Milsom 2003; Rodríguez-Robles 2016). In the case of the GPR data, the MALA ProEx GPR System was used, using the 50 MHz rough terrain antenna, with Tx-Rx separation of 4.19 m, for a penetration depth of about 8-10 m. It is worth mentioning that no topographic correction was needed for this data since the profiling lines were made on flat terrain, with variations of ground level of less than 3 m. A velocity of 10 cm/ns was used for the time-depth conversion.

In the case of the Ground Penetrating Radar (GPR) survey three profiles were performed using the following specifications:

- Presa El Hundido: 77 m long.
- Banco de material: Two profiles of 90 m and 93 m long, respectively.

Both achieved a penetration depth of about 7.5 m. Filtering of GPR data using the RadExplorer 14 software was used to try to remove noise from geological and man-made sources. The following basic filters were used:

- Background removal filter: Removing parallel bands resulting from plane reflectors and bands of low-frequency noise (Butnor *et al.*, 2003; Al-Shiejiri 2013; Rodríguez-Robles 2016).
- Time-zero adjustment: To ensure that the zero time of arrival of the signal corresponds to zero depth, it is necessary to eliminate any lag time before interpreting the radargram.
- Bandpass filtering: This routine is used to increase the signal/noise ratio, using a simple trapeziform zero-phase filter (DECO-Geophysical 2005).

The GPR technique allowed for the best resolution of all the methods used in this study but did not correctly image the dip of fault planes. The reasons for this will be explored in the Discussion section.

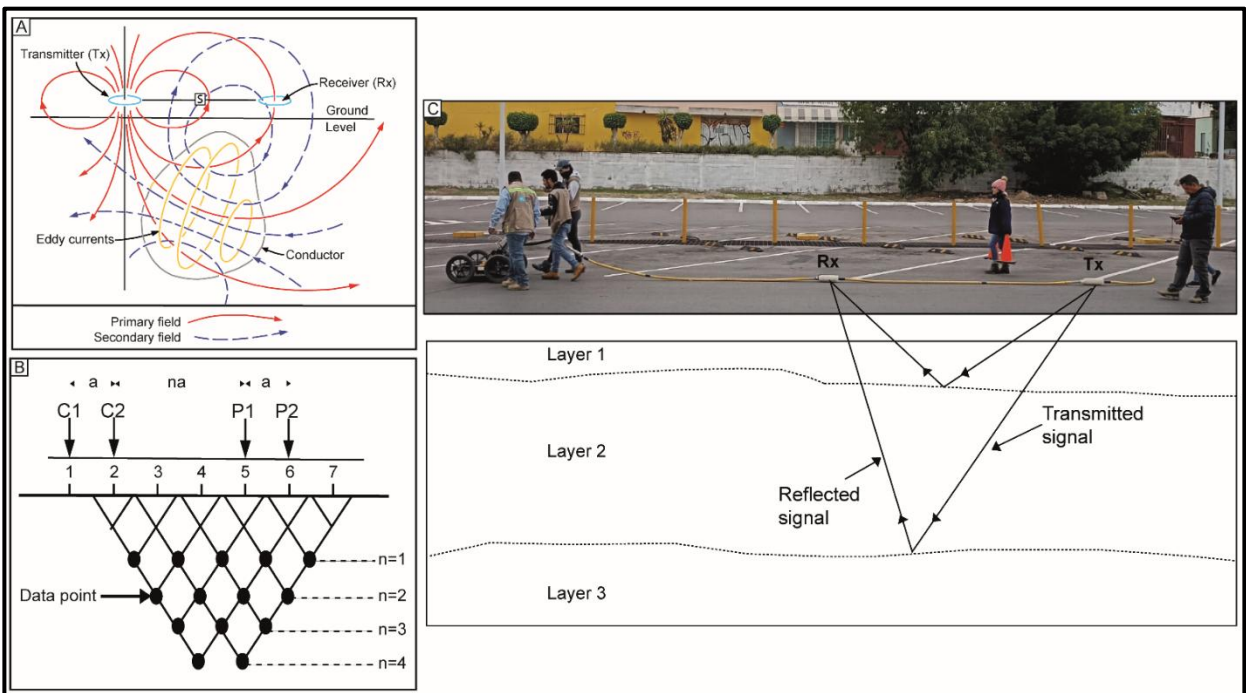


Figure 4 (a) Basic principle of EM surveying method. *S* denotes distance between Tx and Rx coils. Modified after Reynolds (1997). (b) Measurement sequence for building up a resistivity pseudo-section using the Dipole-Dipole array. **C** denotes current electrode, **P** potential electrodes, **a** the electrode spacing, and **n** ground level scanned. After Adepelumi

et al. (2006). (c) Schematic view of the MALA ProEx GRP System surveying a sector of the “Presa El Hundido” site.

4. RESULTS

In this section, the results of the direct measurement of faults and geophysical interpretation at each of the four study sites are presented.

4.1. “Banco de material” site

Fault planes were measured in the field and complemented with Electromagnetic Profiling (EMP) and Ground Penetrating Radar (GPR) measurements. The results of the in-situ measurements are presented in the form of a rose diagram and a stereogram (Figures 5a and 5b). As can be seen in the rose diagram (Figure 5a), which includes data from measured fault planes (9 planes), individual GPS points of ground subsidence spots joined to form fault traces, and resistivity lineaments (14 planes, see location in Figure 6), the NW-SE orientation trend is the most predominant one.

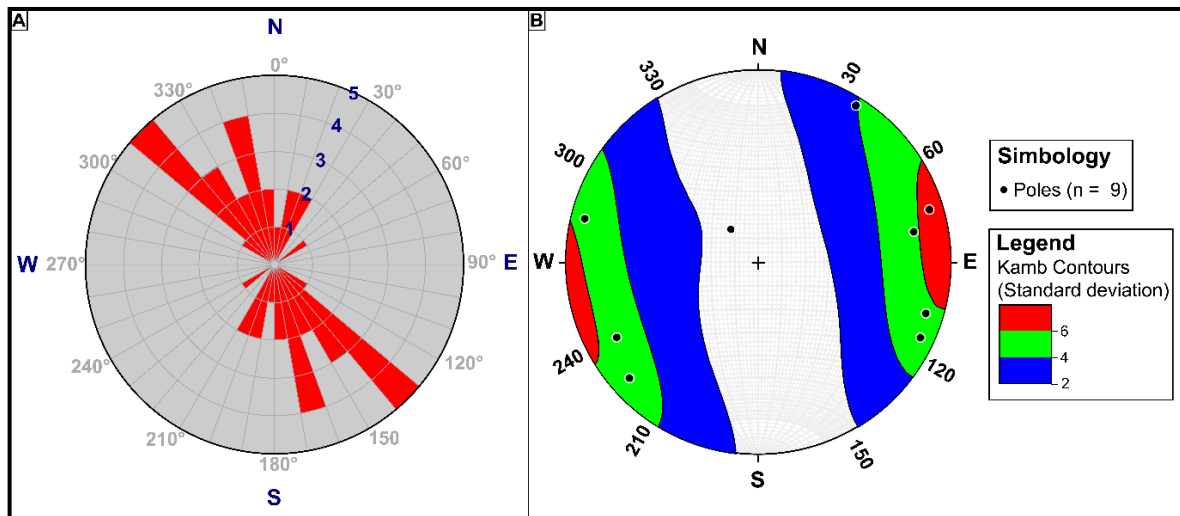


Figure 5 Structural data. (a) Rose diagram from the “Banco de material” site fault planes, fractures on the ground, and apparent resistivity lineaments. (b) Stereogram from outcropping fault planes. Figure 8a data processed using the GeoRose 0.5.2.0 Software

(Yong Technology Inc., 2013). Figure 8b data processed using the Stereonet Software, based on Allmendinger *et al.* (2013) and Cardozo & Allmendinger (2013).

Figure 6 shows the apparent resistivity map resulting of the EMP survey using the MiniExplorer 6L equipment, for an exploration depth of 2.3 m, covering 8 ha of land. High apparent resistivity anomalies related to the presence of unfilled fractures, at least up to 2.3 m depth, are observed in Figure 6. Notice how well the orientation and location of the fractures exposed in the site (dashed red lines in Figure 6) match with those of the apparent resistivity anomalies.

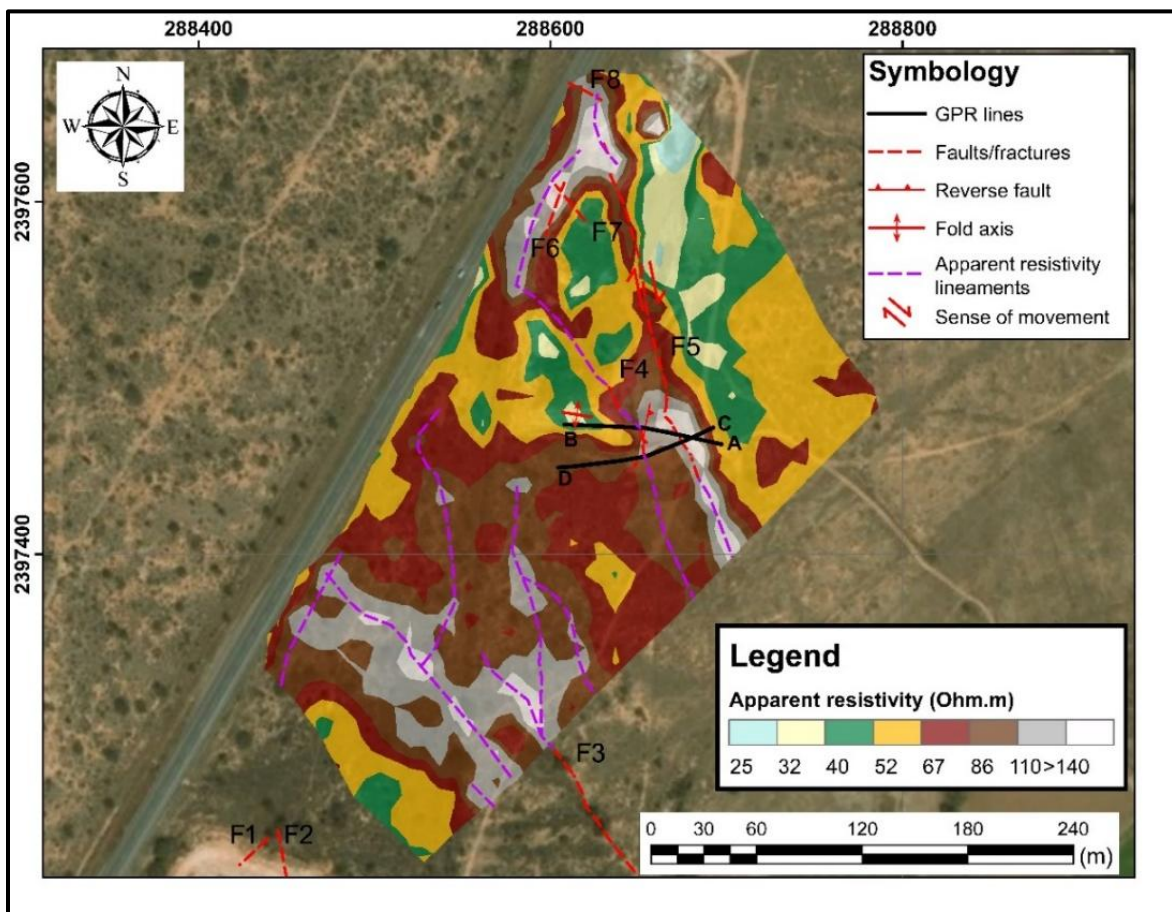


Figure 6 Apparent resistivity mapping results for 2.3 m depth and location of the two GPR sections of this study. Notice how well the measured fractures and high apparent resistivity lineaments (discontinuous lines) agree with the high apparent resistivity anomalies (brown-grey polygons). Processed using ArcMap 10.8, version 10.0.0.10450 (ESRI, 2019).

NW-SE oriented faulting is the predominant one, with the longest fault being around 295 m long, with a maximum fault zone width of about 0.6 m on the surface. Transpressional related deformation can be seen and only affects rhyolitic units at the “Banco de material” site. The compression is mainly shown as low angle faults (Figure 7a) and folding (Figure 7b). This type of fracture causes high apparent resistivity anomalies with values between 80 and 140 Ohm.m (Figure 6).

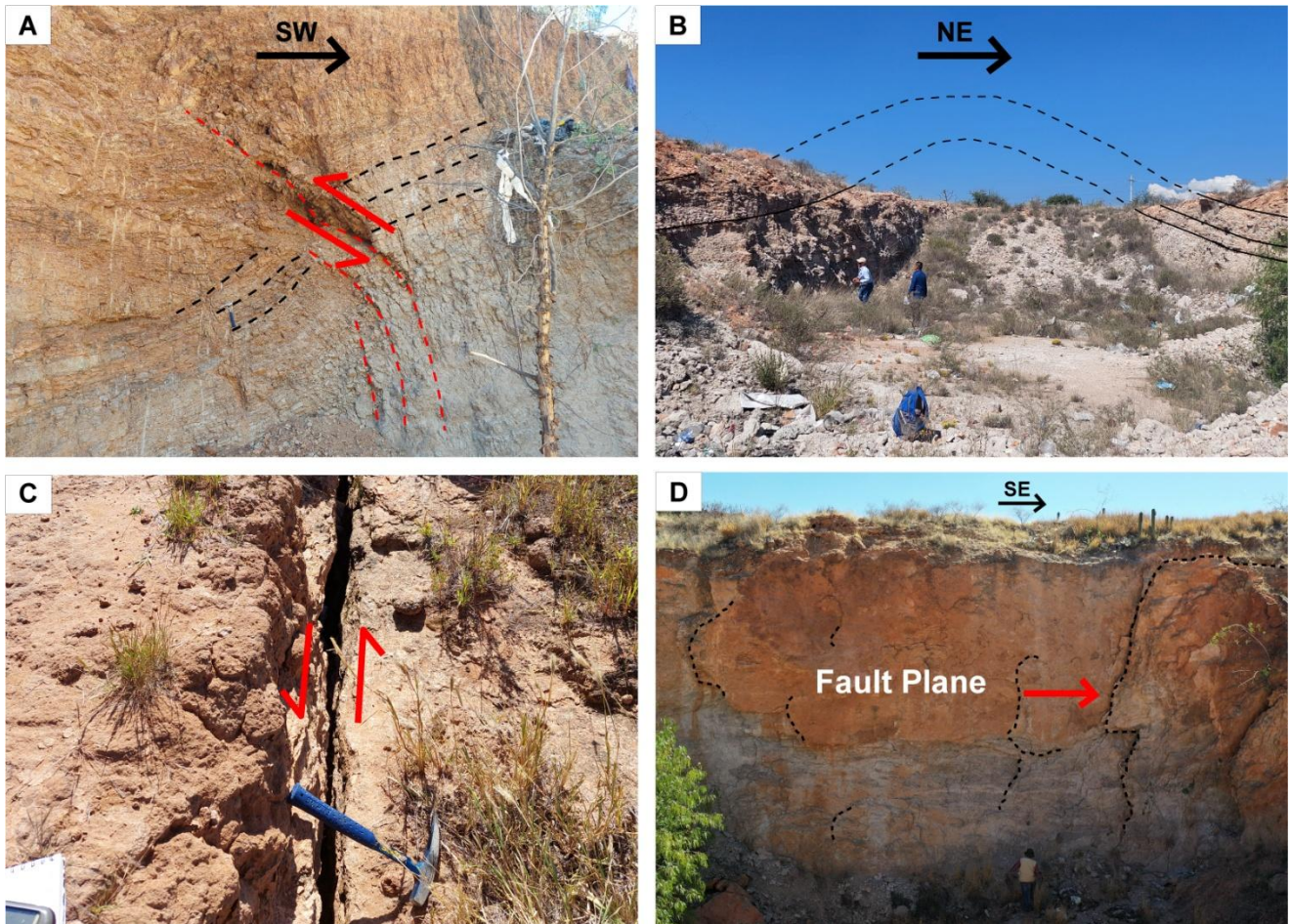


Figure 7 “Banco de material” structures. (a) Positive flower structure affecting tuff deposits (reverse fault in Figure 6). (b) Interpreted antiform structure, with a weathered axis (see approximate location of axis in Figure 6). (c) Transtensional fault (F3 fault in Figure 6), with interpreted right-lateral movement. (d) Meter long kinematic indicators showing right-lateral slip (measured in fault F5, see location in Figure 6).

As can be seen in Figure 7a, this reverse fault seems to have a low angle at shallow depth, while deeper down seems to be almost vertical. Faulting shows mostly strike-slip evidence, with meter long kinematic indicators showing this (Figure 7d). At the southern portion of this same site, faulting seems to change to transtensional style deformation, which causes land subsidence and cracks on the ground (Figure 7c).

Southward from the “Banco de material” site, transtensional style deformation still dominates (as confirmed in a quick visit to a nearby meter long crack on the ground, see location in Figure 2) so this probably means that the rhyolitic units of this site are roughly the limits of both styles of deformation. Transtensional deformation affects mostly Quaternary deposits, so this is the most recent and active style of deformation in this portion of the study area, exposed at surface as vertical unfilled fractures (Figure 7c) causing the highest magnitude apparent resistive anomalies (brown and gray colors in Figure 6).

After EMP helped delineate the areas and trends that are most probable to coincide with subsurface faulting, and to better understand the transpressive and transtensional limits of our study site, two GPR sections were performed, with depths of exploration of about 7.5 m. Because no reflectors are noticeable below 7.5 m, all profiles were cut to this depth (see Figure 8 and 10, and location in Figure 6).

Figure 8 shows GPR section A- B, in which the predominance of transpressive stress can be clearly interpreted (purple discontinuous lines in Figure 8), with the one located near the 25 m mark probably related with our study area main fault (fault F5 in Figure 6). Another important transpressive structure is located approximately in the center of the profile, which approximately matches the reverse fault of Figure 7a. GPR section A-B shows that at depth this fault is clearly related to a positive flower structure (purple discontinuous line). The third compressive structure (green discontinuous line in Figure 8) is probably related to the interpreted fold near the end of this profile (Figure 8b). On the other hand, transtensive structures (orange discontinuous lines in Figure 8) do not seem to be outcropping at present. Figure 9

shows the two main faults which are generating the transpressive structures that can be interpreted in Figure 8.

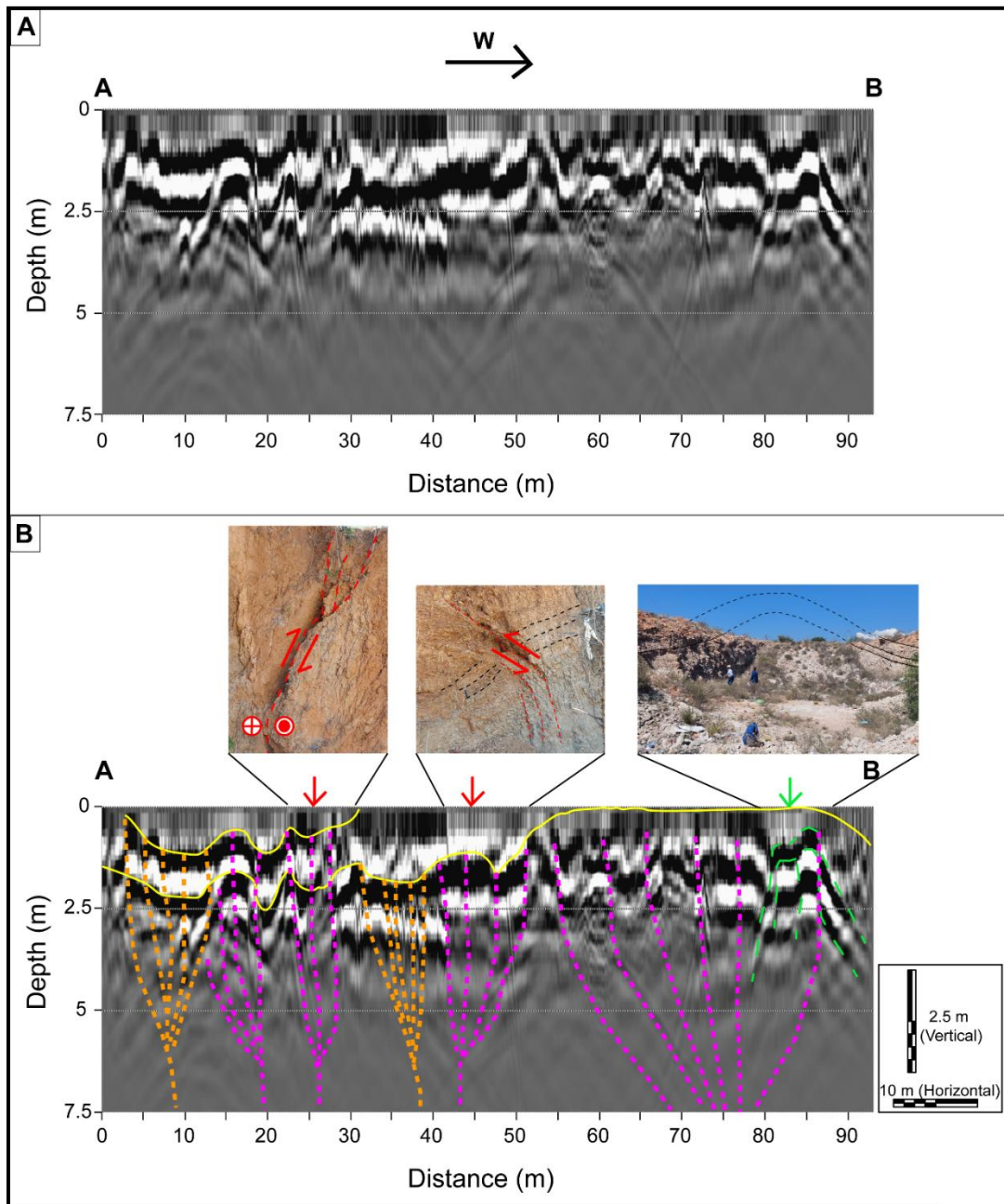


Figure 8 GPR data. (a) GPR section A-B without geological interpretation. (b) GPR section A-B. The red arrows indicate the location in the field of the structures, and the green arrow the approximate location of the interpreted fold axis in Figure 6. Discontinuous lines represent both positive (purple) and negative (orange) flower structures. Solid yellow lines represent layer limits. Notice the good match of in-situ

fault measurements with what is interpreted in the GPR section. Figure 8 also shows how the structures interpreted in the profile look in the field.

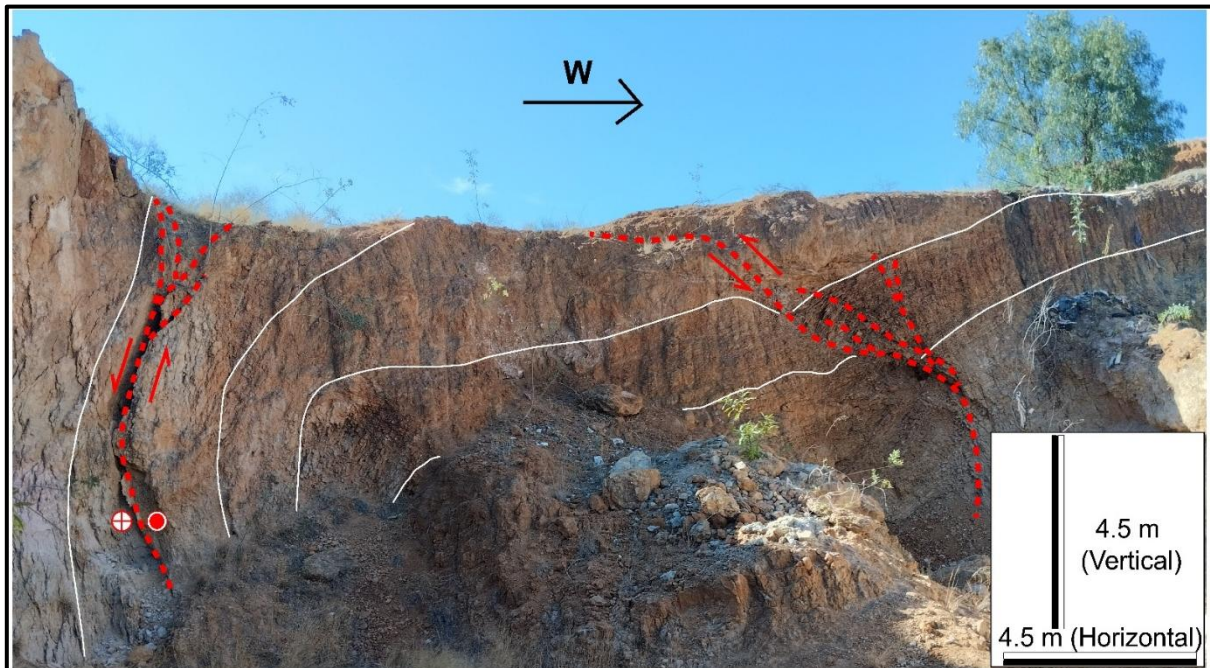


Figure 9 Flower structures (left F5 fault and right reverse faults in Figure 9), which are the main structures in the “Banco de material” site.

GPR section C-D (Figure 10) shows that, contrary to A-B section, transpressive structures are the most abundant (and extended, orange discontinuous lines in Figure 10), which is evidence that, as the separation from the old quarry (where rhyolitic rocks outcrop) increases, subsidence spots and stress-related fractures are the dominant ones. The first of these transpressive structures is probably related to the study area’s main fault (F5 fault in Figure 6). Near the 45 m mark, a compressional structure (purple discontinuous line in Figure 10) can be seen that could match with a probable reverse fault generated by the positive flower structure shown in Figures 7a and 9. Finally, as can be interpreted in both GPR profiles, the maximum fault zone width (of 0.6 m at the surface) could be of the order of at least 40 m.

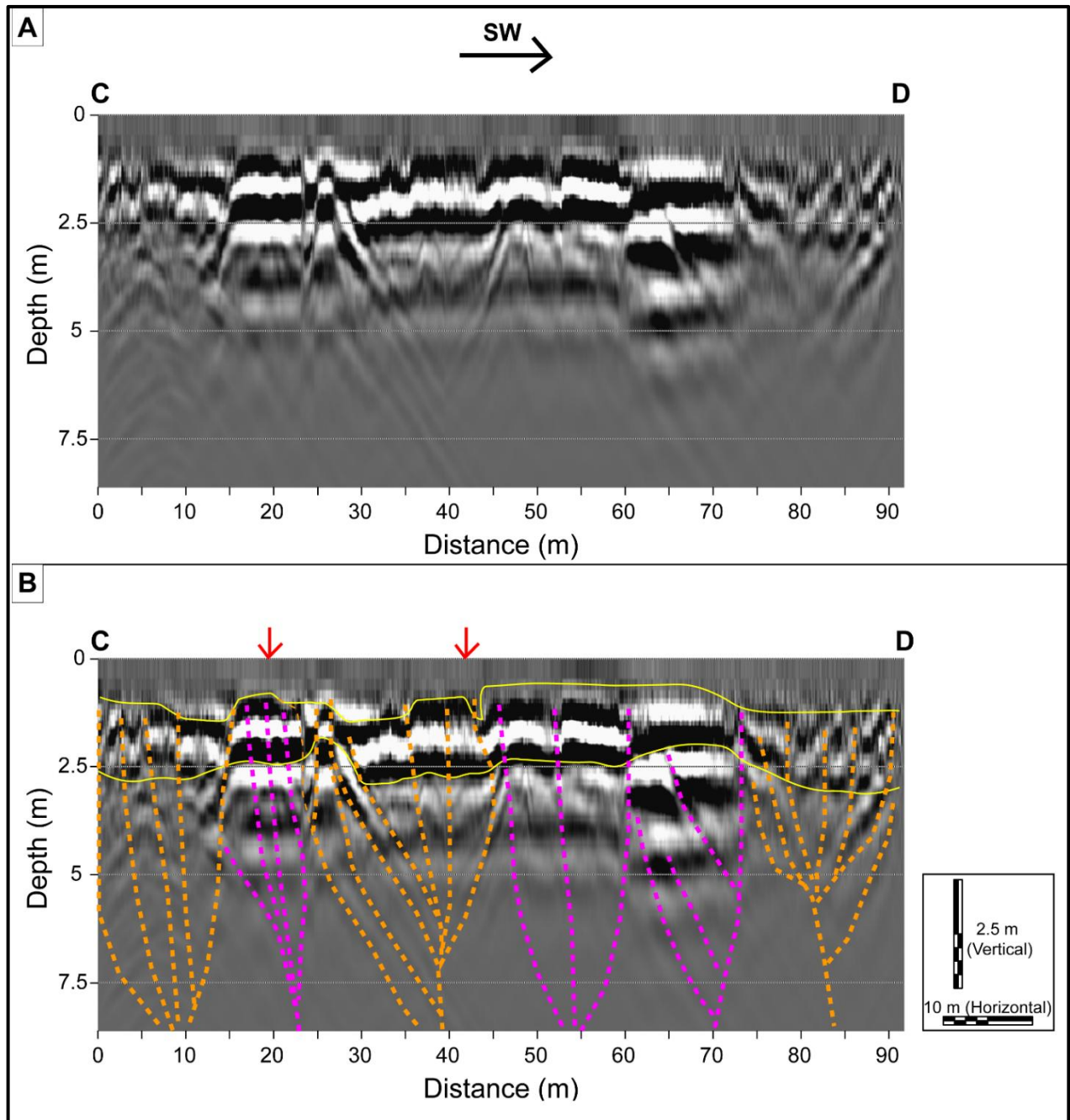


Figure 10 GPR data. (a) GPR section C-D without geological interpretation. (b) GPR section C-D. Red arrows indicate the location in the field of the structures. Discontinuous lines represent both positive (purple) and negative (orange) flower structures. Solid lines represent layer limits. Notice the good match of in-situ measured faults with what is interpreted in the profile.

Figure 11 shows the geological interpretation of GPR line A-B, which cuts across the study area's main structures. Figure 11 makes it clear that transpressive faulting

compresses outcropping rhyolitic units, and it is the dominant structural style on this site.

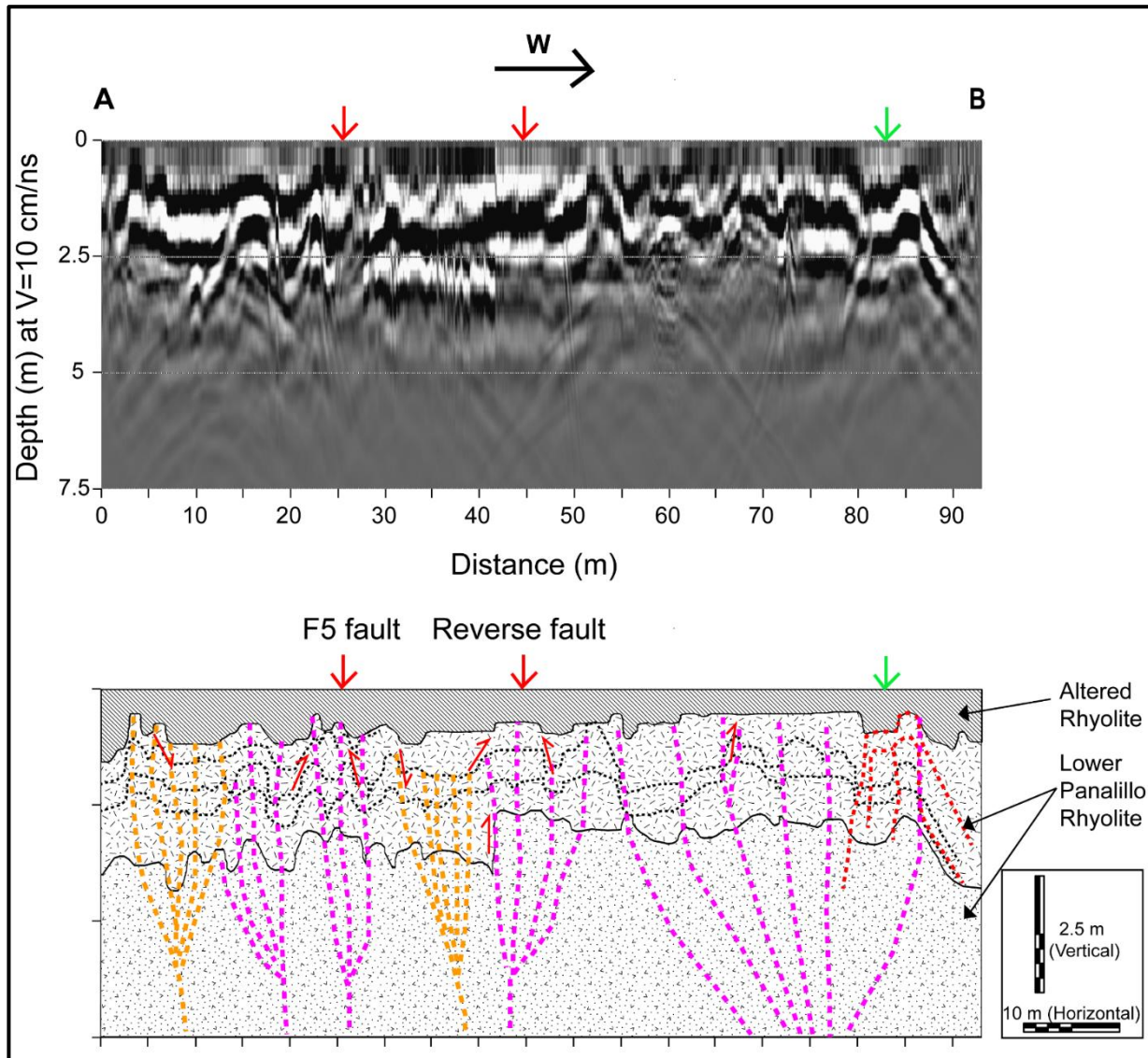


Figure 11 GPR data (top) and interpreted geological section (bottom). Notice the predominance of positive flower type structures (purple discontinuous lines). Black discontinuous lines represent stratification limits.

4.2. “Jaral” site

At this site, in situ measurements were complemented with Electrical Resistivity (ERT). GPR data acquisition is not feasible at this site since cultural noise sources are very abundant. Also, it is worth mentioning that there were no outcrops available in which fault planes could be measured and interpreted using Petit (1987) criteria. Hence, the fault shown in Figure 12 was measured directly on the field by joining several GPS location points, and whose trace was corrected and/or extended using drone photos.

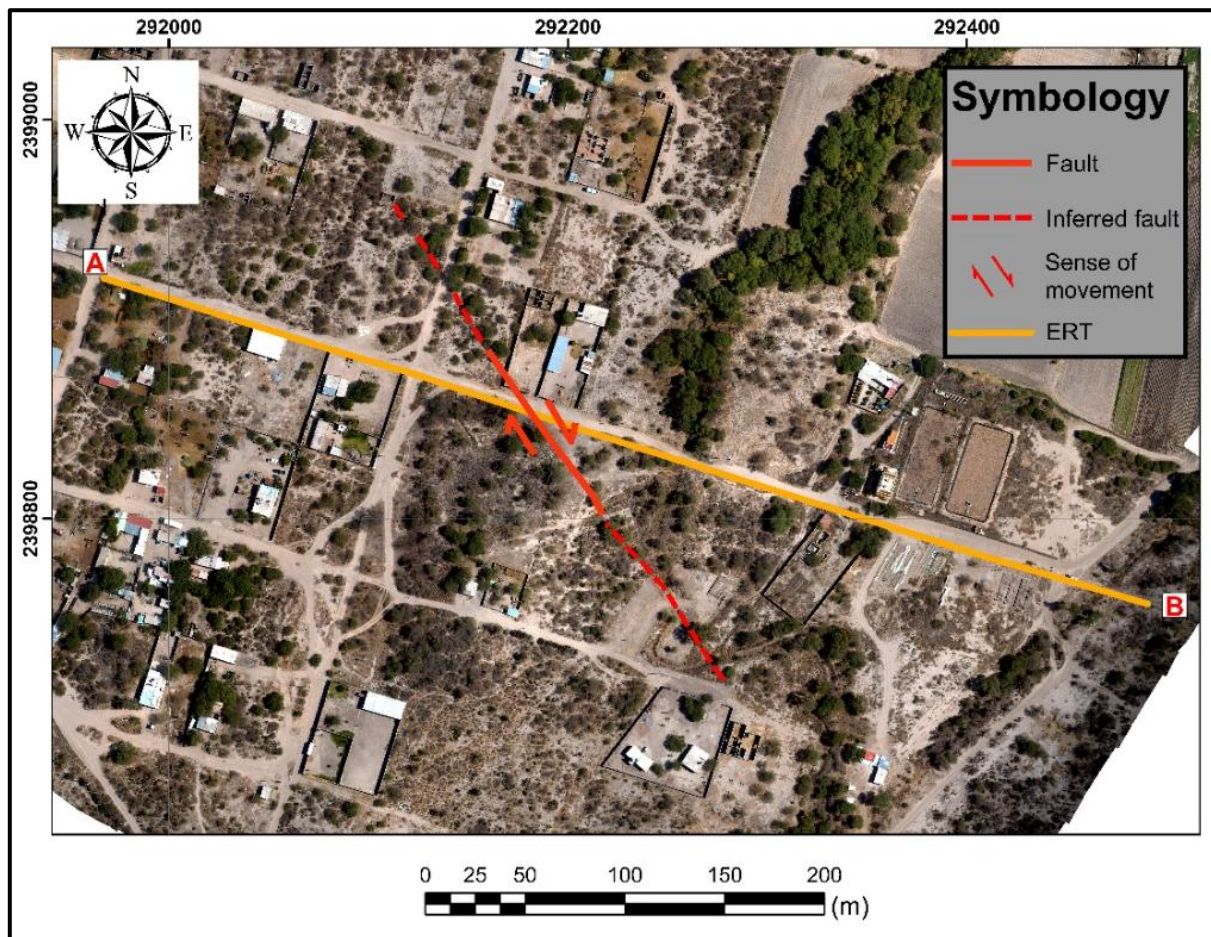


Figure 12 Faulting and location of ERT section at “Jaral” site.

Evidence of fracturing was found along a 100 m long and about 0.4 m wide fault, with NW-SE orientation (see Figure 13). Figure 12 also shows the location of the

ERT performed at this site, which had an extension of approximately 540 m, with electrode separation of 10 m, reaching an exploration depth of about 100 m (see Figure 14).



Figure 13 Ground subsidence spots visible along the main fault trace.

Figure 14 shows the result of the inversion of the ERT performed at this site (top) and the geological interpretation derived from the joint geological and geophysical interpretation (bottom). A Root Mean Square Error (RMS) of 17.8% was achieved after 6 iterations (with a robust inversion), which shows how noisy field data was. The main structure is the fault that runs across the center of the study site. Note the good agreement of what is seen in the field (red arrow) with the interpretation of the fault at depth. Also, there seem to be several secondary fault traces, although they do not outcrop, and tend to join at depth at the center portion of the ERT. The main fault at depth appears to have a high angle plane and puts two layers in contact with resistivity contrasts. Faulting in this site seem to be mainly transpressive in

nature and seem to compress rhyolitic and sedimentary and units. Finally, as can be interpreted in Figure 13, the main fault zone could have a total width of about 120 m.

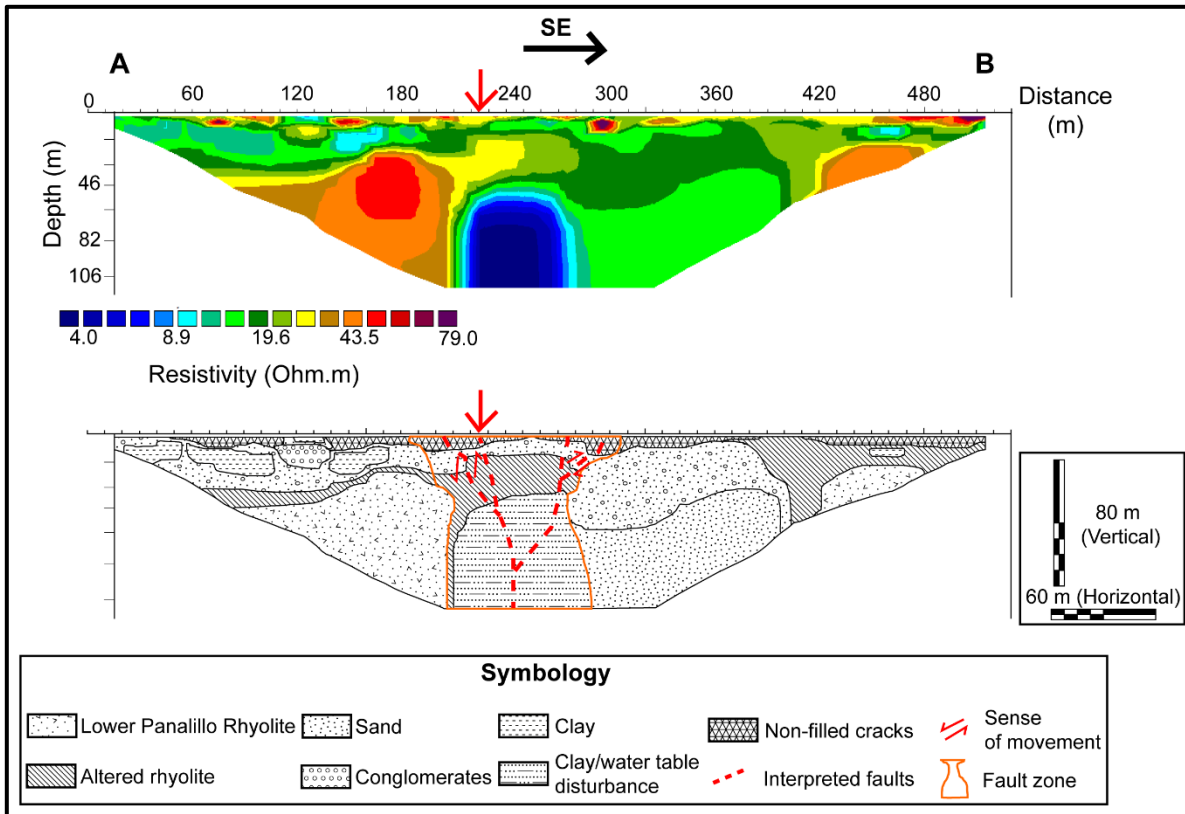


Figure 14 ERT performed on the “Jaral” site (Top) and geological interpretation (bottom). Discontinuous red lines represent possible fault planes, and red arrow represents the field location of the main fault trace. Notice how well the subsurface interpretation of this ERT agrees with the main fault field location, and the predominance of positive flower type structures.

4.3 “Río Jaral” site

NE of the “Jaral” site, at the “Río Jaral” site, faulting changes to a NE-SW regime which, as will be explained later, it is the main faulting direction at the northernmost portion of the study area, especially at the “Presa El Hundido” site. At this site, faulting is evident in the form of a fracture with an extension of about 140 m and an approximate width of about 12 m, which crosses the river (see location in Figure 15).

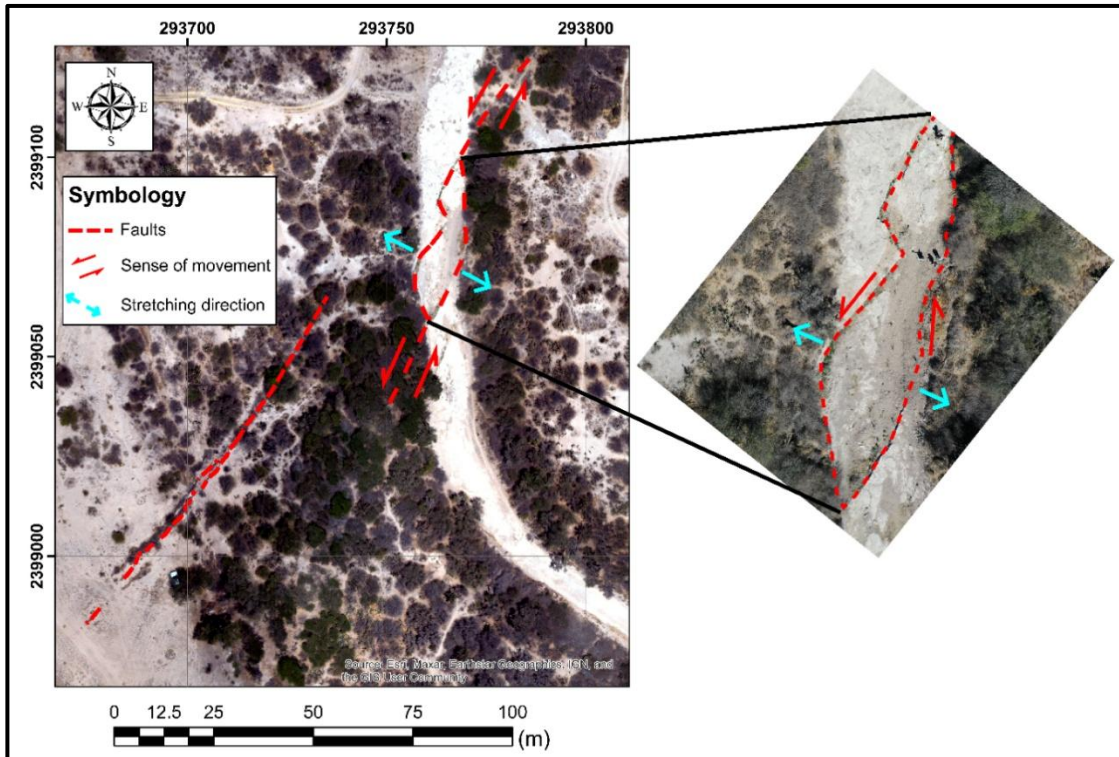


Figure 15 Faulting at “Río Jaral” site. The inset image shows the probable type of fault occurring at this site.

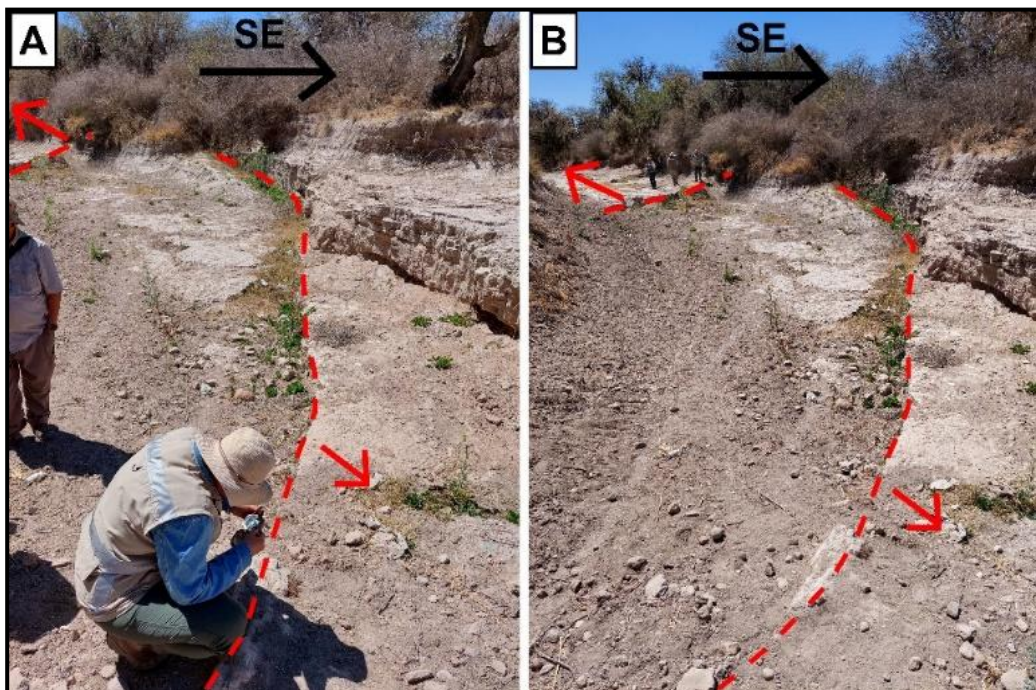


Figure 16 “Río Jaral” site. (a) In-situ measurements at the “Río Jaral” site. (b) Maximum width (of about 8 m) of the main fault zone.

It is worth mentioning that on this site there was only one clear fault plane which could be measured (see Figure 16a), and the maximum length was interpreted using drone photographs, so this is why a stereogram and rosette orientation diagram is not presented. Also, field conditions did not allow for geophysical prospecting.

Faulting is predominantly of the extensional type (see Figures 16a and b), existing anecdotal evidence of water infiltration during the rainy season through these fractures. There is also evidence of a small-scale pull-apart basin structure (see Figure 15), which supports the idea that faulting is transtensional.

4.4 “Presa El Hundido” site

At the northernmost portion of our study area, at the “Presa El Hundido” site both geological and geophysical evidence shows mainly transtensional faulting (Figures 17 and 18), that generates faults with maximum lengths and widths of around 700 m and 12 m, respectively. (Figures 17 and 18d). Similarly to the “Jaral” site, except for the damaged old-dam crest structure, there were no outcrops available in which fault planes could be measured and interpreted using Petit (1987) criteria. Thus, the faults shown in Figure 17 were measured directly on the field by joining several GPS location points, and whose trace were corrected and/or extended using drone photos, and that is why only a rose diagram of the orientation of factures is shown (Figure 17 c).

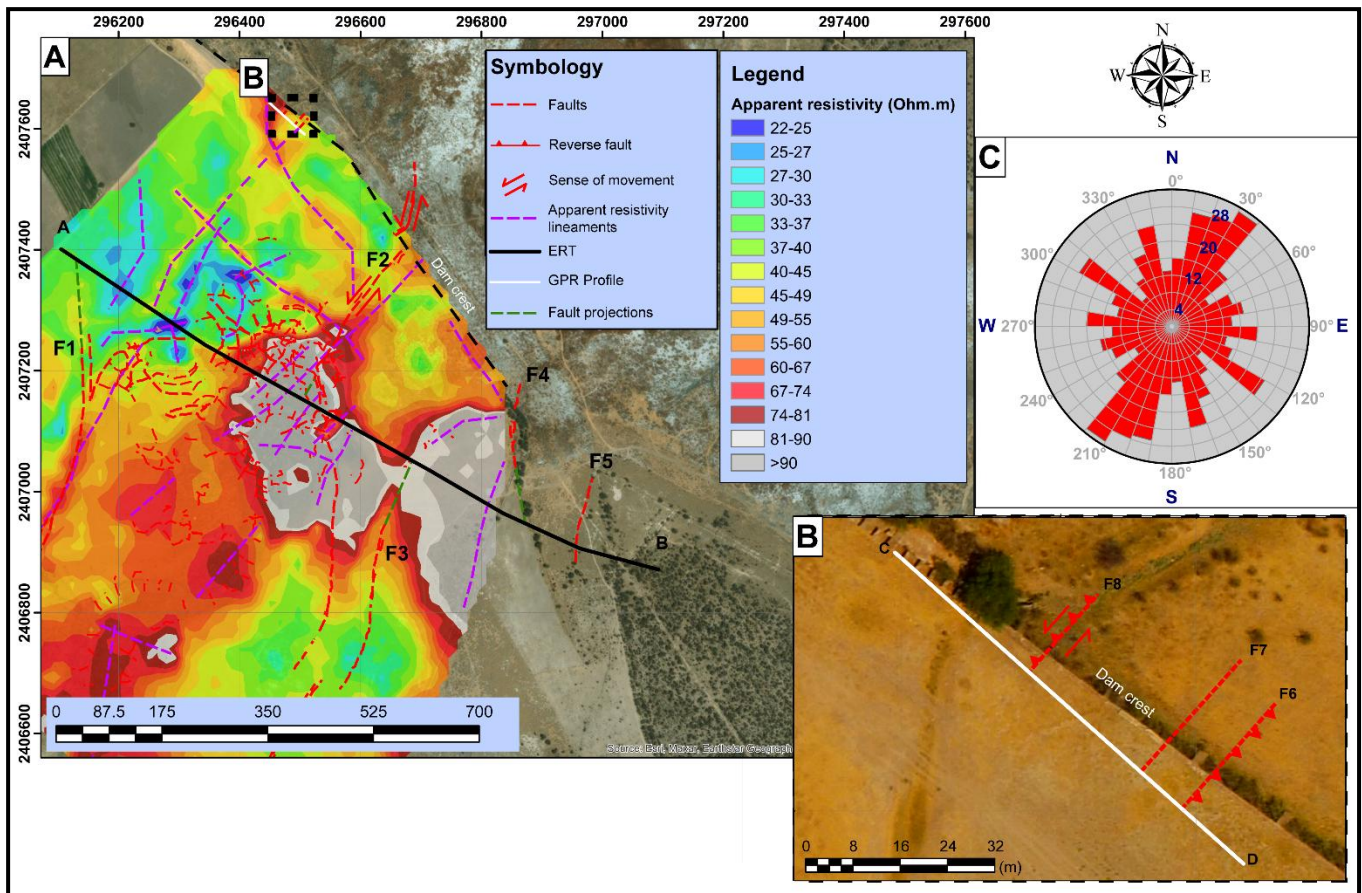


Figure 17 “Presas El Hundido” site. (a) Faulting and location of EMP mapping (for 2.3. m depth), and ERT and GPR sections at “Presas El Hundido”. (b) Zoomed detail of GPR section. (c) Rose diagram from the site’s measured fractures on the ground, and apparent resistivity lineaments data processed using the GeoRose 0.5.2.0 Software (Yong Technology Inc., 2013).

As can be seen in the rose diagram (Figure 17c), which includes data from individual GPS points of ground subsidence spots joined to form fault traces (292 planes, red discontinuous lines in Figure 17), and resistivity lineaments (33 planes, purple discontinuous lines in Figure 17a), the NE-SW orientation trend is the predominant one.

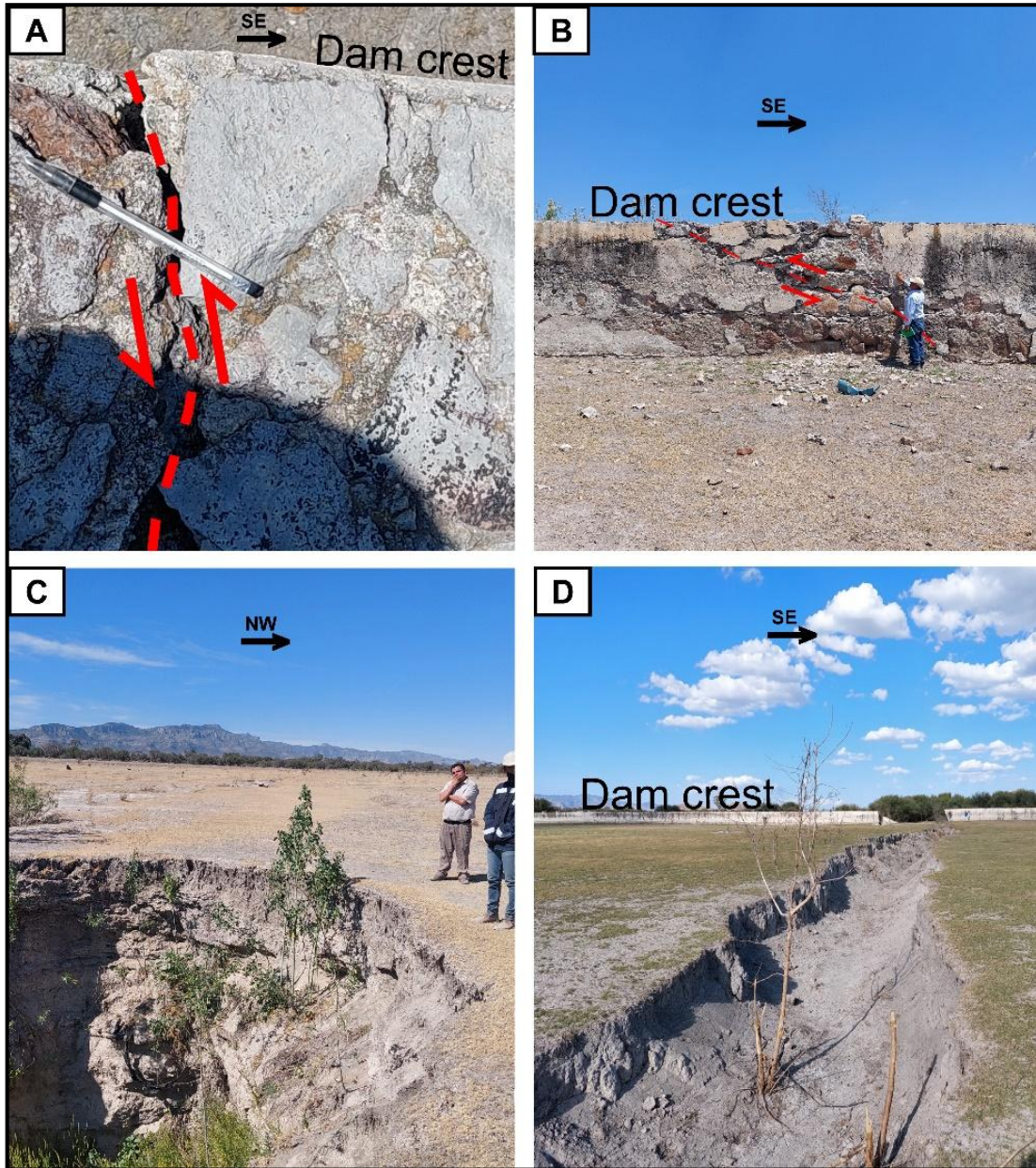


Figure 18 “Presa El Hundido” structures. (a) Left lateral slip evidence on the colonial era dam crest (produced by F8 fault, see location in Figure 17a). (b) Reverse faulting evidence affecting the structure of the colonial period dam crest (F6 fault in Figure 17b). (c) Meter-deep ground subsidence (Near F1 fault, Figure 17a). (d) Meter-long NE-SW oriented (F2) fault cutting across the old dam crest structure (see location of F2 fault in Figure 17a).

The most recent faulting activity however seems to be transpressional and affects the largest man-made structure built on this site, namely the colonial period dam

(Figures 18 a and b). Compressional stress seems to be damaging this abandoned structure, and it is generated by left lateral faulting (Figure 18a).

Figure 17a also shows the results of the EMP mapping, for an exploration depth of 2.3 m. To date, around 95 hectares (ha) of land have been surveyed. The NE-SW trend is still the dominant one. Broadly speaking, areas of high apparent resistivity coincide with the areas of greatest subsidence and in-situ faulting, which outcrops mostly as meter long non-filled cracks (Figures 18c and d). The western sector of this map shows areas of low apparent resistivity, possibly corresponding to fractures filled with moisture and/or clay material, and with areas of greatest plant growth.

Similarly to the “Jaral” site, an ERT was performed along the areas of highest concentration of high apparent resistivity anomalies (see location in Figure 17a and results in Figure 19), which probably match with the subsurface continuation of surface faulting. This ERT had a length of 1120 m, electrode spacing of 10 m, and reached about 120 m deep. Since many of the main faults do not present surface expression in the vicinity of the profile, several of these traces were projected until they intersected the profile line, to visualize their possible underground location (green dashed lines in Figure 11a). After the inversion of this ERT data (Figure 19), an RMS of 12.32% was reached after 5 iterations, with a robust inversion, which denotes that these data are not as noisy as those from the “Jaral” site. Figure 19 also shows the geological interpretation of this ERT section, based on the (sparse) outcrop evidence integrated with the geophysical data.

Fig. 19 shows the possible subsurface continuation of the main faults present in this area. Fault F2 could be the continuation of the main fault that cuts the dam curtain, which in the first 40 m of depth puts zones with contrasting resistivities in contact, and at greater depth seems to generate a zone of low resistivity. Also note that fault F2 is the projection of the data measured in the field, and the high apparent resistivity lineaments (purple arrows in Figure 19) and both agree very well with the interpretation of this fault at depth. Both F3 and F4 faults seem to also have

subsurface continuity. As there are few data points at the SE end of the profile, it is not possible to know with certainty if the interpretation of F5 fault in Figure 19 is correct. Finally, the resistivity lineament around the 220 m mark (Figure 19) could be generating a transpressive structure similar to the one shown in Figure 17b. The tendency that fractures join at depth seems to be stronger than in the ERT performed in the previously visited site (Figure 14).

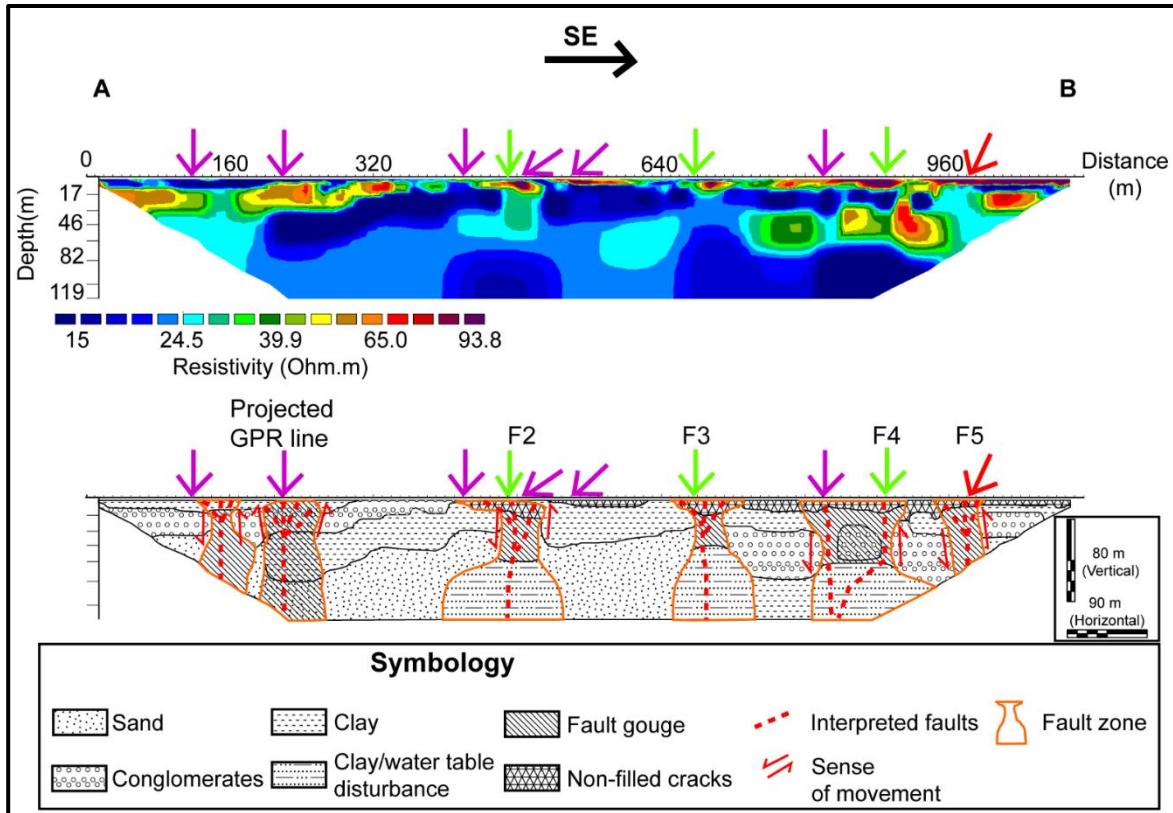


Figure 19 ERT performed on the “Preso El Hundido” site (Top) and geological interpretation (bottom). Discontinuous red lines represent possible faults, green arrows represent the projection of several fault traces close to the profile line, the red arrow represents the field location of a fault trace measured directly in the field, and purple arrows represent apparent resistivity lineaments. Notice the predominance of transpressive structures.

A GPR section was carried out near the left-lateral-reverse fault that is very clearly damaging the structure of the dam (F6 fault in Figure 17a, see detail in Figure 17b). Figure 20 shows the results of the GPR profiling. Notice how compressive stresses are the dominant type that cuts across this section of the dam structure.

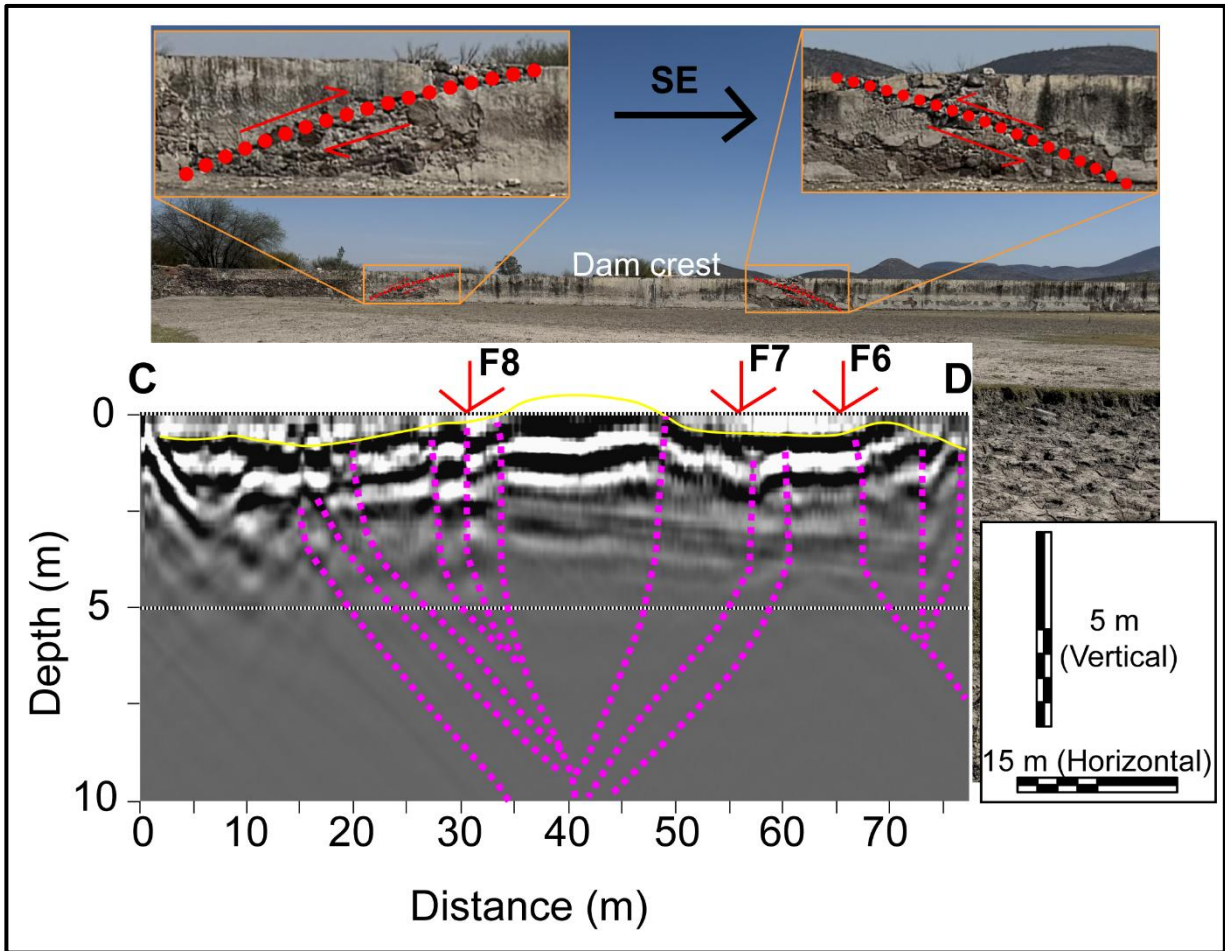


Figure 20 GPR section C-D. Arrows indicate the location in the field of the structures, discontinuous purple lines represent positive flower structures. Solid yellow line represents layer limits. Notice the good match with what is interpreted in the profile. Figure 22 also shows how the structures interpreted in the profile look in the field.

5. DISCUSSION

Most geophysical evidence reveal fault zones which have high resistivity values at surface (generated by non-filled fractures) and progressively decrease until reaching clay-type resistivity values (as low as 4 Ohm.m). This contrasts with similar studies (e.g. Konon *et al.* 2016; Drahor & Berge 2017) in which fault zones are predominantly conductive. Although it is not common, high-resistivity fault related lineaments have been reported by Nobes and Hornblow (2021), and in the study area by Monge-Cerda *et al.* 2024. The phenomena shown in Figures 14 and 19 could be explained by the accumulation of clayey sediments derived from faulting which seep through the non-filled fractures near the surface, or it could be a local disturbance of the water-table, the only exception being the left end of Figure 19 (near the 220 m mark), where faulting is so recent that has not managed to create the mentioned phenomena. Nevertheless, to achieve the correct interpretation of this data, more studies are necessary to ascertain this.

The joint geophysical and geological interpretation also shows that faulting in the studied sites, which can be classified as left (or right) lateral combined with normal (or reverse) types, tend to join at depth to form a single trace. This is evidence of the existence of either positive or negative flower type structures. Positive flower structures generated by NW-SE faults dominate in the “Banco de material” and “Jaral” sites, with meter long right lateral kinematic indicators and reverse faulting surface evidence reinforcing this interpretation at the “Banco de material” site (Figure 7). Geophysical evidence on those sites reveals mostly transpressive structures (Figures 11 and 14). On the other hand, negative flower structures related to NE-SW faulting dominate at the “Presa El Hundido” site, with meter long fractures and subsidence spots being more abundant (Figure 18), although transpressive structures seem to be starting to manifest in the dam crest (Figures 17, 18 and 19). Carpentier *et al.* (2012) also used GPR data to image flower structures along the Alpine fault (New Zealand), although the authors did not differentiate between positive and negative types, and most GPR sections seem to mostly show positive-flower structures.

Figure 21 shows a geological section which cuts across the northern study area, as this is where the largest amount of geological, geophysical and focal earthquake mechanism evidence has currently been recorded (see location in Figure 21).

This section shows faulting near the "Presas El Hundido" site, in which a negative flower structure produced by a left-lateral fault was interpreted. Even though there is evidence of transpressional deformation, the dominant structural style is still transtensional (see Figures 18c and 18d), and it is the one shown on Figure 21. Faulting near the western end of the profile is inferred with geomorphological criteria, but it is probably related to faulting near the "Jaral" and "Banco de material" site, since it has the same strike, so it is most likely generated by a positive flower structure. Figure 21 also shows that, at the "Presas El Hundido" site, the fault zone could potentially have at least 120 m deep, and 979 m wide, which could have both serious seismic hazard and land planning implications, especially for the Villa de Reyes area (see Figure 22).

Figure 22 shows the structural map of the southern portion of the Villa de Reyes Graben, which integrates field, geophysical evidence, and a focal mechanism solution of the September 5, 2021, San Felipe (Guanajuato) earthquake, which had a magnitude M_w of 4.5, and a focal depth of 5 km (SSN 2021). As can be interpreted in Figure 22, NW-SE right lateral oriented faults dominate the southern portion of our study area, while NE-SW left-lateral faults predominate on the northern one (The Río Jaral site is where the change in direction to the structural regime of the "Presas El Hundido" site probably occurs). Faulting is mainly located in quaternary deposits, and at the center of the valley, so this means that these faults are younger than the normal faults which bound the graben. Figure 22 also shows that even though there are several faulting orientations, the most predominant are the ones generated by the faulting that crosses the "Banco de material" and "Presas El Hundido" sites (see both rose diagrams near those sites in Figure 22).

The previously mentioned earthquake focal mechanism solution shows two possible fault planes: NE-SW left lateral and NW-SE right lateral faults, which agrees with our geological, geophysical and structural data (Figure 22). This gives confidence in our interpretation. As can be seen in Figure 22, NW-SE faults (like the ones located in the “Banco de material” site) seem to be the more active ones since this is where epicenters have tended to cluster for the last 30 years.

The coexistence of positive and negative type flower structures within a few meters, like in the “Banco de material” site, although is not so common at the scale of individual strike-slip basins (Barnes *et al.* 2001), the Ground Penetrating Radar sections and field evidence have shown that they could also be present at the metric scale. This interpretation is also supported by the presence of a small (meter long) pull-apart basin in the “Río Jaral” site, which are mostly common at the km scale. This also shows that geological structures and processes can be present at all scales.

Finally, a methodology for the study of active faults was successfully used in the study area (Figure 3):

- First, survey the area for geological evidence of faulting, using standard criteria such as Petit (1987) where available. Paying special attention to man-made structures showing evidence of being affected by faults.
- Second, survey the study area with fast and accurate profiling methods, like Electromagnetic Profiling. With this, the definition of the main apparent resistivity anomalies (whether it be resistive or conductive) that are associated with the subsurface continuation of surface faults will be possible. This will also be of help in mapping the chosen study site’s faulting distribution, showing faults that are not currently outcropping.
- Third, further characterize the previously defined fault zones using more detailed geophysical methods such as Electrical Resistivity Tomography or Ground Penetrating Radar (if field conditions allow it).

- Finally, non-geological evidence such as focal mechanism could be of help in confirming (or not) the type of faults kinematics affecting your study area.

The main limitations of the presented methodology which could hinder correct interpretation are as follows:

- Fault planes dip does not seem to be correctly represented in the Ground Penetrating Radar sections. For example, the most surficial “petals” of both positive and negative structures outcrop as mostly low dip angle planes, but in the geophysical sections they tend to be imaged as if they were almost vertical (see example in Figure 19). This may be due to the low resolution of the method, which is specially intensified in areas with high content of clay deposits (like in the “Presa El Hundido” site). Using a more high-resolution method, for instance, seismic reflection profiles (which also tend not to be as affected by clay content as electromagnetic methods) could help in geophysical sections showing the fault plane’s true dip.
- Electromagnetic Profiling seems to be ideal when clay content is not so abundant (like in the “Banco de material” site). But when clayey deposits are more common, for instance, in the “Presa El Hundido” site, it does not show enough detail of the mapped structures. In this case, using a capacitively-coupled resistivity meter for Resistivity Mapping may be a way of keeping away from this issue.

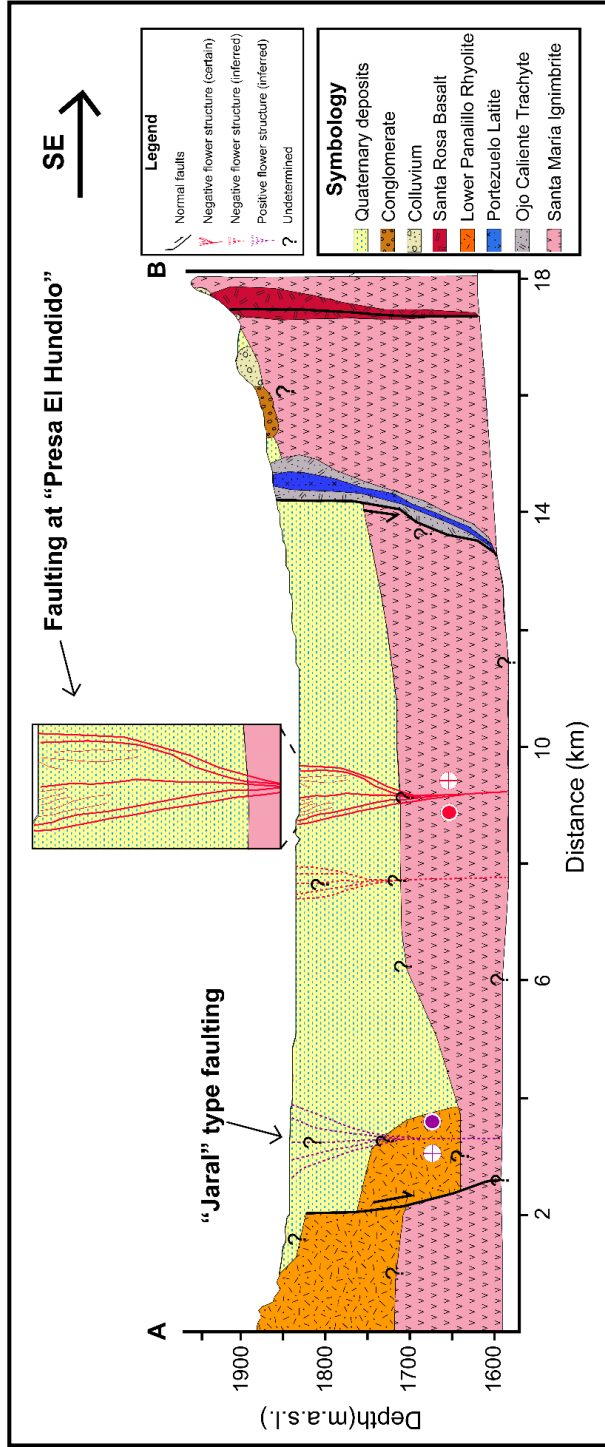


Figure 21 Geological section crossing the northern section of our study area. Notice how the negative flower structure is the dominant structural force at the "Presas El Hundido" site. See location in Figure 22.

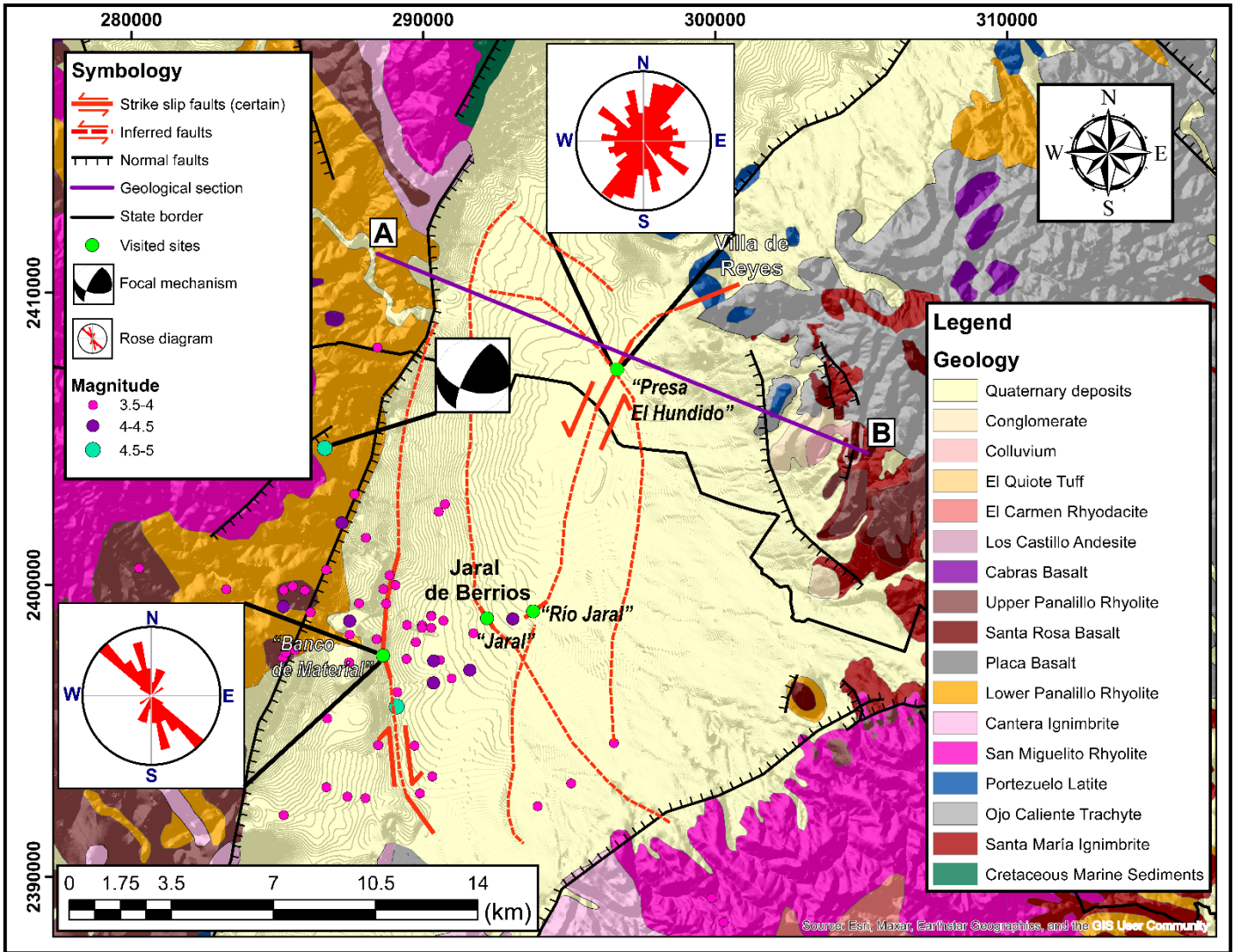


Figure 22 Structural map of the southern portion of the Villa de Reyes Graben. Figure also shows the location of the geological section. Geology and normal faults after López-Loera &Tristán-González (2013), and Soto-García (2022), with modifications and redefinition of faulting limits and geological contacts using Landsat 8 images, processed using ArcMap 10.8, version 10.0.0.10450 (ESRI,2019). Focal mechanism solution after SSN (2021). Epicenter data after SSN (2024). Topographic data after INEGI (2023).

6. CONCLUSIONS

A geological and geophysical study was conducted in the southern portion of the Villa de Reyes Graben, at four sites located in the vicinity of the towns of Villa de Reyes (San Luis Potosí), and Jaral de Berrios (Guanajuato).

Electromagnetic Profiling results show (mainly) high apparent resistivity anomalies, related to the subsurface presence of non-filled fractures which do not always outcrop at surface. These anomalies agreed both in orientation and location with exposed fractures. The Electrical Resistivity Tomography method was used to further characterize the areas defined by Electromagnetic Profiling, showing evidence of nearly vertical fractures at depth, which join at greater depths, which agrees with field evidence of positive and negative flower type structures. Ground Penetrating Radar sections helped in better understanding the transpressional and transtensional structures which were only glimpsed using Electrical Resistivity Tomography sections, since the former method has higher resolution than the latter. Using Ground Penetrating Radar, both positive and negative flower type structures were confirmed as being the ones most related to the faulting that impacts our study site.

Both field and geophysical evidence revealed evidence of mainly NE-SW trending left-lateral faulting on the northern portion of our study area, while NW-SE trending right-lateral faults dominate on the southern portion, which generate both transpressional and transtensional stress fields. This also agrees with focal mechanism and epicenter data from the September 5, 2021, San Felipe (Guanajuato) earthquake, which gives confidence to our interpretation. This study helped establish that there is more than normal type faulting involved in the tectonics of Villa de Reyes Graben.

Finally, the applied methodology for the study of active faults in this study can be useful in both similar and different geological environments, using other geophysical methods depending on the geological and geophysical constraints of each site.

This study shows that faulting that currently has limited extension on the surface not only continues at depth, but also has a wider extension, so the risk of expansion of this faulting is very high. Since the length and width of the fault zones have been defined, both at surface and at depth, this study could have implications both from seismic hazard and land planning points of view, contributing to the decision making of farmers and local landowners when choosing the best locations for their activities. Thus, it is expected that this study to be followed up by more regional studies that contextualize the active tectonics of the study area with other areas within the Central Mesa Tectonic province. It is also expected that, given that the tectonics of the VRG are more complex than previously thought, detailed studies will be carried out within the study area to properly establish how active faulting continues to evolve.

ACKNOWLEDGEMENTS

This work was supported by grants from the Instituto Potosino de Investigación Científica y Tecnológica A.C. (IPICYT) and by the Consejo Nacional de Humanidades, Ciencias y Tecnologías (CONAHCYT). No additional grants to carry out or direct this work were received. Special thanks to Halia Azucena Reynoso-Reynoso for helping with seismic data processing and to Geovanni Daniel Ortiz-Ochoa for helping with the structural data acquisition and processing. We would also like to thank Oscar Guadalupe Almanza-Tovar, Ana Beatriz Rubio-Arellano, Alexa Sofía Sánchez-Barrientos, Karen Hernández-Reyes, Montserrat Lemus-Rueda, Saira Diego-Olmedo, Ulises Gerón-Flores, Ximena Trejo-Martínez, Sarahí Méndez-Torres, Josué Andrade- Hernández, Ariel Yossel Padilla-Guzmán, Diana Martínez-Hernández and Erika Loyola-Martínez for their field work assistance, without which this work would not have been possible.

DATA AVAILABILITY STATEMENT

The data that support the findings of this study are available from the corresponding author upon reasonable request.

REFERENCES

- Adepelumi, A.A., Yi, M.J., Kim, J.H., Ako, B.D., & Son, J.S., (2006) Integration of surface geophysical methods for fracture detection in crystalline bedrocks of southwestern Nigeria. *Hydrogeology Journal* 14, 1284-1306. <https://doi.org/10.1007/s10040-006-0051-2>
- Ahmad, N., Xiaodong, L., Zhijun, G., & Abbas, A., (2020) Electrical resistivity imaging of active faults in palaeoseismology: case studies from Karachi Arc, southern Kirthar Fold Belt, Pakistan. *NRIAG Journal of Astronomy and Geophysics* 9(1), 116-128. <https://doi.org/10.1080/20909977.2020.1722524>
- Allmendinger, R.W., Cardozo, N., & Fisher, D.M., (2011) *Structural geology algorithms: Vectors and tensors*. Cambridge University Press, London.
- Al-Shiejiri, S.J.D., (2013) *Investigation of Subsidence Phenomena by GPR Technique and Geotechnical Evaluation in Baghdad City* [Doctoral Dissertation]. University of Baghdad.
- Aray-Castellano, J.C., Lacan, P., Garduño-Monroy, V.H., Ávila-García, J., Gómez-Cortés, J., Audmard-M, F.A., Lázaro-Mancilla, O., & Bandy, W., (2021) Geophysical characterization of a potentially active fault in the Agua Fría micrograben, Los Azufres, México. *Boletín de la Sociedad Geológica Mexicana* 73(2), A040121. <https://doi.org/10.18268/BSGM2021v73n2a040121>
- Barnes, P.M., Sutherland, R., Davy, B., & Delteil, J., (2001) Rapid creation and destruction of sedimentary basins on mature strike-slip faults: An example from the offshore Alpine Fault, New Zealand. *Journal of Structural Geology* 23(11), 1727-1739. [https://doi.org/10.1016/S0191-8141\(01\)00044-X](https://doi.org/10.1016/S0191-8141(01)00044-X)
- Blindow, N., (2009). Ground Penetrating Radar. In: Kirsch, R. (Ed.) *Groundwater Geophysics: A Tool for Hydrogeology*, Springer, Verlag Berlin Heidelberg, pp. 227-252.
- Botero-Santa, P.A., Xu, S., Nieto-Samaniego, Á.F., & Alaniz-Álvarez, S.A., (2020) Efecto de las fracturas de enfriamiento en la formación de fallas normales: El ejemplo de Santa María del Río, San Luis Potosí, México. [Influence of

- cooling fractures on the formation of normal faults: a case study in Santa María del Río, San Luis Potosí, México]. *Boletín de la Sociedad Geológica Mexicana* 72(1), <https://doi.org/10.18268/bsgm2020v72n1a011019>
- Bran, D.M., Tassone, A., Menichetti, M., Cerredo, M.E., Lozano, J.G., Lodolo, & E., Vilas, J.F., (2018) Shallow architecture of Fuegian Andes lineaments based on Electrical Resistivity Tomography (ERT). Evidences of transverse extensional faulting in the central Beagle Channel area. *Andean Geology* 45(1), 1-34. <http://dx.doi.org/10.5027/andgeov45n1-3002>
- Butnor, J.R., Doolittle, J.A., Johnsen, K.H., Samuelson, L., Stokes, T., & Kress, L., (2003) Utility of ground-penetrating radar as a root biomass survey tool in forest systems. *Soil Science Society of America Journal* 67, 1607-1615. <https://doi.org/10.2136/sssaj2003.1607>
- Cardozo, N., & Allmendinger, R.W., (2013) Spherical projections with OSXStereonet. *Computers and Geosciences* 51, 193-205. <https://doi.org/10.1016/j.cageo.2012.07.021>
- Carpentier, S. F. A., Green, A. G., Langridge, R., Boschetti, S., Doetsch, J., Abächerli, A. N., Horstmeyer, H., & Finnemore, M., (2012) Flower structures and Riedel shears at a step over zone along the Alpine Fault (New Zealand) inferred from 2-D and 3-D GPR images. *Journal of Geophysical Research: Solid Earth* 117(B2). <https://doi.org/10.1029/2011JB008749>
- Cauich-Kau, D.D.A., Cardona-Benavides, A., Castro-Larragoitia, G.J. & Rúde, T.R., (2021) Understanding Arsenic and Uranium Sources and Mobility in Groundwater Flow Systems from Two Areas in San Luis Potosi, Mexico: Cerritos and Villa de Reyes Basins. *Lehr-und Forschungsgebiet Hydrogeologie* No. RWTH-2021-09796. <https://doi.org/10.18154/RWTH-2021-09796>.
- Cinti, F.R., Pauselli, C., Livio, F., Ercoli, M., Brunori, C.A., Ferrario, M.F., Volpe, R., Civico, R., Pantosti, D., Pinzi, S., De Martini, P.M., Ventura, G., Alfonsi, L., Gambillara, R., & Michetti, A.M., (2015) Integrating multidisciplinary, multiscale geological and geophysical data to image the Castrovillari fault

- (Northern Calabria, Italy). *Geophysical Journal International* 203(3), 1847–1863. <https://doi.org/10.1093/gji/ggv404>
- DECO-Geophysical, (2005) *User Manual: RadExplorer 1.4, the Software for GPR data processing and interpretation*. Mala Geoscience, Moscow.
- Drahor, M. G., & Berge, M. A., (2017) Integrated geophysical investigations in a fault zone located on southwestern part of İzmir city, Western Anatolia, Turkey. *Journal of Applied Geophysics* 136, 114-133. <https://doi.org/10.1016/j.jappgeo.2016.10.021>
- Del Pilar-Martínez, A., Nieto-Samaniego, A.F., Alaniz-Álvarez, S.A., & Ángeles-Moreno, E., (2020) Geology of the southern Mesa Central of Mexico: recording the beginning of a polymodal fault system. *Journal of Maps* 16(2), 199-211. <https://doi.org/10.1080/17445647.2020.1719911>
- ESRI, (2019) ArcMap 10.8 (Version 10.0.0.10450) [Software]
- Figueroa-Miranda, S., Tuxpan-Vargas, J., Ramos-Leal, J.A., Hernández-Madrigal, V.M., & Villaseñor-Reyes, C.I., (2018) Land subsidence by groundwater over-exploitation from aquifers in tectonic valleys of Central Mexico: A review. *Engineering Geology* 246, 91-106. <https://doi.org/10.1016/j.enggeo.2018.09.023>
- Galone, L., Villani, F., Colica, E., Pistillo, D., Baccheschi, P., Panzera, F., Galindo-Zaldívar, J., & D'Amico, S., (2024) Integrating near-surface geophysical methods and remote sensing techniques for reconstructing fault-bounded valleys (Mellieha valley, Malta). *Tectonophysics* 875, 230263. <https://doi.org/10.1016/j.tecto.2024.230263>
- Geotomo Software, (2002) Red2DInv (Version 3.4) [Software]
- Golden Software, (2019) Surfer 16 (Version 16.3.408) [Software]
- Gunda, G.K.T., Balaji, S., Champati-Ray, P.K., Bhat, G.R., Balakrishna, & Kannaujia, S., (2020) Geophysical Characterization of the Active Fault Geometry and Trends in Tectonic Deformation in the Shallow Stratigraphy along Active Faults, South Andaman, India. *Journal of the Geological Society India* 95, 286–292. <https://doi.org/10.1007/s12594-020-1427-y>

- Hasan, M., Shang, Y., Meng, H., Shao, P., & Yi, X., (2021) Application of electrical resistivity tomography (ERT) for rock mass quality evaluation. *Scientific Reports* 11(1), 23683. <https://doi.org/10.1038/s41598-021-03217-8>
- Henry, C.D., & Aranda-Gómez, J.J., (1992) The real southern Basin and Range: Mid to late Cenozoic extension in Mexico. *Geology* 20, 701-704. [https://doi.org/10.1130/0091-7613\(1992\)020<0701:TRSBAR>2.3.CO;2](https://doi.org/10.1130/0091-7613(1992)020<0701:TRSBAR>2.3.CO;2)
- Instituto Nacional de Estadística y Geografía (INEGI), (2013) Continuo de Elevaciones Mexicano. <https://www.inegi.org.mx/app/geo2/elevacionesmex/> (accessed 10 April 2023).
- Kuria, Z.N., Woldai, T., Van Der Meer, F.D., & Barongo, J.O., (2010) Active fault segments as potential earthquake sources: Inferences from integrated geophysical mapping of the Magadi fault system, southern Kenya Rift. *Journal of African Earth Sciences* 57, 345-359. <https://doi.org/10.1016/j.jafrearsci.2009.11.004>
- Konon, A., Ostrowski, S., Rybak-Ostrowska, B., Ludwiniak, M., Śmigielski, M., Wyglądała, M., Uroda, J., Kowalczyk, S., Mieszkowki, R., & Kłopotowska, A., (2016) Mnin restraining stepover—evidence of significant Cretaceous–Cenozoic dextral strike-slip faulting along the Teisseyre-Tornquist Zone?. *Acta Geologica Polonica* 66(3), 429-449. <https://doi.org/10.1515/agp-2016-0019>
- Labarthe-Hernández, G., Tristán-González, M., & Aranda-Gómez, J.J., (1982) *Revisión estratigráfica del Cenozoico de la parte central del Estado de San Luis Potosí*. [Stratigraphic revision of the Cenozoic of central part of the State of San Luis Potosí]. Universidad Autónoma de San Luis Potosí, San Luis Potosí.
- Loke, M.H., & Barker, R.D., (1996) Rapid least-squares inversion of apparent resistivity pseudosections using a quasi-Newton method. *Geophysical Prospecting* 44, 131–152. <https://doi.org/10.1111/j.1365-2478.1996.tb00142.x>
- Loke, M.H., (2021) *Tutorial: 2-D and 3D Electrical Imaging Surveys. RES2DINV ver. 3.59. 2D Resistivity and IP inversion program*. Geotomo Software, Penang.

- López-Loera, H., &Tristán-González, M., (2013) Geología y magnetometría aérea del Graben de Villa de Reyes, San Luis Potosí, Mesa Central de México: Implicaciones tectónicas y geohidrológicas. [Geological and aeromagnetic mapping of the Villa de Reyes Graben, San Luis Potosí, Mesa Central of México: Hydrogeological and tectonic implications]. *Boletín de la Sociedad Geológica Mexicana* 65(1), 137-156. <https://doi.org/10.18268/BSGM2013v65n1a11>
- Martos, J.R., (2012) *Fault Mapping with the Refraction Microtremor and seismic refraction methods along the Los Osos Fault Zone* [Master Dissertation]. California Polytechnic State University.
- McNeill, J.D., (1980) *Electromagnetic terrain conductivity measurements at low induction numbers, technical note TN-6*. Geonics Limited, Ontario.
- Milsom, J., (2003) *Field Geophysics*. John Wiley & Sons Ltd, London.
- Monahan, S.M., (2013) *Investigating Fault Structure Using Electrical Resistivity Tomography* [Master Dissertation]. California Polytechnic State University
- Monge-Cerda, F. E., Delgado-Rodríguez, O., Ramos-Leal, J. A., & Sánchez-Higueredo, L. E. (2024) Geoelectrical characterization of non-filled active faults in Jaral de Berrios, Guanajuato, México. *Journal of Applied Geophysics* 227, 105431. <https://doi.org/10.1016/j.jappgeo.2024.105431>
- Nieto-Samaniego, A.F., Alaniz-Alvarez, S.A., & Camprubí, A., (2005) La Mesa Central de México: estratigrafía, estructura y evolución tectónica cenozoica. [Mesa Central of México: Stratigraphy, structure, and Cenozoic tectonic evolution]. *Boletín Sociedad Geológica Mexicana* 57(3), 285-318. <https://doi.org/10.18268/bsgm2005v57n3a3>
- Petit, J.P., (1987) Criteria for the sense of movement on fault surfaces in brittle rocks. *Journal of Structural Geology* 9(5-6), 597-608. [https://doi.org/10.1016/0191-8141\(87\)90145-3](https://doi.org/10.1016/0191-8141(87)90145-3)
- Porras, D., Carrasco, J., Carrasco, P., & González, P.J., (2022) Imaging extensional fault systems using deep electrical resistivity tomography: A case study of the Baza fault, Betic Cordillera, Spain. *Journal of Applied Geophysics* 202, 104673. <https://doi.org/10.1016/j.jappgeo.2022.104673>

- Reynolds, J., (1997) *An Introduction to Applied and Environmental*. John Wiley and Sons, West Sussex.
- Rodríguez-Robles, U., (2016) *Geoeohydrological mechanism in semiarid tropical forests: spatial and temporal use of water of two coexisting forest tree species* [Doctoral Dissertation]. Instituto Potosino de Investigación Científica y Tecnológica (IPICYT).
- Sasaki, Y., (1992) Resolution of resistivity tomography inferred from numerical SIMULATION1. *Geophysical Prospecting* 40(4), 453-463. <https://doi.org/10.1111/j.1365-2478.1992.tb00536.x>
- Servicio Sismológico Nacional (SSN), (2021) Secuencia Sísmica del 4 a 6 de septiembre de 2021, Guanajuato-San Luis Potosí (M 4.5). [Seismic Sequence from 4 to 6 September 2021, Guanajuato-San Luis Potosí (M 4.5.)]. National Seismological Survey website. <http://www.ssn.unam.mx> (accessed 7 September 2021).
- Servicio Sismológico Nacional (SSN), (2024) Earthquake Catalog. National Seismological Survey website. <http://www2.ssn.unam.mx:8080/catalogo/> (accessed 22 March 2024).
- Soto-García, A.G., (2022) *Análisis estructural del Graben de Santa Rosa, San Luis Potosí y Guanajuato*. [Structural Analysis of the Santa Rosa Graben, San Luis Potosí and Guanajuato] [Master Dissertation] Universidad Autónoma de San Luis Potosí (UASLP).
- Stewart, J.H., (1998) Regional characteristics, tilt domains, and extensional history of the late Cenozoic Basin and Range province, western North America. *Special Paper of the Geological Society of America* 47-74. <https://doi.org/10.1130/0-8137-2323-X.47>
- Suski, B., Brocard, G., Authemayou, C., & Consenza, B., (2010) Localization and characterization of an active fault in an urbanized area in central Guatemala by means of geoelectrical imaging. *Tectonophysics* 480, 88-698. <https://doi.org/10.1016/j.tecto.2009.09.028>

- Thabit, J.M., & Al-Zubedi, A.S., (2015) Evaluation of three important electrode arrays in defining the vertical and horizontal structures in 2D imaging surveys. *Iraqi Journal of Science* 56(2B), 1465-1470.
- Tristán-González, M., (1986) *Estratigrafía y tectónica del graben de Villa de Reyes, en los estados de San Luis Potosí y Guanajuato, México, Folleto Técnico 107*. [Stratigraphy and tectonics of the Villa de Reyes Graben, in the states of San Luis Potosí and Guanajuato, México, Technical Report number 107]. Universidad Autónoma de San Luis Potosí (UASLP), San Luis Potosí.
- Tristán-González, M., Aguillón-Robles, A., Barboza-Gudiño, J.R., Torres-Hernández, J.R., Herve, B., López-Doncel, R., Rodríguez-Ríos, R., & Labarthe-Hernández, G., (2009) Geocronología y distribución espacial del vulcanismo en el Campo Volcánico de San Luis Potosí. [Geochronology and spatial distribution of de vulcanism inside de Volcanic Field of San Luis Potosí]. *Boletín de la Sociedad Geológica Mexicana* 61 (3), 287-303.
- Wang, Z., Cai, X., Yan, J., Wang, J., Liu, Y., & Zhang, L., (2017) Using the integrated geophysical methods detecting active faults: A case study in Beijing, China. *Journal of Applied Geophysics* 156, 82-91. <https://doi.org/10.1016/j.jappgeo.2017.01.030>
- Yong Technology Inc., (2013) GeoRose (Version 0.5.2.0) [Software].

Chapter 5-. Active faulting and its relationship with regional hydrogeological regimes: a case study in the Villa de Reyes Graben

This chapter is based on an article where Aeromagnetic, epicenter, and major ion data was used to establish the extent to which the southern portion of the Villa de Reyes Graben faults can act as contaminant pathways, and also to confirm and/or redefine the structural style established on Chapter 4, by authors: M.Sc. Fabián Esteban Monge-Cerda, Dr. José Alfredo Ramos-Leal, Dr. Omar Delgado-Rodríguez, Dr. José Ramón Torres-Hernández, and Dr. Mayla Alhelí Ramos-Vázquez. It was submitted for publication to **Pure and Applied Geophysics**.

Active faulting and its relationship with regional hydrogeological regimes: a case study in the Villa de Reyes Graben, Central México

Fabián Esteban Monge-Cerda¹ • José Alfredo Ramos-Leal^{1*}(0000-0003-4715-7411) • Omar Delgado-Rodríguez¹(0000-0001-7027-2560) • José Ramón Torres-Hernández²(0000-0002-0624-0780) • Mayla Alheli Ramos-Vázquez ¹(0000-0001-9155-4313)

¹División de Geociencias Aplicadas, Instituto Potosino de Investigación Científica y Tecnológica A.C. (IPICYT), San Luis Potosí, 78216, México

² Facultad de Ingeniería, Universidad Autónoma de San Luis Potosí, San Luis Potosí, 78290, México

*Corresponding autor: jalfredo@ipicyt.edu.mx

Abstract

The Villa de Reyes Graben is a tectonic basin where structural studies have focused mainly on normal faulting, but little attention has been given to the active strike-slip faults in its interior. This study integrates aeromagnetic, geoelectric, hydrogeochemical, and 3D aeromagnetic analysis, to study the likelihood that active faults act as contaminant pathways, and the way these active faults influence the regional hydrogeological regime. Aeromagnetic data shows anomalies with similar orientation of mapped faults, and alternates zones of magnetic lows and highs, which could be interpreted as both positive and negative flower structures influencing the area. The western sector of the study area shows the lowest magnetic anomaly values, which also agrees with the cluster of recent seismic activity epicenters. Geoelectric data show how water infiltration takes place through shallow non-filled fractures, which alter the water table at greater depths. Hydrogeochemical profiles across the area reveal that meteoric water influence tends to increase near the more tectonically active western sector and decrease in the less active eastern sector. Geothermometer analysis shows that geothermal water influence appears to be non-existent. Finally, 3D faulting analysis suggests that surface faults affecting the study area appear to merge at depth, which could indicate that the tectonics of the area are controlled by flower structures. This study reveals which zones could act as either barriers or pathways for contaminants, which could have implications for land use planning in the study area.

Keywords: Aeromagnetic data, hydrogeochemical analysis, positive and negative flower structures, active faulting, Villa de Reyes Graben.

1. Introduction

The link between geological faults and groundwater has been extensively studied for several years (Caine et al., 1996; Bense & Person, 2006; Grauch & Hudson, 2007; Bense et al., 2013; Cilona et al., 2015; Boubaya, 2017; Fronzi et al., 2021; Hacıoğlu et al., 2021; Jolie et al., 2021; Meneisy et al., 2021; Piña-González et al., 2021; Bustamante-Orozco et al., 2023).

In the previously mentioned studies, the two most widely used methods to study the role of faults in regional hydrogeological regimes are aeromagnetic (AM) and hydrogeological methods. AM methods have a great number of applications such as geotectonic studies, geologic mapping, and solid minerals, as well as oil and natural gas prospecting, city stability evaluation, geologic hazard prediction, and other geoscience studies (Zou et al., 2013). For example, Meneisy et al. (2021) used AM, ground-based magnetic and satellite imagery data to delineate surface and subsurface structures to clarify its impacts on groundwater flow direction, and to establish the thickness of the aquifer in the study area (Wadi El Amal, Aswan, Egypt). The surface water movement was shown to be towards lake Nasser (SW of the study area), while AM data interpretation showed a NW-SE structural trend, which may increase the potentiality of ground-water flow from that lake to the aquifer beneath the fracture system. Finally, the depth to the water table ranges from 77 to 89 m, and depth to the basement based on AM data was found to be more than 300 to 700 m below the ground surface. Bustamante-Orozco et al. (2023) interpreted magnetic

and gravimetric subsurface responses in the western portion of the Grijalva basin, México, to identify and delimit areas of rock units with aquifer potential, especially faulted areas. Several filters were used, but the Tilt Derivative (TDR) was the most useful for both data types, and for better delineation of geophysical lineaments associated with the study area's structural style. Of all these lineaments, the ones located in the central-northern portion are the most promising of having aquifer potential.

On the other hand, hydrogeological methods have been mostly applied to study fault zone permeability to assess aquifer potential and the likelihood of fault zones acting as contaminant pathways. For instance, Ciloná et al. (2015) combined structural and hydrogeological data to interpret the hydraulic-head drop measured across a fault (named Shear Zone fault) within the sandstones and shales of the Chatsworth Formation in Southern California, USA. Hydraulic heads based on 30 wells data show a drop of 75 m across this fault, which the authors interpret to be a result of the low conductivity of the fault core. The authors conclude that the results of their study are consistent with numerical modeling, which requires a low-permeability fault core to simulate the observed hydraulic head differences. Piña-González et al. (2021) performed analyses that include hydrochemical (Multivariate cluster and Principal Components Analyses (PCA)), mineralogical, and satellite images to identify the main processes that contribute to the concentration of total inorganic arsenic (iAs) in groundwater within the northern portion of the Laguna Seca aquifer in Guanajuato, México. The groundwater samples were classified in two groups according to their chemical composition: Cluster II had the highest temperature,

mineralization, and it was more influenced by a regional flow than Cluster I. The newly mapped geological faults allowed the interpretation of the origin of iAs in both clusters, which comes from regional flows impacted by pumping, and the highest concentration of iAs probably comes from the added impact of the deepest, hottest regional flows ascending through geological faults.

As can be noticed in the cited examples, both methods are usually applied separately, and their application for studying the link between faults and contaminant pathways to aquifers has yet to be made. Moreover, most of those studies do not deal with the relationship between active geological faults and groundwater. In this study, AM data has been used with the main objective of establishing the extent to which active faults can be pathways for contaminants by comparing four AM profiles, with major ions sections, while a Giggenbach (1991) diagram was used to define the origin of these waters. It is also one of the goals of this study to assess if geological structures mapped in previous studies (e.g. Monge-Cerda et al., 2025, sites “Banco de material” and “Presa El Hundido” from that study, Fig. 1) can play a role in the hydrogeological regime of the studied area.

1.1. Study Area

The study area is located in the States of San Luis Potosí and Guanajuato inside the bigger tectonic structure of the Villa de Reyes Graben (VRG, Fig. 1) a ~ 100 km long valley mainly filled with Quaternary deposits, with thickness that ranges from 50 to 250 m (Tristán-González, 1986), and it is located in the southern portion of the tectonic province known as the Mesa Central. To date, no studies have been made to assess the role of active geological faults in this area’s regional aquifer. Two sites

from the Monge-Cerda et al. (2025) study were visited to corroborate some of the structures described in that work, and to find new ones if possible (Fig. 1)

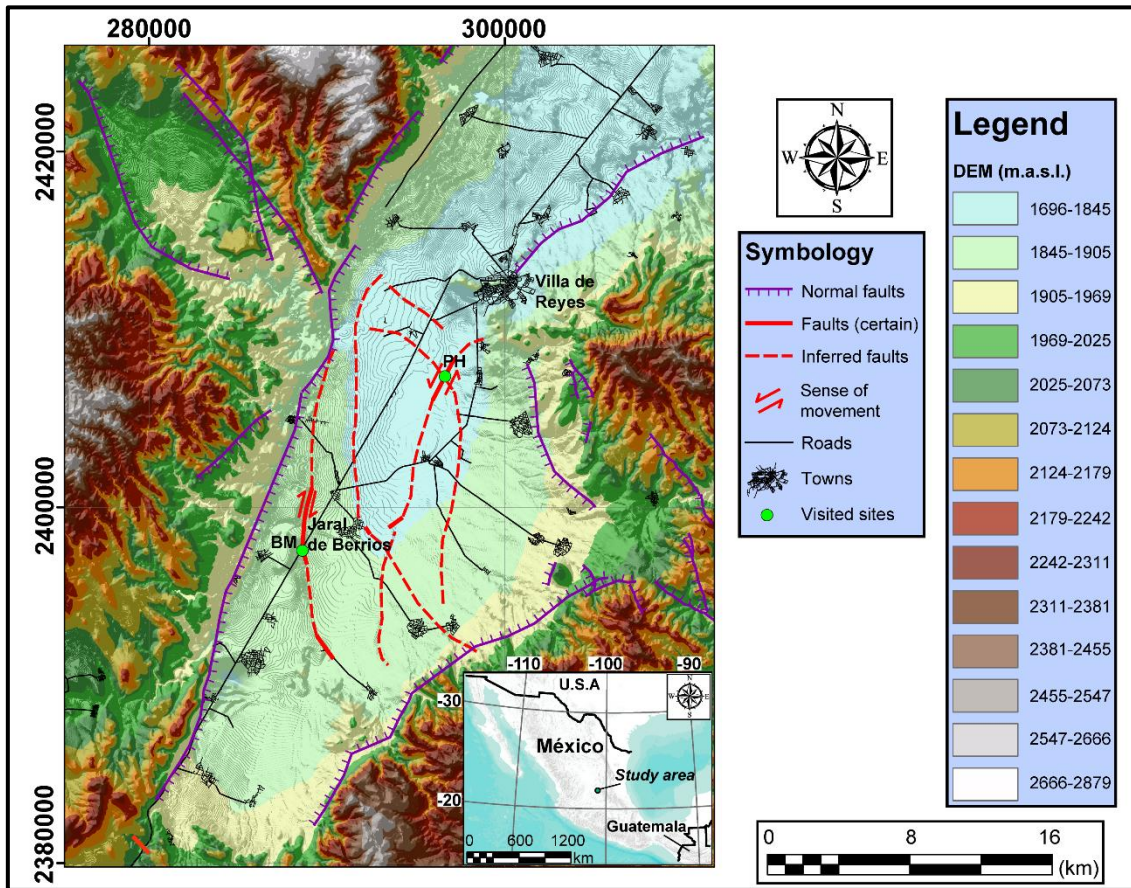


Fig. 1 Study area located in central region of Mexico (Municipalities of Villa de Reyes in the State of San Luis Potosí (north) and Jaral de Berrios in the State of Guanajuato (south)). Two visited sites: “Banco de material” (BM) and “Presas El Hundido” (PH). Modified after Labarthe-Hernández (1982), López-Loera & Tristán-González (2013), Soto-García (2022), INEGI (2023), and Monge-Cerda et al. (2025)

2. Fault zone permeability

Caine et al. (1996) defined the primary components of upper-crustal fault zones as fault core, damage zone, and protolith (Fig. 2a). Fluid properties of a fault zone may change, for example, the core may act as a conduit during deformation and as a barrier when open pore space is filled by mineral precipitation during deformation. The fault core is defined as the structural, lithologic, and morphologic portion of a fault zone where most of the displacement is accommodated. Grain-size reduction and/or mineral precipitation generally yield fault cores with lower porosity and permeability, which leads to fault cores that act as barriers to fluid flow. The damage zone is the network of subsidiary structures that bound the fault core and may enhance fault zone permeability relative to the core and the undeformed protolith. Fracture density in the fault core is usually significantly less than in the damage zone, thus, the permeability of the fault core may be dominated by the grain-scale permeability of the fault rocks, whereas the damage zone permeability is dominated by the hydraulic properties of the fracture network (fracture dominated permeability).

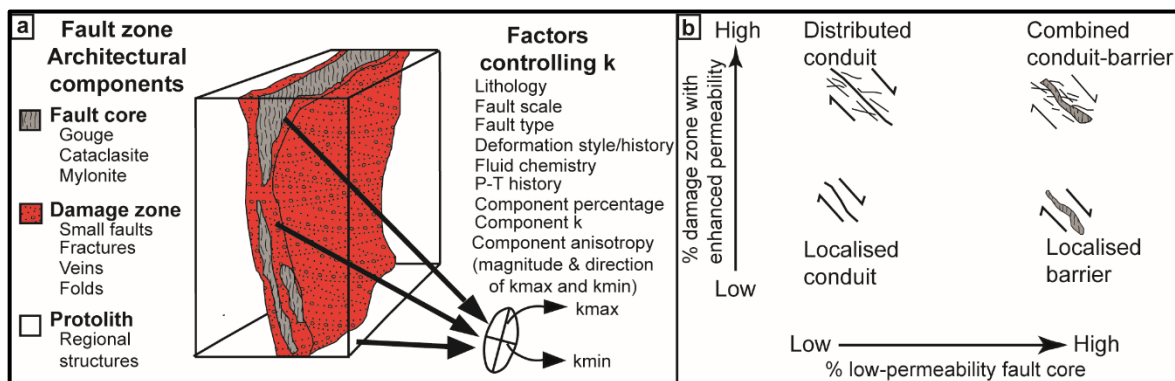


Fig.2 a Conceptual model of a fault zone. The ellipse represents relative magnitude and orientation of the bulk two-dimensional permeability (k) tensor that might be associated

with each distinct architectural component of fault zone. Modified after Caine et al. (1996).

b Description of fault behavior based on the proportion of fault core to damage zone. After
Bense et al. (2013)

The fault core (FC), as the zone of the most intense strain, is generally found in the center of the fault zone and accommodates most of the displacement within the fault zone. The damage zone (DC) has secondary structures such as fractures and minor faults, which take up the remainder of strain within the fault zone. In the FC-DZ framework a measurable fault thickness is defined as perpendicular to the fault strike which is the sum of the fault core and damage zone thickness. The thickness of fault zones increases with fault throw or displacement. This trend is relatively consistent for different types of faults (normal, reverse and strike-slip) in a range of rock types. As mentioned before, fault permeability seems to be greater in and around the DZ, peaking closely to the FC before dropping drastically, probably because of more fracture density in the DZ, where fluid infiltration would concentrate (Caine et al., 1996; Bense et al., 2013).

3. Geological, hydrogeological and structural context of the Villa de Reyes Graben

3.1 Geology and structure

The Villa de Reyes Graben (VRG) is a tectonic basin located inside the Physiographic Province known as the Mesa Central of México, which is an elevated plateau covered by Cenozoic volcanic rocks, encompassing portions of the states of Aguascalientes, Durango, Guanajuato, Jalisco, San Luis Potosí, and Zacatecas (Nieto Samaniego et al., 2007; Botero-Santa et al., 2020; Cauich-Kau et al., 2021). In the following section, a summary of the geology and structure of the study area is

presented for the reader to have a better understanding of the VRG faulting dynamics.

3.1.1. Geology

The VRG mostly includes rocks belonging to the Volcanic Field of San Luis Potosí (VFSLP), Volcanic Complex Sierra de San Miguelito (VCSSM), and Volcanic Complex of Santa María del Río (VCSMR). These fields consist mostly of volcanic rocks that vary from dacites to high silica rhyolites (formed between 32 and 29 Ma), with around 80% of these rocks having an effusive origin, while the rest are pyroclastic products associated with fractures through which the magmas came out (Labarthe-Hernández et al., 1982; Tristán-González, 1986; Tristán-González et al., 2009).

3.1.2. Structural geology

The VRG originated mainly during crustal normal faulting (Fig. 3) that occurred during crustal breakage processes, and which were the main conduits where magma ascended around 32 Ma. The beginning of the subsidence started with the spill of the Latita Portezuelo lavas, and culminated with the formation of the Cantera Ignimbrite, between 32 and 27 Ma (Tristán-González, 1986). The best-defined episodes of extensional tectonics (28, 23 and 12 Ma), appear to be part of regionally extensional intervals, associated with the Basin and Range province of California, Arizona, New Mexico, and Texas (Henry & Aranda-Gómez, 1992; Stewart, 1998; López-Loera & Tristán-González, 2013). This work's study area is located in the southern sector of the Mesa Central, which compared with the northern sector, is

more seismically active and this explains the VRG's recent fault activity (Nieto-Samaniego et al., 2005; Monge-Cerda et al., 2025). This active faulting seems to be taking place since colonial times ("Presa el Hundido" site, Monge-Cerda et al., 2025), as evidenced by reparations being made to the dam structure affected by faulting, identified in field-visits for this work (See Figs 1 and 7b).

3.2 Hydrogeology

The main aquifer that encompasses the study area is defined as the Jaral de Berrios-Villa de Reyes aquifer, labeled by Comisión Nacional del Agua, CONAGUA (National Water Commission) with the code 2412. This aquifer is located in central Mexico, covering northern Guanajuato, corresponding to the Jaral de Berrios Valley, and southeast San Luis Potosí, corresponding to the VRG, with a total area of 2370 km² (CONAGUA, 2023).

3.2.1. Aquifer type

According to the aquifer constitution, it can be described vertically in two parts: the upper aquifer is a perched, unconfined and embedded aquifer located in the alluvial fill of the graben, with a saturated thickness between 5 to 25 m. Since the static level is found to be between 0.5 and 6 m deep, water extraction is done with dug wells and by manual traction for domestic uses and, to a lesser extent, mechanically for irrigation of small plots for self-consumption. The lower aquifer is constituted by alluvial, lacustrine, pyroclastic deposits as well as fractured volcanic rocks within the graben. Thickness varies between 200 and 450 m, and piezometric levels are found between 40 to 120 m (Cauich-Kau et al., 2021; CONAGUA, 2023).

3.2.2. Piezometric levels

According to Carillo-Rivera et al. (1992), the water table levels for shallow groundwaters (upper aquifer) in the Villa de Reyes valley closely follow local topography, which indicates a general flow pattern towards the axis of the valley and north-eastward along the direction of surface drainage. On the other hand, for deep groundwaters (lower aquifer), the piezometric surface has been substantially modified by water extraction over the past decades. Nevertheless, a similar flow direction which is influenced by topography is apparent.

Similarly, according to Cauich-Kau et al. (2021), groundwater flow presents a direction from the recharge areas (mountain ranges) towards the central part of the valley, however to the northeast of Villa de Reyes groundwater flow takes a northeast direction, probably related to zones with high exploitation. Similar results to the latter author are reported here, using piezometric data from CEAG (2021), with the difference that in the piezometric level map (Fig. 3) water overexploitation zones are more evident near the most populated communities (Jaral de Berrios and Villa de Reyes), which is to be expected.

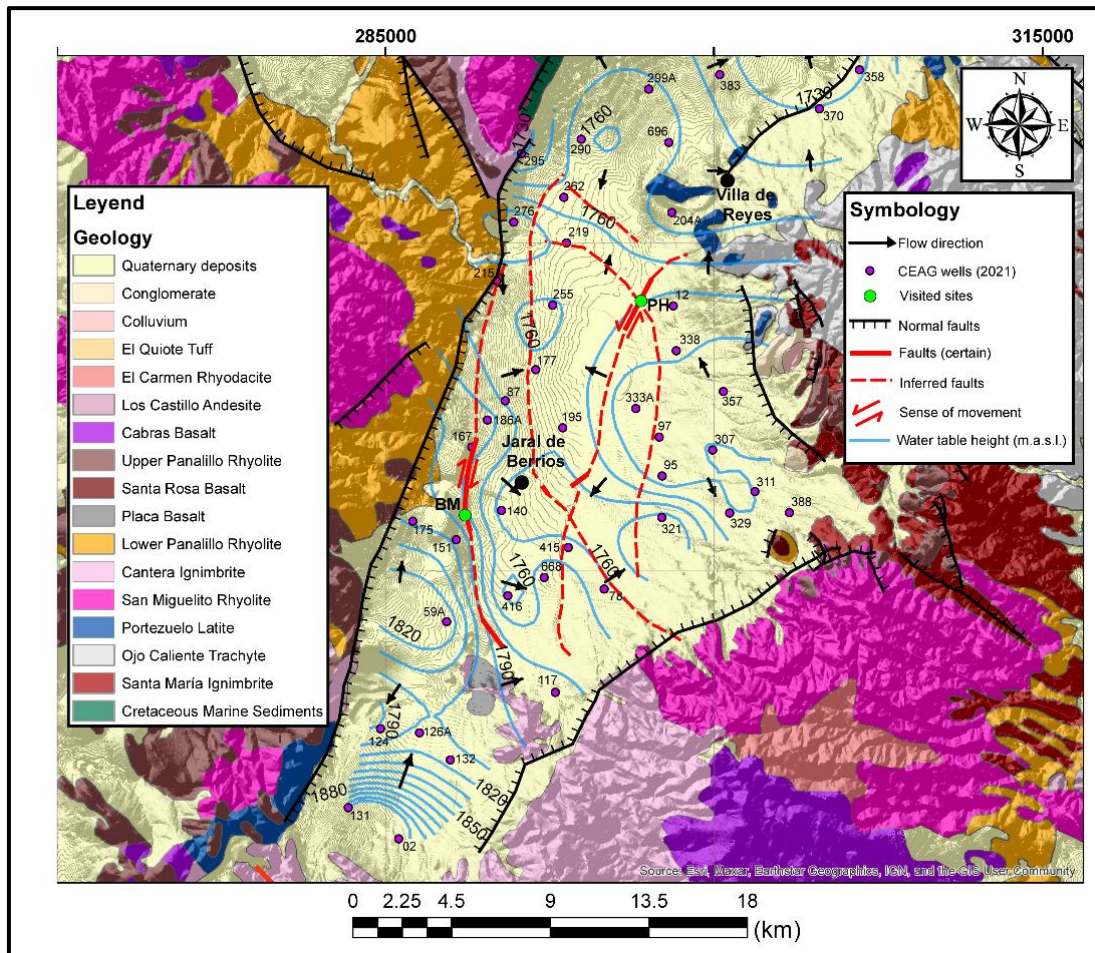


Fig. 3 Piezometric levels for the deep aquifer and geology for the southern portion of the VRG. BM and PH stands for the visited sites “Banco de material” and “Presas El Hundido”, respectively, which were visited for validating the type of faulting. Modified after López-Loera & Tristán-González (2013), CEAG (2021), Soto-García (2022), INEGI (2023), Monge-Cerda et al (2024), and Monge-Cerda et al (2025). Piezometric levels processed using Surfer 16 (Golden Software, 2019)

4. Methods and data processing

4.1 Aeromagnetic (AM) data

Regarding the AM data, the aeromagnetic prospection of the study area was carried out in 1996 by the Mexican Geological Survey (SGM, 1996), using an Islander BN2-B27 aircraft equipped with a Scintrex CS-2 brand Cesium vapor magnetometer with a resolution of 0.001 nanoteslas (nT). The flight height was 450 m with N-S bearing lines at every km in the N-S direction. The data was provided by the IPICYT Geophysics Laboratory and processed using Oasis montaj 8.4 software (Geosoft, 2015). From this analysis, several maps were obtained:

4.1.1. Residual Magnetic Field Map (RMF)

This map, which was provided by the IPICYT Geophysics Laboratory, is obtained by subtracting the International Geomagnetic Reference Field (IGRF) from the Total Magnetic Field (TMF) data, which can be seen in Fig. 4a.

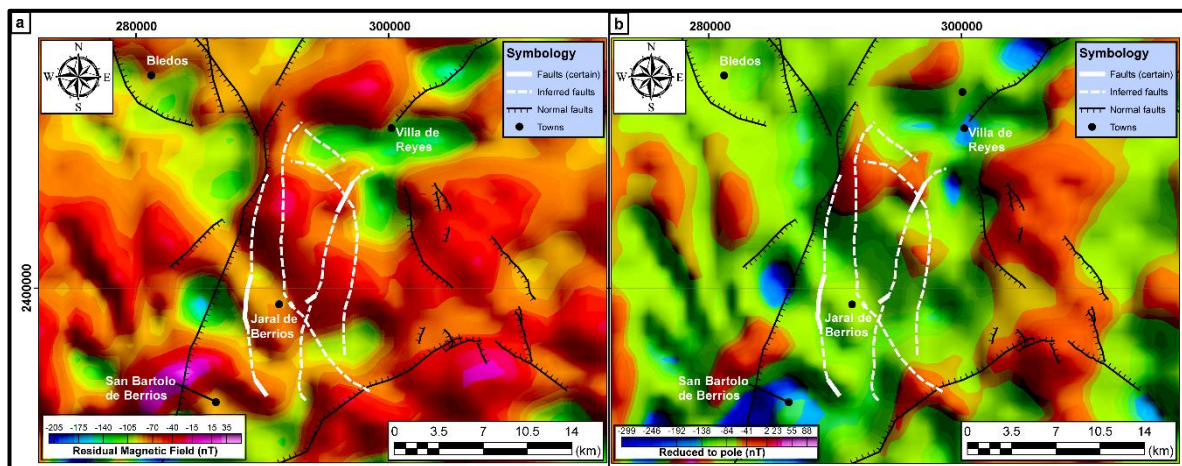


Fig. 4 a Residual Magnetic Field and b Residual Magnetic Field Reduced to Pole map.

Faults after López-Loera & Tristán-González (2013), Soto-García (2022) and Monge-

Cerda et al. (2025)

4.1.2. Residual Magnetic Field Reduced to Pole (RMFRP)

This method simplifies interpretation because for subvertical contacts (including faults), it transforms their asymmetric responses to simpler symmetric and antisymmetric forms (Ganiyu et al., 2012). Thus, one of the advantages of using the RMFRP is that the magnetic anomalies are located directly above the sources that cause them (López-Loera & Tristán-González, 2013).

As can be seen in Fig. 4b, the anomalies are more clearly defined in that map, and the data tends to be less noisy. This map was also used as a basis for the creation of the maps that will be explained in the remainder of this report.

After the RMFRP was obtained, two basic filters were used:

1) Downward continuation: Using this filter, the horizontal resolution of anomalies and their sources by continuing the field downward is increased. By doing this, the sources of the field resulting in shorter wavelengths are amplified and sharpened. This filter is especially useful for “eliminating” the influence of magnetic sources above the desired depth of exploration. Since this filter amplifies shorter wavelengths, it is ideal to map near surface faults (Ravat, 2007; Abedi et al., 2013).

2) Vertical and horizontal derivatives: The derivatives in both x (horizontal) and z (vertical) directions sharpen the edges of magnetic anomalies and give clearer contrasts between geological units and structures (e.g., lineaments, faults, etc.), and enhances shallow wavelengths that result from near surface structures (Sunny 2018). In this case of this work’s study area, we used the second derivatives for two mains reasons:

- The resolution, and hence, the number of structures that can be identified are increased.
- The first horizontal derivative showed a gap between the fault locations and the peak anomaly of up to 1000 m when compared to the second derivative, probably because the first derivative imaged deeper structures than the second one.

4.2 Electrical Resistivity Tomography (ERT) and Electromagnetic Profiling (EMP) data

Data from Monge-Cerda et al. (2024) from the “Banco de material” site was used to better understand, as will be explained later, the higher infiltration that takes in the western portion of the study area when compared to the east side of the study area. ERT was obtained in that study using the Dipole-Dipole array, which offers high horizontal resolution (Thabit & Al-Zubedi, 2015), which is ideal for mapping vertical contacts. The data from Monge-Cerda et al. (2024), with maximum penetration depths of around 50 m and electrode separation of 5 m, was merged with the ERT performed by Hernández-Bocanegra (2023), with a maximum penetration depth of around 120 m with electrode separation of 10 m. In this way, we can maintain the higher shallow resolution of the former study, while also having the greater penetration depths of the latter.

Even though data from only an ERT line on one of the study sites was used, the resistivity phenomena present at the “Banco de material” (shallow high resistivity to low resistivity at depth) is present at the remaining study sites (Monge-Cerda et al.,

2025), so the conclusions reached in this work can probably be projected to the other study sites.

EMP data is also taken from Monge-Cerda et al., (2024), which was obtained using the The Czech-made CMD MiniExplorer 6L (Slingram method) for an exploration depth of 2.3 m. This rapid acquisition method allows to better visualize the true distribution of faulting, and the apparent resistivity lineaments that seem to be associated with the interpreted subsurface continuation of faulting.

4.3 Hydrogeological data

The major ion and temperature data was provided by the Comisión Estatal de Agua de Guanajuato, CEAG (The Guanajuato State Water Commission), based on the sampling of 26 wells distributed throughout the study area (not shown of Figs because of presentation reasons), for the dry and rainy season of **2020**. On the other hand, the piezometric data was also provided by the CEAG, but for 57 monitoring wells, and the sampling survey was conducted in the year **2021** (Fig. 3). Both major ion and water table data were processed and interpolated using Surfer 16 (Golden Software, 2019). The Giggenbach (1991) ternary Cl-SO₄-HCO₃ plot is useful for illustrating the proportions of major anions in geothermal water, and the labels on the plot indicate associations with different parts of a geothermal system or different types of geothermal system (Powell & Cumming, 2010). For the purposes of this paper, only wells with water temperatures of more than 35 °C were used to establish if those waters had a geothermal origin, or if they could be heated waters by fault activity. The ternary plot was made using the free EXCEL spreadsheet Liquid-Analysis-V3, which was released with the Powell & Cumming (2010) paper.

5. Results

5.1 Aeromagnetic (AM) maps

Fig. 5 shows the main results of the aeromagnetic data analysis. Four maps were made for this purpose: second vertical derivative (Fig. 5a, section A-B); second horizontal derivative (Fig. 5b, section C-D) which is especially useful for mapping vertical contacts (e.g. faults); two downward continuations at 50 m and 400 m (Fig. 5c and d, sections E-F and G-H). The last two filters, even though they do not represent true depth, are useful to characterize the influence of active faults at depths that approximate the 50 m and 400 m, respectively.

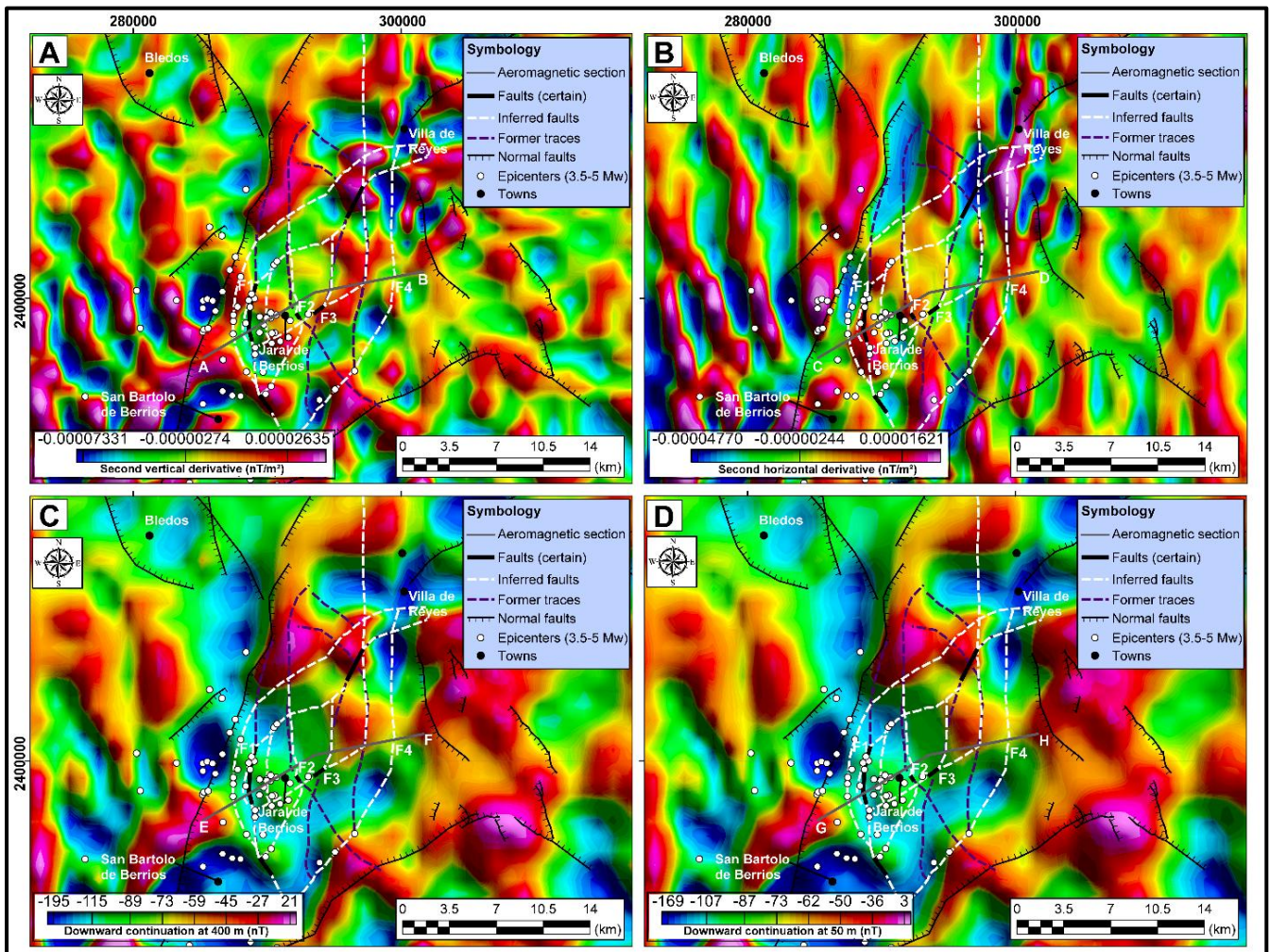


Fig. 5 Aeromagnetic maps. **a** Second vertical derivative. **b** Second horizontal derivative. **c** Downward continuation at 400 m. **d** Downward continuation at 50 m. Notice how the previously mapped fault traces orientations were fine-tuned with the magnetic anomalies. Data was processed with the Oasis montaj 8.4 software (Geosoft, 2015)

Also shown in this map is the seismicity between 1993 and 2024, with magnitudes from 3 to 5 Mw, and focal depths of 5-6 km (SSN, 2024). As can be seen in Fig. 5, broadly speaking, the orientation of the main faults of the study area agrees with the orientations of the aeromagnetic anomalies, and there seems to be alternating zones of low and high anomalies. These maps were also useful to better adjust the location of most inferred faults (by Monge-Cerda et al., 2025), which were delineated using geomorphological. In this work AM data was integrated with earthquake epicenter data, and in-situ fault measurements criteria (Fig. 6), to fine tune those traces (white dashed lines in Fig. 5). Fig. 5 also shows that faulting in the area is more extended than previously thought, with the longest one being at least 30 km long (fault F3 in Fig. 5), with a mainly NE-SW orientation.

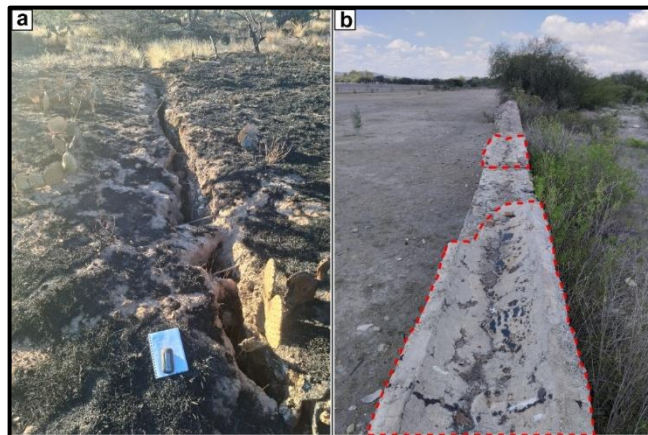


Fig. 6 a Cracks on the ground generated by F1 fault (see location in Fig. 8). **b** Repairs made on the colonial era dam structure (discontinuous polygon)

5.2 Aeromagnetic (AM) sections

Fig. 7 shows four sections which cut across the main faults studied in a SW-NE direction (see location in Fig. 5). These sections reveal the good agreement between the previously mapped confirmed faults and the aeromagnetic anomalies, and the water level drop around the most faulted areas. The faulting influenced anomalies show mostly low values, except in the second horizontal derivative section which is characterized by high values (section C-D, Fig. 7). There are also, as can be seen in Figs. 5 and 7, three new faults that were delineated in this work mainly with epicenter criteria, that do not seem to generate magnetic anomalies peaks.

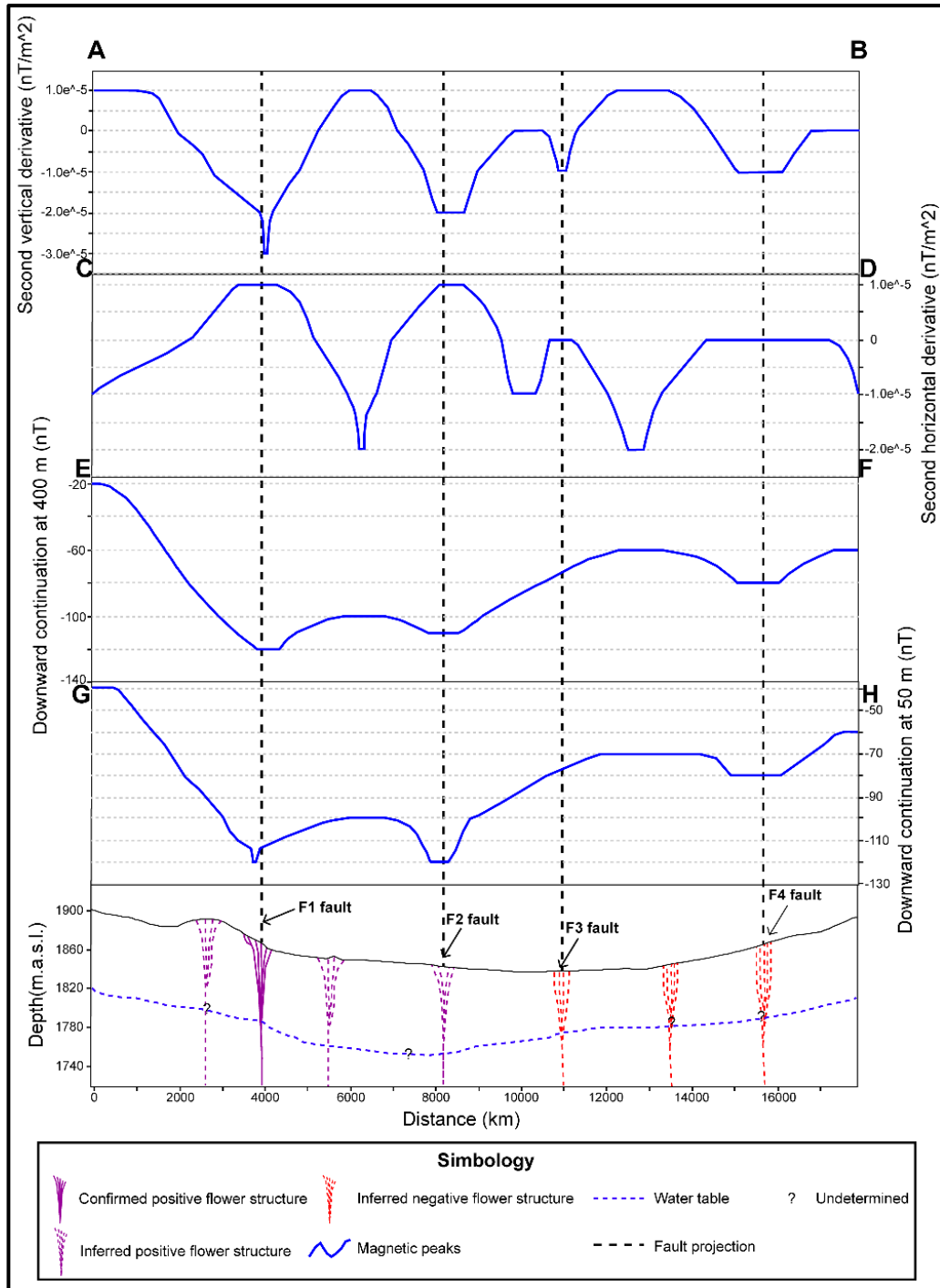


Fig. 7. Aeromagnetic sections. From top to bottom: Second vertical derivative; Second horizontal derivative; Downward continuation at 400 m; Downward continuation at 50 m; topographic relief showing the water table drop around faulted areas. It is especially clear in this Fig. how well the main fault traces agree with AM anomalies and how new traces

can be delineated. Water table levels after CEAG (2021), and faults after Monge-Cerda et al. (2025)

5.3 ERT and EM data

Fig. 8 shows EMP data and the location of the ERT of Monge-Cerda et al. (2024), which was performed in the “Banco de material” site (see location in Fig. 1). EMP data shows that faulting is more extended than outcrop faulting makes apparent, and that several apparent resistivity lineaments are most likely related to non-outcropping faulting. Fig. 8 also shows the location of the non-filled fault represented in Fig. 7, which is the way all faults outcrop on this site, hence the high-resistivity anomalies preponderance in the EMP map.

Fig. 9 shows the merging of ERT data from Monge-Cerda et al. (2024) and Hernández-Bocanegra (2023), with a maximum penetration depth of around 120 m. Shallow high-resistivity generating faulting, especially around the site’s main fault (fault FF), seem to change to low resistivity values (of 4-6 Ohm.m), and the fault zone seem to become wider and alters the water table. Shallow traces also seem to join in a single trace around FF fault.

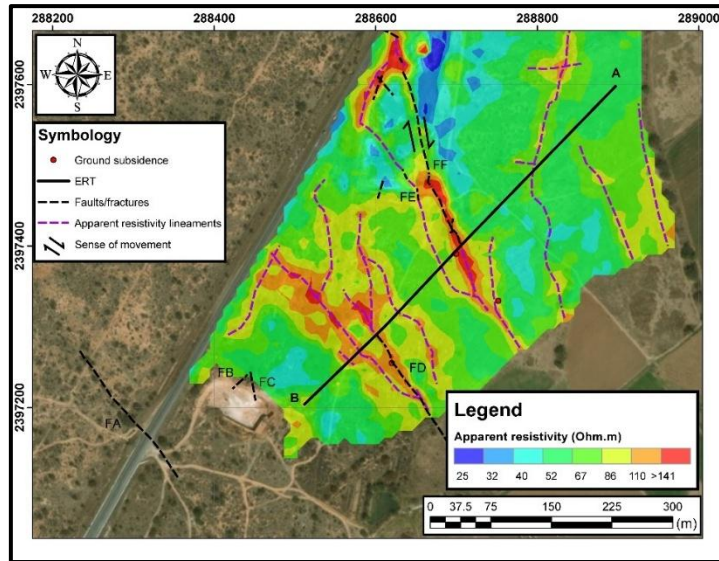


Fig. 8 EMP, ERT and faulting distribution data for the “Banco de material” site (see location in Fig. 1). Modified after Monge-Cerda et al. (2024)

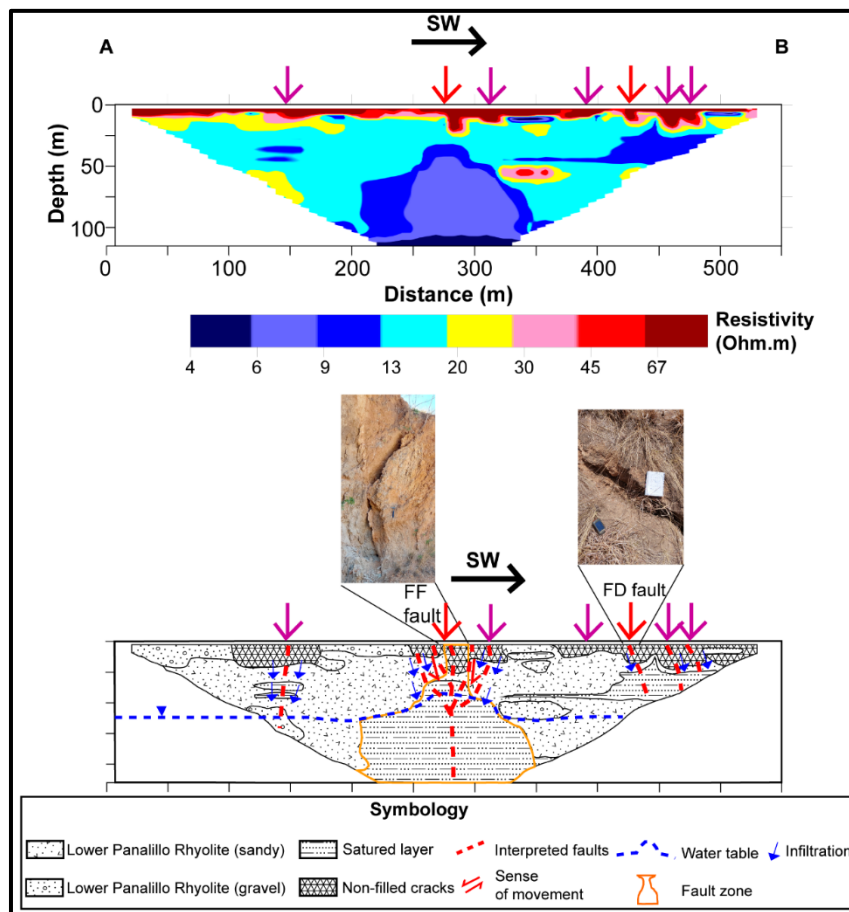


Fig. 9 ERT A-B and faulting distribution for the “Banco de material” site. From left to right, second and fifth arrows represent in-situ measurements of faults, while rest of the arrows the location of high apparent resistivity lineaments. Water table data after CEAG (2021), taken from well 151 (see location in Fig. 3). Geology after Tristán-González (1986) and in-situ geology description

5.4 Hydrogeochemical maps

The results of the major ion analysis of this work are presented in Fig. 10, by comparing the concentrations of chloride (section A-B, Fig. 10a), HCO_3 (section C-D, Fig. 10b) and NO_3 (section E-F, Fig. 10c) for the dry and rainy season of 2020. Also shown in this map is the seismicity between 1993 and 2024, with magnitudes from 3 to 5 Mw, and focal depths of 5-6 km (SSN, 2024). This makes evident how faulting is influencing the water table height, which is especially strong in the western sector of the study area, showing water table height contrasts of up to 30 m (Fig. 10).

Low chloride concentrations entry points (both in the dry and rainy season), in the southern and northern ends of the study area, and a high-chloride plume in the Villa de Reyes area can be identified (Fig. 10a). HCO_3 concentrations (Fig. 10b) show a similar trend, but in the rainy season there seems to be a higher influx of this ion. Finally, there seems to be a NO_3 contamination source near the Villa de Reyes and Bledos area (Fig. 10c).

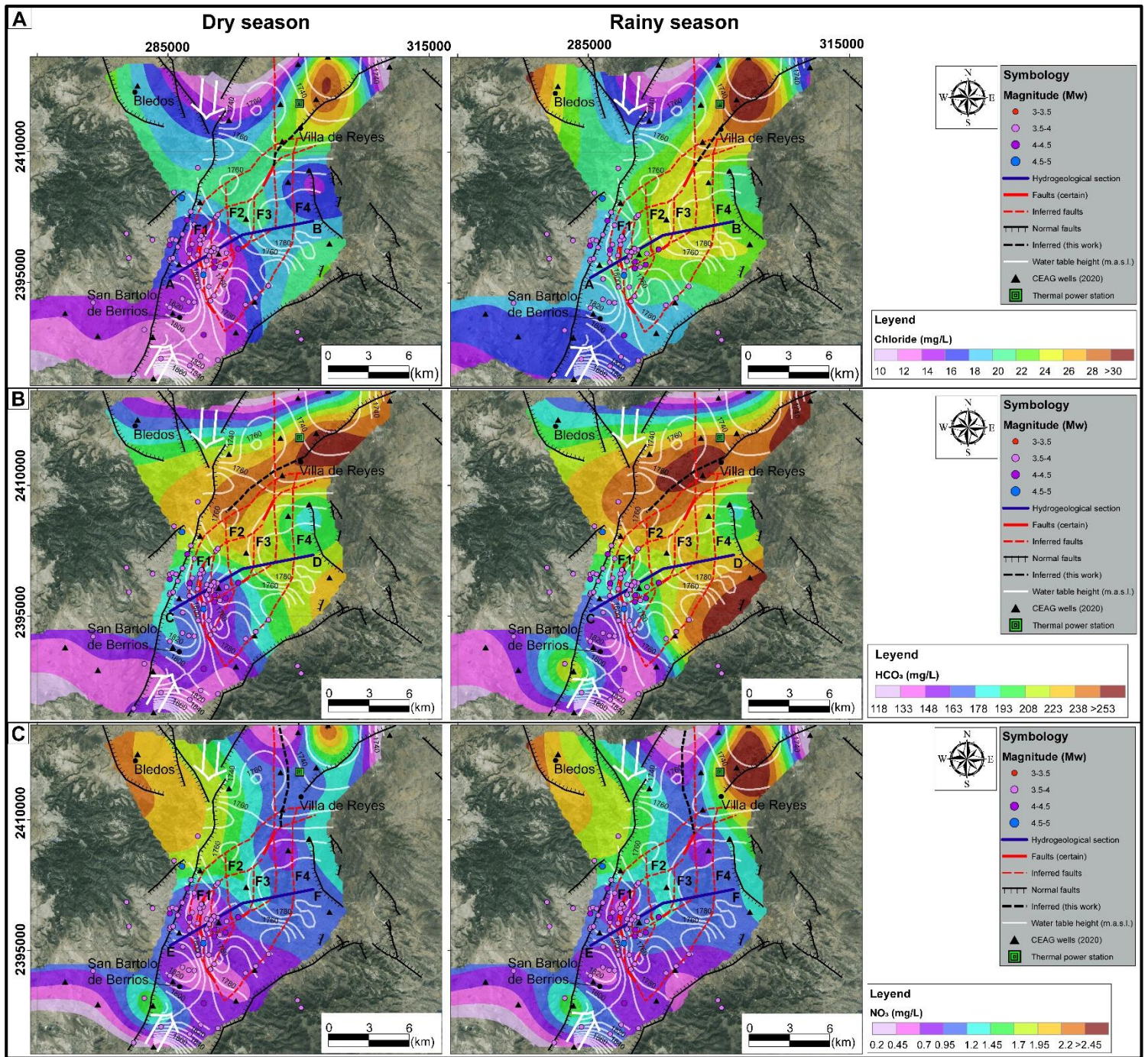


Fig. 10 Hydrogeochemical maps for the dry and rainy season. **a** Chloride. **b** SO_4 . **c** NO_3 . Notice how well the previously mapped fault traces orientations agree with the major ion anomalies. Arrows represent major ions entry points. Contours processed using the Surfer 16 software (Golden Software, 2019). Ion data after CEAG (2020)

5.5 Hydrogeochemical sections

Fig. 11 shows four sections for the same ions as the maps in Fig. 10, and the influence of faulting in the water table height. These sections more explicitly manifest how the western end of the study area is the most active one. Chloride concentrations also dramatically increase in the rainy season (blue line) when compared with HCO_3 and NO_3 .

In the rainy season, chloride (blue line) increases from west to east. In the dry season (red line), chloride content shows low anomalies in the western sector around fault zones, whereas towards the eastern values are stable around 18 mg/L.

HCO_3 increases continuously in the rainy season, until it reaches stable values of 223 mg/L. For the dry season HCO_3 shows low concentrations of around 146 mg/L in the western sector near faulted areas, while in the eastern part of the study area this concentration increases and stabilizes at 206 mg/L.

For the rainy season, NO_3 shows concentrations of 0.95 mg/L in the western portion of the study area and decreases to 0.7 mg/L around the fault zone and increases until reaching 1.2 mg/L and slowly decreases again to 0.95 mg/L towards the east. For the dry season nitrate values start at 0.95 mg/L, decrease to 0.45 mg/L around faulted areas, and increase again in the center of the study area to 1.2 mg/L, and finally decrease to 0.95 mg/L in the eastern portion of the study area.

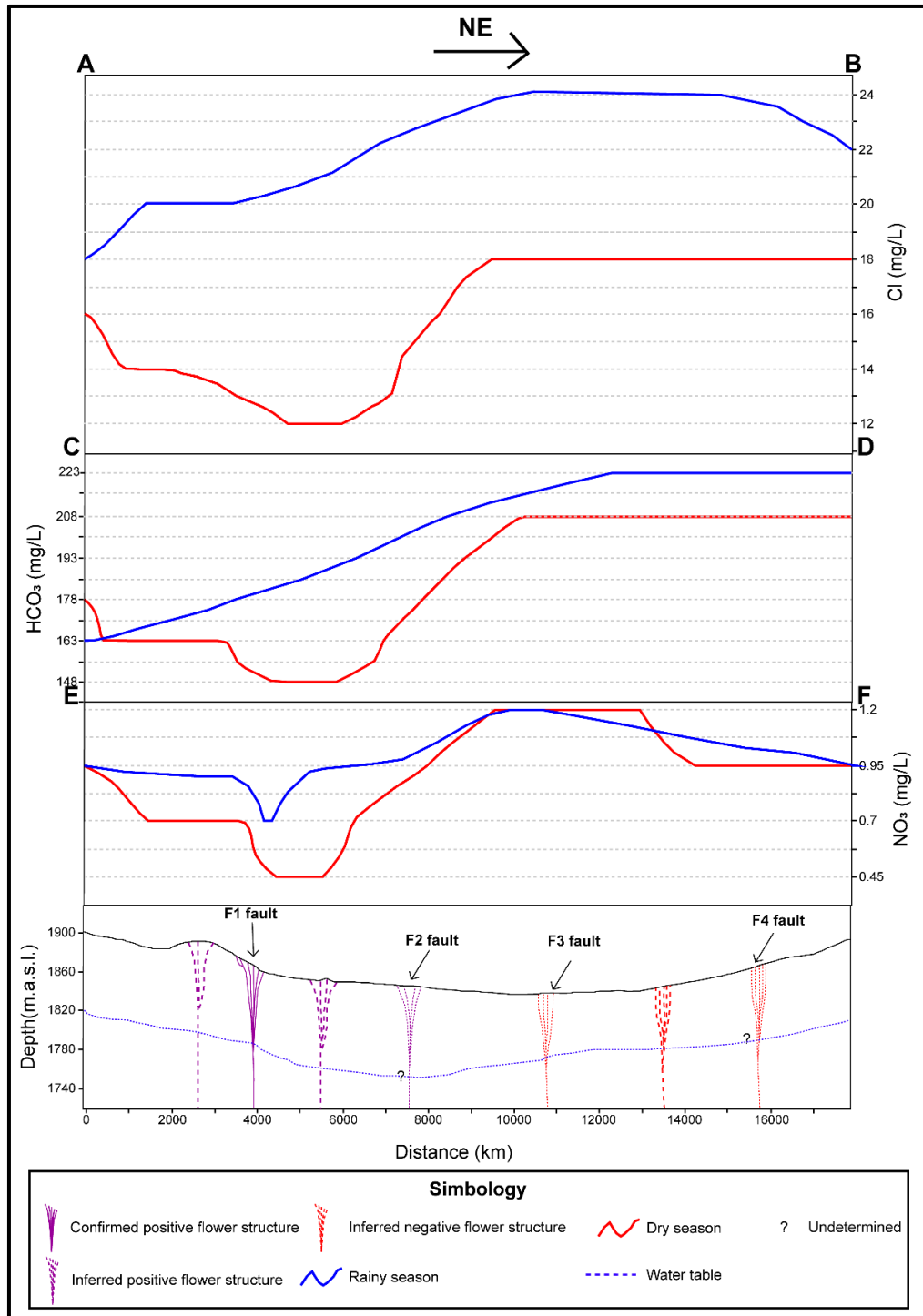


Fig. 11 Hydrogeochemical sections. From top to bottom: Chloride; SO₄; NO₃; topographic relief showing the water table drop around faulted areas. Notice how clear the western end faults show the lowest concentrations of major ions

5.6 Temperature map and Giggebach (1991) diagram

To ascertain the influence of faulting in the exploration wells around the study area, a temperature map was made to look for thermal anomalies associated with deep faults. As it is shown in Fig. 12, in general, faulted areas show the highest temperatures, which is especially true for the eastern portion of the study area, where wells with up to 40° C form NW-SE trending lineaments, which could be associated with several geomorphological lineaments in the eastern side of the study area. Five wells with higher temperatures were chosen to analyze them using the ubiquitous Giggenbach (1991) diagram to find out if those waters had a geothermal origin, which according to Fig. 12 they clearly do not have.

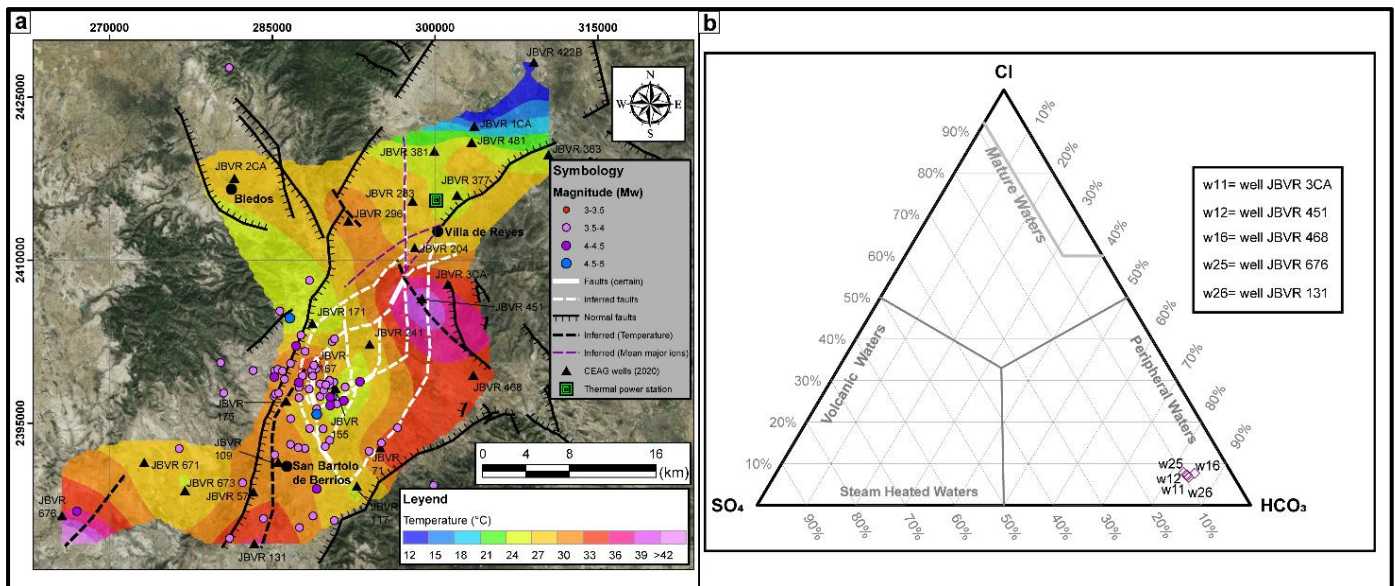


Fig. 12 a Temperature map, showing several high-temperature lineaments which could be associated with deep faults and **b** Giggenbach (1991) geothermal plot. Temperature contours processed using the Surfer 16 software (Golden Software, 2019) and the ternary plot was made using the free EXCEL spreadsheet Liquid-

Analysis-V3 by Powell & Cumming (2010)

6. Discussion

AM maps (Fig. 5) mostly show alternating low-high magnetic anomalies, which could be explained by the recently discovered positive and negative flower structures which seem to be controlling the structural style in the Villa de Reyes Graben (VRG, Monge-Cerda et al., 2025), and also makes evident that the faulting style does not significantly change in the first ,approximately, 400 m of the basin fill, since the number and orientations of faults remains unchanged throughout this thickness. Of all the used filters, the ones that seem to show more resolution are the second horizontal and vertical derivatives, since they show more fault traces than the downward continuation maps (Fig 5a and 5b). AM data clearly shows that the western sector of the study area is the most active one, both from a seismicity (Fig. 5) and AM standpoint (Figs 5 and 7), because of cluster concentration and lower peaking anomalies, respectively. Several smaller traces were also delineated but do not generate significant AM anomalies, which could be due to these faults being younger and/or less active than major faults.

The AM data also evidences how faulting in the area is more extended than previously thought, with the longest one being at least 30 km long (fault F3 in Fig. 5), with a mainly NE-SW orientation, which also agrees with orientation regime change to a NE-SW trend around this area documented by Monge-Cerda et al. 2025. Of all the AM maps, the most useful seem to be the Second Horizontal Derivative since it clearly shows the best agreement of faulting orientations and locations with the magnetic anomalies (Fig, 5b). This data also helped delineate the study area's faulting as probably being produced by a pull apart basin, which agrees with outcrop

scale evidence in the area (“Río Jaral” site in Monge-Cerda et al. (2025)), inside which there is both transtensional as well as transpressional stress fields (Monge-Cerda et al., 2025).

ERT shows how these faults, which outcrop as high resistivity generating non-filled fractures which mainly alter rhyolitic rocks, seem to change to low resistivity values and alter the water table level in fracture FF (Fig. 9). In this main fracture, there is a change from high resistivity values to highly conductive values at greater depths (more than 50 m). This conductive anomaly expands in the form of an inverted funnel, becoming very narrow at the surface, expanding with a certain gradient from approximately 40 m to 70 m, until it loses that gradient and stabilizes upon reaching the water table. It is very likely that this fracture is acting as a narrow conduit, like an injection well, where rainwater infiltrates and loses gradient upon reaching the water table. This illustrates how water may infiltrate through fractures located in the more active western sector, since the ERTs from Monge-Cerda et al. (2025) show the change from shallow high resistivity to low conductive values at depth, so the results of this work can probably be projected to the study sites of Monge-Cerda et al. (2025), and thus roughly describe the behavior of water infiltration on the locations of those sites. The faulting on this site seems to be generating mainly by flower structures (in Fig. 9, probably a negative-type structure), which corroborates Monge-Cerda et al. (2025) findings. The fault of core of FF fault (first red arrow from left to right in Fig. 9) seems to be less permeable than the damage zone (surrounding faults) since the saturated layer’s main source of infiltration appears to be these surrounding faults (compare with Fig. 2a). There are also two other infiltration zones

shown in Fig. 9, where the most important one seems to be generating a perched aquifer-like structure (southwest end of Fig. 9). EMP data shows how faulting is more extensive than previously thought, and how high-resistivity lineaments are associated with subsurface faults.

HGC maps (Fig. 10) reinforce the geological and geophysical interpretation that the western sector of the study area is more active, mainly because:

- The water table height clearly controls the distribution of the isophreatic curves when compared to the eastern sector, evidenced by the higher gradient of those curves.
- Ion concentration is lower in this zone, both in the rainy season and the dry season.

Western sector faults, being very seismically active, and outcropping mostly as non-filled fractures (Monge-Cerda et al., 2025), which manifest new traces themselves in practically each new visit to the study area (Fig. 6a), allow for easier contaminant penetration, especially in the rainy season. Since rainwater normally presents lower contents of the major ions analyzed in this work, which is especially true for chloride content in the rain season (Figs. 10a and 11), the low concentrations of these ions in the western sector support this interpretation. The western side faults can be classified as a distributed conduit system (Fig. 2b).

On the other hand, for the eastern sector faults, since they are not very seismically active but still show recent activity, the fault core is not as permeable when compared with the damage zone (secondary faults). This sector faults probably act as barriers, since faulting derived material (i.e. fault gouge) from recent activity “clog” these

fractures and make it harder for contaminants to penetrate in the aquifer, which explains the higher content of major ions not normally present in rainwater (Figs 10 and 11). The western sector faults can probably be classified as a combined conduit-barrier system (Fig. 2b).

Faulting orientation also shows good agreement with the major ion anomalies, both for the dry and rainy season, so this is also evidence of the tectonic control exerted by fault on the ion distribution and concentrations.

Temperature data (Fig. 12) makes evident that a geothermal origin for the study area's high-temperature water is not possible, since the Giggenbach (1991) diagram indicates a peripheral water origin. The high temperatures could be explained by shallow water being heated by faulting activity, or the previously documented radon decay processes in the study area (Hernández-Bocanegra, 2023).

Since the AM data showed that faulting distribution and orientation is similar for, approximately, the first 400 m of the basin fill (Fig. 5), a 3D model was made for three approximate exploration depths (Fig. 13): 400 m, 1 km and 2 km, which also integrates the findings of the shallow AM data. As can be seen in the 3D model, at shallow depths, fault traces seem to be more numerous and widely distributed, with similar orientations and number of faults for the 400 m and 1 km exploration depths. On the other hand, at 2 km deep, shallower faults seem to join in a smaller number of traces,

This seems to be reinforcing both this study and Monge-Cerda et al. (2025) interpretation of positive and negative flower type structures both at the regional and

basin scale, and this study's finding in the pull-apart basin structural style of the tectonics of the VRG.

The predominance of high magnetic values at the 2 km depth of exploration could be indicating that the basement is reached at this structural level. Nevertheless, more studies are necessary to ascertain this.

Finally, as in any geoscientific work, several sources of uncertainty have arisen:

- Since AM data was obtained in the year 1996, data for major ions from the year 2020, and water table levels from 2021, this could give way to errors in interpretation, and since most of this data was obtained before the seismic sequence of September 2021 (SSN, 2021), the structural impact on the hydrogeology of the area could not be as well displayed as it should, so cautious interpretation of the results of this work are necessary. Nevertheless, the good agreement between AM and structural data, and the more dynamic fracture distribution in the western sector of the study area (e.g. "Banco de material" site Fig. 1 and 6) which shows the most structural influence in the water table height and ion orientation and concentration (respectively), gives more confidence in this study's interpretation. Also, since tectonic phenomena tend to start before major earthquake events, we hope the results of this work are the best possible approximation of the tectonics of the VRG.
- As most ion data was obtained inside the main fault zones, this could raise concerns about sampling representativeness. However, as mentioned before, the water table height and ion distribution are clearly influenced by these

faults, showing less influence as the distance from the faulted areas is increased, so this work's interpretation seems to be adequate.

- As flight lines from AM data are every km in the N-S direction, and the sections are practically E-W, the magnetic data between each line (which is interpolated) might lose detail of small faults between those lines. Still, since the structures affecting the VRG are of the regional scale, the main structures in this basin are most likely being well imaged in this work.

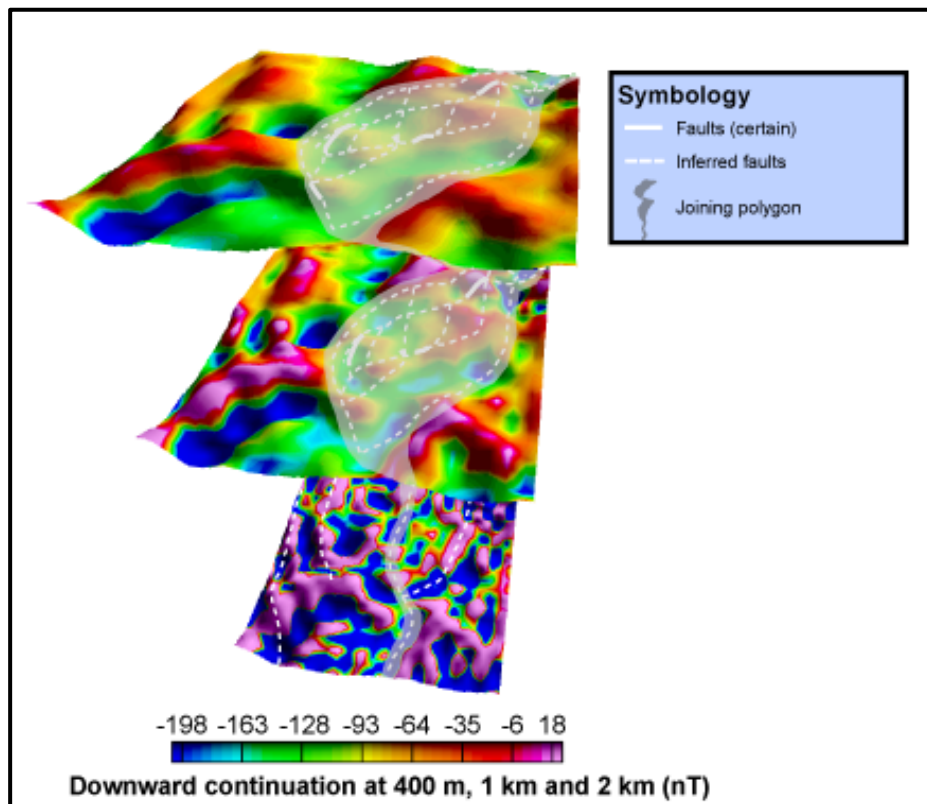


Fig. 13 3D model showing three downward continued (approximate) explorations depths: 400 m, 1 km and 2 km. Notice how shallower faults seem to join in a single trace at depth, suggesting the existence of a positive-negative flower structure. The shallow part of the faulting suggests a pull-apart basin-like structural style

7. Conclusions and recommendations

7.1 Conclusions

- Aeromagnetic maps show anomalies with the same orientations and seem to alternate areas of low and high anomalies, which may be due to alternating positive and negative flower structures. These maps also helped to fine-tune the location of the inferred fault traces and show the pull-apart nature of the structural of the southern portion of the Villa de Reyes Graven (VRG).
- The aeromagnetic profiles show the good coincidence of the fault traces with the magnetic anomalies, with the lowest anomaly values occurring in the western sector, which is the most active of the studied area.
- Geoelectric data makes evident that water infiltrates through non-filled fractures (which generate high-resistivity anomalies), and that when it reaches the water table the resistivity anomalies widen and become low value (as low as 4-6 Ohm.m). This also illustrates how infiltration may take place in the more seismically active western sector. The faulting seems to be predominantly generated by a negative-type flower structure, and the fault core of the faults appears to be less permeable than the surrounding faults (damage zone).
- Hydrogeochemical maps and profiles reveal that, broadly speaking, the ion content is lower in the western sector of the study area compared to the eastern sector, since the western sector is the most active one, allowing low chloride, HCO_3 and NO_3 meteoric waters to pass through unfilled fractures. The eastern sector, on the other hand, is not as active, and the material derived from this

activity which has had enough time to accumulate in a significant way probably prevents the infiltration of these ions.

- Temperature maps show wells with temperatures of more than 40° C, which form anomalies with a NW-SE orientation. However, according to the Giggenbach (1991) diagram, these high temperature points do not have a geothermal origin and are rather surface waters heated by active faulting.
- The final model shows a greater number of faults on the surface, which decrease and tend to unite at depth, which could support the initial theory that all the faults that occur within the Villa de Reyes Graben are caused by positive-negative flower structures.
- This work reveals which areas of the southern portion of the Villa de Reyes Graben could act as barriers (eastern sector) or pathways (western sector) for contaminants, which could have implications for land use planning in the study area.
- It is expected that this study will serve as a basis for understanding how the faulting within this graben extends across the Mesa Central, which will help understand the active tectonics in the San Luis Potosí valley and surrounding areas.

7.2 Recommendations

- The update of AM, monitoring of the piezometric levels, water quality and major ion data from the area would facilitate the correct correlation between these data and the recent (and future) seismicity of the VRG.

- Additional indicators such as isotope analysis would aid in reaching more robust conclusions regarding the origin of the water in the Jaral de Berrios-Villa de Reyes aquifer. Likewise, the use of other geophysical to image deep structures such as magnetotellurics (MT) and seismic reflection would enhance the deep structural interpretation of AM data.

Acknowledgements This study was initiated in the framework of a Ph. D. thesis at the Department of Geosciences of the Instituto Potosino de Investigación Científica y Tecnológica (IPICYT). The authors would like to thank Anayeli Pineda-Román for the help with the aeromagnetic data processing, and David Ernesto Torres-Gaytán of the IPICYT Geophysics' Laboratory for facilitating the aeromagnetic data. Special thanks to Paola Itzel Hernández-Bocanegra for providing the deep ERT data, and the Comisión Estatal de Agua de Guanajuato for kindly contributing with all the hydrogeological data used in this work.

References

- Abedi, M., Gholami, A., & Norouzi, G.H. (2013). A stable downward continuation of airborne magnetic data: A case study for mineral prospectivity mapping in Central Iran. *Computers and Geosciences*, 52, 269-280. <https://doi.org/10.1016/j.cageo.2012.11.006>.
- Bense, V.F., & Person, M.A. (2006). Faults as conduit-barrier systems to fluid flow in siliciclastic sedimentary aquifers. *Water Resour Res* 42(5). <https://doi.org/10.1029/2005WR004480>
- Bense, V.F., Gleeson, T., Loveless, S.E., Bour, O., & Scibek, J. (2013). Fault zone hydrogeology. *Earth Science Rev*, 127, 171-192. <http://dx.doi.org/10.1016/j.earscirev.2013.09.008>
- Botero-Santa, P.A., Xu, S., Nieto-Samaniego, Á.F., & Alaniz-Álvarez, S.A. (2020). Efecto de las fracturas de enfriamiento en la formación de fallas normales: El ejemplo de Santa María del Río, San Luis Potosí, México. [Influence of cooling fractures on the formation of normal faults: a case study in Santa María del Río, San Luis Potosí, México]. *Bol Soc Geol Mex*, 72(1). <https://doi.org/10.18268/bsgm2020v72n1a011019>

- Boubaya, D. (2017). Combining resistivity and aeromagnetic geophysical surveys for groundwater exploration in the Maghnia plain of Algeria. *J Geol Res*, 2017(1), 1309053. <https://doi.org/10.1155/2017/1309053>
- Bustamante-Orozco, M.R., Medrano-Pérez, O.R., Neri-Flores, I., & Ángeles-Cordero, E. (2023). Interpretación de datos aeromagnéticos y gravimétricos satelitales para la identificación de zonas con potencial acuífero en la porción oeste de la cuenca Grijalva, México. [Interpretation of aeromagnetic and satellite gravimetric data for the identification of zones with aquifer potential on the western Grijalva basin, México]. *Bol Soc Geol Mex*, 75(1). <http://dx.doi.org/10.18268/BSGM2023v75n1a031122>
- Caine, J.S., Evans, J.P., & Forster, C.B. (1996). Fault zone architecture and permeability structure. *Geol*, 24(11), 1025-1028. [https://doi.org/10.1130/0091-7613\(1996\)024<1025:FZAAPS>2.3.CO;2](https://doi.org/10.1130/0091-7613(1996)024<1025:FZAAPS>2.3.CO;2)
- Carrillo-Rivera, J.J., Clark, I.D., & Fritz, P. (1992). Investigating Recharge Of Shallow And Paleo-Groundwaters In The Villa De Reyes Basin, SLP, Mexico, With Environmental Isotopes. *Appl Hydrogeol*, 1(4), 35–48. <https://doi.org/10.1007/s100400050025>
- Cauich-Kau, D.D.A., Cardona-Benavides, A., Castro-Larragoitia, G.J., & Rude, T.R. (2021). Understanding Arsenic and Uranium Sources and Mobility in Groundwater Flow Systems from Two Areas in San Luis Potosi, Mexico: Cerritos and Villa de Reyes Basins. *Lehr-und Forschungsgebiet Hydrogeologie* No. RWTH-2021-09796. <https://doi.org/10.18154/RWTH-2021-09796>.
- Cilona, A., Aydin, A., & Johnson, N.M. (2015). Permeability of a fault zone crosscutting a sequence of sandstones and shales and its influence on hydraulic head distribution in the Chatsworth Formation, California, USA. *Hydrogeol J*, 23(2), 405. <https://doi.org/10.1007/s10040-014-1206-1>
- Comisión Estatal de Agua de Guanajuato (CEAG) (2020). Calidad del Agua 2020, acuífero Jaral de Berrios-Villa de Reyes (Water quality 2020, Jaral de Berrios-Villa de Reyes aquifer) [Data set].
- Comisión Estatal de Agua de Guanajuato (CEAG) (2021). Historia de Piezometría 2015-2021, acuífero Jaral de Berrios-Villa de Reyes (Piezometric levels history 2015-2021, Jaral de Berrios-Villa de Reyes aquifer) [Data set].
- Comisión Nacional del Agua (CONAGUA) (2023). Actualización de la disponibilidad media anual de agua en el acuífero Jaral de Berrios-Villa de Reyes (2412), Estado de San Luis Potosí. Ciudad de México. (Update of the average annual water availability in the Jaral de Berrios-Villa de Reyes aquifer (2412), State of San Luis Potosi. Mexico City). CONAGUA. Retrieved June 1, 2023, from https://sigagis.conagua.gob.mx/gas1/Edos_Acuiferos_18/sanluispotosi/DR_2412.pdf

- Fronzi, D., Mirabella, F., Cardellini, C., Caliro, S., Palpacelli, S., Cambi, C., Valigi, D., & Tazioli, A. (2021). The role of faults in groundwater circulation before and after seismic events: Insights from tracers, water isotopes and geochemistry. *Water*, 13(11), 1499. <https://doi.org/10.3390/w13111499>
- Ganiyu, S.A., Badmus, B.S., Awoyemi, M.O., Akinyemi, O.D., & Olurin, O.T. (2013). Upward continuation and reduction to pole process on aeromagnetic data of Ibadan Area, South-Western Nigeria. *Earth Science Res*, 2(1), 66. <https://doi.org/10.5539/esr.v2n1p66>
- Geosoft (2015). Oasis montaj (Version 8.4) [Software]
- Giggenbach, W.F. (1991). Chemical techniques in geothermal exploration. In: D'Amore F (ed) Applications of geochemistry in geothermal reservoir development : series of technical guides on the use of geothermal energy. United Nations, pp 119-144
- Grauch ,V.J.S., & Hudson, M.R. (2007). Guides to understanding the aeromagnetic expression of faults in sedimentary basins: Lessons learned from the central Rio Grande rift, New Mexico. *Geosph*, 3(6), 596-623. <https://doi.org/10.1130/GES00128.1>
- Hacıoğlu, Ö., Başokur, A.T., & Diner, Ç. (2021). Geothermal potential of the eastern end of the Gediz basin, western Anatolia, Turkey revealed by three-dimensional inversion of magnetotelluric data. *Geother*, 91, 102040. <https://doi.org/10.1016/j.geothermics.2020.102040>
- Henry, C.D., & Aranda-Gómez, J.J. (1992). The real southern Basin and Range: Mid to late Cenozoic extension in Mexico. *Geol*, 20, 701-704. [https://doi.org/10.1130/0091-7613\(1992\)020<0701:TRSBAR>2.3.CO;2](https://doi.org/10.1130/0091-7613(1992)020<0701:TRSBAR>2.3.CO;2)
- Hernández-Bocanegra, P.I. (2023). Exploración geofísica e hidrogeoquímica en el graben de Villa de Reyes, para estudiar el origen de las fallas activas y sus implicaciones en el acuífero. [Geophysical and hydrogeochemical exploration inside the Villa de Reyes Graben, to study the area's active faulting and its effects on the aquifer]. Dissertation, Instituto Potosino de Investigación Científica y Tecnológica (IPICYT).
- Instituto Nacional de Estadística y Geografía (INEGI) (2023). Continuo de Elevaciones Mexicano. INEGI. Retrieved April 1, 2023, from <https://www.inegi.org.mx/app/geo2/elevacionesmex/>
- Jolie, E., Scott, S., Faulds, J., Chambefort, I., Axelsson, G., Gutiérrez-Negrín, L.C., Regenspurg, S., Ziegler, M., Ayling, B., Richter, A., & Zemedkun, M.T. (2021). Geological controls on geothermal resources for power generation. *Nat Rev Earth Environ*, 2(5), 324-339. <https://doi.org/10.1038/s43017-021-00154-y>
- Labarthe-Hernández, G., Tristán-González, M., & Aranda-Gómez, J.J. (1982). Revisión estratigráfica del Cenozoico de la parte central del Estado de San Luis Potosí. [Stratigraphic revision of the Cenozoic of central part of the State

of San Luis Potosí]. Technical Report. Universidad Autónoma de San Luis Potosí, San Luis Potosí.

- López-Loera, H., & Tristán-González, M. (2013). Geología y magnetometría aérea del Graben de Villa de Reyes, San Luis Potosí, Mesa Central de México: Implicaciones tectónicas y geohidrológicas. [Geological and aeromagnetic mapping of the Villa de Reyes Graben, San Luis Potosí, Mesa Central of México: Hydrogeological and tectonic implications]. *Bol Soc Geol Mex*, 65(1), 137-156. <https://doi.org/10.18268/BSGM2013v65n1a11>
- Meneisy, A.M., & Al Deep, M. (2021). Investigation of groundwater potential using magnetic and satellite image data at Wadi El Amal, Aswan, Egypt. *Egypt J Remote Sens Space Science*, 24(2), 293-309. <https://doi.org/10.1016/j.ejrs.2020.06.006>
- Monge-Cerda, F.E., Delgado-Rodríguez, O., Ramos-Leal, J.A., & Sánchez-Higuero, L.E. (2024). Geoelectrical characterization of non-filled active faults in Jaral de Berrios, Guanajuato, México. *J Appl Geophys*, 227, 105431. <https://doi.org/10.1016/j.jappgeo.2024.105431>
- Monge-Cerda, F.E., Ramos-Leal, J.A., Delgado-Rodríguez, O., Torres-Hernández, J.R., Belmonte-Jiménez, S.I., & Torres-Gaytán, D.E. (2025). Geophysical, geological and tectonic study of active faulting inside the Villa de Reyes Graben, Central Mexico. *Near Surf Geophys* (in press). <https://doi.org/10.1002/nsg.70019>
- Nieto-Samaniego, A.F., Alaniz-Alvarez, S.A., & Camprubí, A. (2005). La Mesa Central de México: estratigrafía, estructura y evolución tectónica cenozoica. [Mesa Central of México: Stratigraphy, structure, and Cenozoic tectonic evolution]. *Bol Soc Geol Mexic*, 57(3), 285-318. <https://doi.org/10.18268/bsgm2005v57n3a3>
- Piña-González, V., Miranda-Avilés, R., Hernández-Anguiano, J.H., Knappett, P.S., Morales-Martinez, J.L., Puy-Alquiza, M.D.J., Naves, A., Bian, J., Liu, J., Ramírez-González, L.M., Navarro-Céspedes, J.M., & Li, Y. (2022). Influence of geological faults on dissolved arsenic concentrations in an overexploited aquifer with shallow geothermal heat. *Appl Geochem*, 144, 105395. <https://doi.org/10.1016/j.apgeochem.2022.105395>
- Powell, T., Cumming, W. (2010). Spreadsheets for geothermal water and gas geochemistry. Stanford Geothermal Workshop
- Ravat, D. (2007). Upward and downward continuation. In D. Gubbins, & E. Herrero-Bervera (Eds.) *Encyclopedia of Geomagnetism and Paleomagnetism* (pp. 974-976). Springer, Dordrecht,
- Servicio Geológico Mexicano (SGM) (1996). Datos aeromagnéticos Villa de Reyes (SLP)-Guanajuato (Aeromagnetic data Villa de Reyes (SLP)-Guanajuato) [Data set]

- Servicio Sismológico Nacional (SSN) (2021). Secuencia Sísmica del 4 a 6 de septiembre de 2021, Guanajuato-San Luis Potosí (M 4.5). [Seismic Sequence from 4 to 6 September 2021, Guanajuato-San Luis Potosí (M 4.5)]. National Seismological Survey website. Retrieved September 7, 2021, from <http://www.ssn.unam.mx>
- Soto-García, A.G. (2022). Análisis estructural del Graben de Santa Rosa, San Luis Potosí y Guanajuato. [Structural Analysis of the Santa Rosa Graben, San Luis Potosí and Guanajuato]. Dissertation, Universidad Autónoma de San Luis Potosí (UASLP)
- Stewart, J.H. (1998). Regional characteristics, tilt domains, and extensional history of the late Cenozoic Basin and Range province, western North America. *Spec Pap Geol Soc Am*, 47-74. <https://doi.org/10.1130/0-8137-2323-X.47>
- Sunny, A.A. (2018). Derivatives and analytic signals: improved techniques for lithostructural classification. *Malays J Geosci*, 2(1), 01-08. <https://doi.org/10.26480/mjg.01.2018.01.08>
- Thabit, J.M., Al-Zubedi, A.S. (2015). Evaluation of three important electrode arrays in defining the vertical and horizontal structures in 2D imaging surveys. *Iraqi J Sci*, 56(2B), 1465–1470.
- Tristán-González, M. (1986). Estratigrafía y tectónica del graben de Villa de Reyes, en los estados de San Luis Potosí y Guanajuato, México. [Stratigraphy and tectonics of the Villa de Reyes Graben, in the states of San Luis Potosí and Guanajuato, México]. Technical Report number 107. Universidad Autónoma de San Luis Potosí (UASLP), San Luis Potosí.
- Tristán-González, M., Aguillón-Robles, A., Barboza-Gudiño, J.R., Torres-Hernández, J.R., Herve, B., López-Doncel, R., Rodríguez-Ríos, R., & Labarthe-Hernández, G. (2009). Geocronología y distribución espacial del vulcanismo en el Campo Volcánico de San Luis Potosí. [Geochronology and spatial distribution of de vulcanism inside de Volcanic Field of San Luis Potosí]. *Bol Soc Geol Mex*, 61 (3), 287-303.
- Zou, C., Zhang, G., Zhu, R., Yuan, X., Zhao, X., Hou, L., Wen, B., & Wu, X. (2013). *Volcanic Reservoirs in Petroleum Exploration*. Elsevier Inc, San Diego.

Declarations

Funding This work was supported by grants from the Instituto Potosino de Investigación Científica Tecnológica A.C. (IPICYT) and by the Consejo Nacional de Humanidades Ciencia y Tecnología (CONAHCYT). No additional grants to carry out or direct this work were received.

Conflict of interest The authors have no relevant financial or non-financial interests to disclose.

Author contributions **Fabián Esteban Monge-Cerda**: Conceptualization, Methodology, Visualization, Investigation, Writing-original draft, Writing - review and editing. **José Alfredo Ramos-Leal**: Conceptualization, Methodology, Writing-review and editing, Supervision. **Omar Delgado-Rodríguez**: Conceptualization, Methodology, Writing-review and editing, Supervision. **José Ramón**

Torres-Hernández: Conceptualization, Methodology, Writing-review and editing, Supervision. **Mayla Alheli Ramos-Vázquez:** Writing-review and editing.

Data availability Data used during the current study is available from the corresponding author on reasonable request.

Chapter 6-. Discussion

A four-part methodology for the study of active faults was established in this work and was applied in the southern sector of the Villa de Reyes Graben (VRG). The **first part** involves field work for surveying active faulting, which in the VRG mostly outcrop as non-filled fractures and ground subsidence spots. Outcrop evidence tends to be scarce, but fault planes that show kinematic indicators exhibit mostly right-lateral NW-SE faulting in the southern portion of the study area and left-lateral NE-SW faulting in the northern portion.

The **second part** of the methodology uses of Electromagnetic Profiling (EMP) mapping as a first step in detecting fault zones and was first tested on the “Banco de material” site, proving to be very successful since the location of the fractures measured in the field matched with the geophysical anomalies, and also revealed fractures that have not reach the surface yet, as shown by the Electromagnetic Profiling (EMP) map (see Fig. 6; Chapter 3). EMP data show that non-filled surficial fractures mostly generate high-resistivity responses. This contrasts with similar studies (e.g. Konon *et al.*, 2016; Drahor & Berge, 2017; Nabi *et al.*, 2020; among many others) in which faulted areas are predominantly conductive, since fault zones tend to accumulate fault gouge, mineralization and water content. High-resistivity fault related lineaments have been reported by Nobes & Hornblow (2021) and are explained by prolonged periods of dry weather that can dry out (i.e. leave fractures “empty”) the near-surface expression of faults, therefore increasing the electrical resistivity. This agrees with the present study’s interpretation since the Villa de Reyes Graben (VRG) is located within an area of low precipitation (average annual precipitation of 435 mm/yr, according to CONAGUA (2023), with most fractures outcropping as open cracks on the ground, which explains the high resistivity values.

The **third part** of this methodology involves the use Electrical Resistivity Tomography and Ground Penetrating Radar (GPR), as methods to further

characterize the resistivity lineaments defined by EMP. At depths greater than 20 m, ERT data revealed on all sites (Fig. 7 in Chapter 3 and Figs 14 and 19 in Chapter 4) that fault zones reach low resistivity values, which could be generated by the accumulation of clayey sediments derived from faulting, or by a local disturbance of the water-table, but more studies are needed to establish this. ERT data also helped establish that the faulting affecting the southern sector of the VRG is predominantly geological in nature, with no man-made component triggering it, since most fault traces are located below the local water table (e.g. Fig. 9 in Chapter 5), which means that faulting (and ground subsidence) is not being generated by over-exploitation of the area's aquifer, in which case fault traces would be predominantly located above the water table. This contrasts with other locations such as Querétaro and Celaya (Guanajuato), where anthropogenic (especially intense groundwater abstraction) activity exacerbates the effects of geological faulting (Figueroa-Miranda *et al.*, 2018). With the application of Electric Resistivity Tomography (ERT), but especially with the high-resolution Ground Penetrating Radar (GPR) method, the study area's outcropping faults which can be classified as left-right lateral combined with normal-reverse type faults, were shown to join at depth to form a single trace. This is evidence of the existence of positive or negative flower structures, generated by transpressional or transtensional stress fields (respectively), which until now have not been reported in the study area. Transpressional (right-lateral) NW-SE orientated structures dominate at the "Banco de material" and "Jaral" sites, with field evidence such as meter long right-lateral kinematic indicators, reverse faults and folds, affected man-made structures, and geophysical evidence mostly showing the sub-surface continuation of that geological evidence. The northern sector of the study area ("Río Jaral" and "Presa El Hundido" sites) is dominated by NE-SW (left-lateral) trending transtensional structures, with field evidence such as meter long non-filled fractures, subsidence spots, and negative type flower structures shown on geophysical sections, although, transpressional structures seem to be starting to manifest in the dam crest at the "Presa El Hundido" site. The maximum dimensions for the active faulting impacting the southern sector of the VRG was established of 700 m in length and 979 m wide ("Presa El Hundido" site, see Fig. 21 in Chapter 4).

The fault activity at this site appears to be taking place since at least colonial times (around 500 years ago), since the colonial dam crest has evidence of being repaired from that time (see Fig. 6b in Chapter 5).

The **fourth part** of this methodology involves the use of non-geological evidence which in the case of this work we used focal mechanism solutions evidence. The modeled change of trend from NW-SE (south of the study area) to NE-SW (north) is supported by a focal mechanism solution evidence of the September 5, 2021, San Felipe (Guanajuato) earthquake (SSN,2021) which shows two fault planes: NE-SW left lateral and NW-SE right lateral faults, which agrees with this study's findings. This work also shows the coexistence of positive and negative type flower structures within a few meters, like in the "Banco de material" site. Although this is not so common on the scale of individual strike-slip basins (Barnes *et al.*, 2001), GPR sections revealed that they can be present at the metric scale.

The four-part methodology was useful for surveying active faulting starting from an outcrop to a regional scale. To study the basin scale, the Aeromagnetic (AM) method permitted surveying to maximum depths of 2 km. AM data both helped in confirming the mapped faults based on EMP, ERT, GPR, and epicenter data, and adjusting geomorphologically inferred traces (Figs 5 and 7 in Chapter 5). This data also showed that faulting is longer than previously thought, with maximum lengths of 30 km at the northern limit of the study area. AM data also helped establish the study area's structural style as probably being produced by a pull-apart basin (which agrees with outcrop scale evidence in the area, e.g. "Río Jaral" site, Chapter 4), inside which there is both transtensional as well as transpressional stress fields.

According to epicenter data from the seismic sequence of the September 5, 2021, San Felipe (Guanajuato) earthquake (SSN, 2024), the western portion of the study area is more tectonically active than the eastern part. Additionally, fractures which manifest as new traces in practically each new visit to the "Banco de material" site (see Fig. 6a in Chapter 5), support this claim. This evidence is crucial for

understanding the major ion behavior in the area: fault activity (“Banco de material” type faulting) in the western sector seem to allow low chloride, HCO_3 and NO_3 rainwater to pass more freely, since faulting activity has not had sufficient time to accumulate enough fault related material that would not let it infiltrate. As can be seen in Figs 5 and 7 in Chapter 5, the eastern sector of the study area is not as significantly active from a tectonic point of view compared to the western sector, (e.g. the “Presa El Hundido” site, Fig. 22, Chapter 4). Therefore, fault gouge and related fluids have had enough time to accumulate and fault planes can act as barriers for low chloride, HCO_3 and NO_3 rainwater, since those ions concentrations are higher than in the western sector, both in the dry and rainy season.

The structural-geophysical model derived from the integration of AM, major ion, and geological data shows that both the distribution and orientation of faults is constant for the first 1000 m of the southern sector of the VRG. Conversely, at 2000 m depth, shallower faults seem to join and form a smaller number of traces. This reinforces the interpretation of the presence of positive and negative flower structures made in Chapter 4 of this study. This also means that these types of transpressive and transtensive structures are present at the outcrop, regional, and basin scales.

References

- Barnes, P.M., Sutherland, R., Davy, B., and Delteil, J., (2001) Rapid creation and destruction of sedimentary basins on mature strike-slip faults: An example from the offshore Alpine Fault, New Zealand. *Journal of Structural Geology* 23(11), 1727-1739. [https://doi.org/10.1016/S0191-8141\(01\)00044-X](https://doi.org/10.1016/S0191-8141(01)00044-X)
- Comisión Nacional del Agua (CONAGUA) (2023) Actualización de la disponibilidad media anual de agua en el acuífero Jaral de Berrios-Villa de Reyes (2412), Estado de San Luis Potosí. Ciudad de México. (Update of the average annual water availability in the Jaral de Berrios-Villa de Reyes aquifer (2412), State of San Luis Potosi. Mexico City).
- Drahor, M. G., and Berge, M. A., (2017) Integrated geophysical investigations in a fault zone located on southwestern part of İzmir city, Western Anatolia,

- Turkey. *Journal of Applied Geophysics* 136, 114-133.
<https://doi.org/10.1016/j.jappgeo.2016.10.021>
- Figueroa-Miranda, S., Tuxpan-Vargas, J., Ramos-Leal, J.A., Hernández-Madrigal, V.M., and Villaseñor-Reyes, C.I., (2018) Land subsidence by groundwater over-exploitation from aquifers in tectonic valleys of Central Mexico: A review. *Engineering Geology* 246, 91-106.
<https://doi.org/10.1016/j.enggeo.2018.09.023>
- Konon, A., Ostrowski, S., Rybak-Ostrowska, B., Ludwiniak, M., Śmigielski, M., Wyglądała, M., Uroda, J., Kowalczyk, S., Mieszkowki, r., and Kłopotowska, A., (2016) Mnin restraining stepover—evidence of significant Cretaceous–Cenozoic dextral strike-slip faulting along the Teisseyre-Tornquist Zone?. *Acta Geologica Polonica* 66(3), 429-449. <https://doi.org/10.1515/agp-2016-0019>
- Nabi, A., Liu, X., Gong, Z., and Ali, A., (2020) Electrical resistivity imaging of active faults in palaeoseismology: case studies from Karachi Arc, southern Kirthar Fold Belt, Pakistan. *NRIAG Journal of Astronomy and Geophysics* 9(1), 116-128. <https://doi.org/10.1080/20909977.2020.1722524>
- Nobes D. C., Hornblow S. M., 2021. Not all faults are conductive: the effects of seasonal weather changes on the near-surface expression of faults. *Geophysical Prospecting*, 69(7), 1503-1514. . <https://doi.org/10.1111/1365-2478.13126>
- Servicio Sismológico Nacional (SSN), (2021) Secuencia Sísmica del 4 a 6 de septiembre de 2021, Guanajuato-San Luis Potosí (M 4.5). [Seismic Sequence from 4 to 6 September 2021, Guanajuato-San Luis Potosí (M 4.5)]. National Seismological Survey website. <http://www.ssn.unam.mx> (accessed 7 September 2021).
- Servicio Sismológico Nacional (SSN), (2024) Earthquake Catalog. National Seismological Survey website. <http://www2.ssn.unam.mx:8080/catalogo/> (accessed 22 March 2024).

Chapter 7-. Conclusions and recommendations

7.1 Conclusions

The southern sector of the Villa de Reyes Graben, because of its geological, tectonic and climatic conditions, proved to be the perfect experimental area to try the methodology for studying active faults developed in this work. The **first** and **second parts** of this methodology, field geological survey and Electromagnetic Profiling Method (EMP) mapping, yielded excellent results showing non-filled active faults that generate high resistivity values (EMP), and also reveal faults traces that have not outcropped yet and the true width of fault zones (which are usually only a few centimeters wide at outcrops). The **third** and **fourth** parts of this methodology (Electrical Resistivity Tomography (ERT) and Ground Penetrating Radar (GPR)) further allowed to characterize these faults, where at depths greater than 20 m generate wider and lower resistivity anomalies when compared to shallow depths. This is probably caused by a local disturbance of the water table, but at present there is not enough data to ascertain this. ERT was especially useful for confirming that active faulting is predominantly geological and not man-made, as was first thought at the beginning of this study, which contrasts with other locations where anthropogenic activity can exacerbate geological faulting. The structural style of the southern sector of VRG was defined as NW-SE trending right-lateral faults (southern portion) and NE-SW left-lateral faults (northern portion). These faults can generate both transtensive (negative flower) and transpressive (positive flower) structures, which can alternate along the same fault trace. Nevertheless, negative flower structures are more common in the northern portion of the study area (although transpressive structures are starting to manifest in the “Presa El Hundido” site), whereas positive flower structures in the southern sector. This active faulting seems to be taking place since at least 500 years ago, given that the old colonial era dam structure at the “Presa El Hundido” shows evidence of being repaired around that time. The **fourth part** of the methodology, which involves the use of focal mechanism solutions evidence, confirmed the trend and fault type change

interpretation based on geological and geophysical evidence, while epicenter location showed that the western sector is more active than the eastern one.

Aeromagnetic (AM) and epicenter data allowed to go from a local and regional to a basin scale, and also helped fine tune the location and structure of the faults mapped using the previously mentioned four-part methodology and showed that the southern sector of the VRG is being faulted by a pull-apart like structure, which can display inside it both transpressive and transtensive structures. AM data revealed alternating high and low magnetic anomalies, which could be caused by the previously mentioned alternating positive-negative flower structures. Hydrogeochemical (HGC) data confirmed that the western sector of the VRG is more active, since it shows stronger meteoric water influence when compared to the eastern sector. Finally, the 3D structural model showed more numerous shallow faults joining at depth, which confirms the presence of a positive-negative flower type structure. In this way, this structural style seems to control the tectonics of the VRG at the outcrop, regional and basing scale.

This work is a first step towards a greater and broader understanding of the tectonics of the VRG, the southern sector of the Mesa Central structural province, and its relationship with neighboring active structures. The width, length and depth definition of faulting at the southern portion of the VRG could also have serious implications both from a seismic hazard and land planning points of view.

7.2 Recommendations

- Updating and continuing the monitoring of the piezometric, water quality and major ion data from the area would allow the correct correlation between all these data and the recent (and future) seismicity of the VRG.
- Establishing a seismic and active-faulting monitoring network would allow better understanding of the distribution of epicenters at shallow depths, and hence the location of faults that have not outcrop yet.

- Likewise, updating the current Aeromagnetic database would be helpful for better adjusting the different types of faults and structures that are negatively influencing the study area.
- An Induced Polarization survey along the ERT profiles would help establish if the high to low resistivity change of fault planes is being caused by a local water table disturbance, or by the accumulation of fault-derived fault gouge.